UNIVERSITÀ
DEGLI STUDI
DI TRIESTE

# UNIVERSITÀ DEGLI STUDI DI TRIESTE

## XXXVI CICLO DEL DOTTORATO DI RICERCA IN

### INGEGNERIA INDUSTRIALE E DELL'INFORMAZIONE

# MODELLING AND DESIGN OF VOLTAGE CONTROL SYSTEMS FOR THE ENERGY TRANSITION

Settore scientifico-disciplinare: ING–IND/33


DOTTORANDO
**FABIO MARZOLLA**

COORDINATORE
**PROF. FULVIO BABICH**

SUPERVISORE DI TESI
**PROF. GIORGIO SULLIGOI**

CO-SUPERVISORE DI TESI
**PROF. ANDREA VICENZUTTI**


**ANNO ACCADEMICO 2022/2023**

# Sommario

Lo scopo della tesi è di presentare gli studi effettuati per la definizione di un nuovo regolatore di tensione secondaria per la rete di trasmissione nazionale, dotato delle capacità necessarie a gestirne l'evoluzione a seguito della transizione energetica e dall'attuazione di politiche contro il cambiamento climatico.

L'attuale architettura di controllo della tensione presenta limitazioni dovute all'obsolescenza delle tecnologie impiegate, alla progettazione basata sul precedente modello monopolistico del mercato elettrico, ed alla struttura di controllo fondata sull'assunzione di invarianza della struttura della rete e dei flussi di potenza. Inoltre, alcune delle ipotesi fondanti per l'attuale regolatore di tensione potrebbero risultare non più valide a causa dell'incremento di fonti di energia rinnovabile distribuita che gradualmente sostituirà la generazione basata su fonti fossili. Risulta di interesse lo sviluppo di una nuova architettura di controllo basata sulle caratteristiche attuali della rete elettrica nazionale, in grado di sfruttare le nuove fonti rinnovabili, capace di gestire le dinamiche operative della rete di trasmissione e con caratteristiche di robustezza superiori all'attuale.

In particolare, il primo capitolo della tesi presenta la struttura di regolazione gerarchica di tensione e la sua evoluzione, approfondendo i suoi componenti e le diverse logiche di controllo.

Il secondo capitolo descrive gli aspetti critici dell'attuale architettura di regolazione della tensione italiana. Vengono mostrati studi approfonditi, per mezzo di simulazioni e ricostruzioni di eventi di rete realmente accaduti, per convalidare presenza e natura di eventuali criticità.

Nel terzo capitolo si effettua una rassegna dello stato dell'arte riguardante nuove architetture e strategie di regolazione della tensione, volendo identificare possibili soluzioni per le criticità messe in evidenza. Si dimostra l'assenza di proposte applicabili alla rete italiana nel contesto di una realizzazione nel breve termine. Sono presentati due approcci controllistici promettenti in tale senso: *Decoupling* e *Linear Quadratic Regulator with Integral actions* (considerati i più coerenti con gli obiettivi di gestione della rete elettrica futura).

Il quarto capitolo tratta le implementazioni delle architetture di controllo che, sfruttando gli approcci controllistici del capitolo tre, consentano la realizzazione di regolatori secondari integrabili nell'attuale struttura di controllo, seguendo le esigenze elencate in precedenza.

Il quinto capitolo presenta il modello linearizzato di una porzione di rete di trasmissione italiana utilizzato per i test delle strutture di controllo di cui il capitolo quattro. Sono presentate le ipotesi per la costruzione del modello matematico ed i risultati di simulazioni eseguite, utili a valutare le prestazioni dinamiche delle architetture di controllo, a seguito di differenti perturbazioni del sistema.

Il sesto capitolo presenta due studi riguardanti l'implementazione della soluzione identificata nel capitolo precedente, considerando la disponibilità delle misure dal campo e le esigenze della rete di trasmissione italiana. Quest'attività consente il passaggio da un modello matematico ideale, utilizzato unicamente per la definizione degli algoritmi di controllo, ad un modello che più si avvicini alla realizzazione effettiva.

Il settimo capitolo presenta un nuovo modello di rete, capace di emulare il sistema elettrico in esame in modo più fedele rispetto al modello utilizzato nel capitolo sei. Tale modello non-lineare della rete è basato su calcoli di *load-flow* ricorsivi. Esso consente di analizzare uno ampio spettro di punti di lavoro, riflettendo con precisione il comportamento di una rete reale. Le simulazioni del nuovo controllore secondario con il nuovo modello di rete sono presentate al fine di validarne le prestazioni.

# Abstract

The purpose of this thesis is to present the research studies for the definition of a new secondary voltage regulator for the national transmission network. This regulator must be capable of managing the power system evolution caused by the energy transition and the application of climate change policies.

The current voltage control architecture limitations are mainly due to the technological obsolescence, the design based on the prior monopolistic model of the energy market, and the control structure based on the assumption of both network structure and power flows invariance. Furthermore, due to the increase of distributed renewable energy sources, which will eventually replace fossil fuel-based generation, several fundamental hypotheses for the existing voltage regulator may no longer be valid. For these reasons, the design of a new voltage control architecture is of interest. It should be based on the present national energy grid properties, able of utilizing new renewable sources, controlling the operational dynamics of the transmission network, and having robustness qualities superior to the current one.

The first chapter of the thesis describes the hierarchical voltage regulation structure and its evolution, going into its components and various control logics.

The second chapter describes the critical aspects of the current Italian voltage regulation architecture. In-depth studies are shown, through simulations and reconstructions of network events that actually occurred, to validate the presence and nature of any critical issues.

In the third chapter, a review of the state of the art is carried out regarding new architectures and voltage regulation strategies, aiming to identify possible solutions for the critical issues highlighted. The absence of proposals applicable to the Italian network in the context of short-term implementation is demonstrated. Two promising control approaches in this sense are presented: *Decoupling* and *Linear Quadratic Regulator with Integral actions* (considered the most consistent with the management objectives of the future electricity grid).

The fourth chapter is concerned with the implementation of control architectures that use the control techniques of chapter three, enabling the design of secondary regulators. Those regulators can be integrated into the current control structure while sticking to the previously specified requirements.

The fifth chapter shows a linearized model of a portion of the Italian transmission network that was used to evaluate the control structures mentioned in chapter four. The hypotheses for the mathematical model's design and the results of simulations performed are described, which are valuable for considering the dynamic performance of control structures after various system disturbances. The best solution is examined in depth in the following chapters.

The sixth chapter includes two studies on the execution of the previous chapter's solution, taking into account the availability of field measurements and the needs of the Italian transmission network. This activity enables the shift from an ideal mathematical model, which is only used to define control algorithms, to a model that is closer to actual control implementation.

The seventh chapter presents a new network model, capable of representing the electrical system with more accuracy than the model used in chapter five. This new non-

linear model of the network is based on recursive *load-flow* calculations. It enables the analysis of a broad range of operational points, precisely mirroring the behaviour of a real network. Simulations of the new secondary controller with the new network model are presented in order to validate its performance.

# Contents

# Glossary

**AVR** Automatic Voltage Regulator

**CN** Control Node

**CVR** Coordinated Voltage Regulation

**FP** First Procedure

**HIL** Hardware In the Loop

**HV** High Voltage

**HVDC** High Voltage Direct Current

**LQR** Linear Quadratic Regulator

**LQRI** LQR with Integral Actions

**MIMO** Multiple Input Multiple Output

**MV** Medium Voltage

**OLTC** On Load Tap Changer

**PI** Proportional Integral

**PMU** Phasor Measurament Unit

**PN** Pilot Node

**PVC** Primary Voltage Control

**PVR** Primary Voltage Regulator

**RES** Renewable Energy Sources

**RPFM** Recoursive Power Flow Model

**RPR** Reactive Power Resource

**SCADA** Supervisor Control And Data Acquisition

**SIL** Software In the Loop

**SP** Second Procedure

**SISO** Single Input Single Output

**SVC** Secondary Voltage Control

**SVR** Secondary Voltage Regulator

**TCSC** Thyristor Controlled Series Capacitor

**TVC** Tertiary Voltage Control

**TVR** Tertiary Voltage Regulator

**TSO** Transmission System Operator

# Introduction

The climate change and the greenhouse gases emissions reduction policies are heavily affecting electrical power systems. To guarantee a limitation in global warming, the EU sets demanding policies for ensuring climate neutrality in 2050 [1]. Consequently, the already challenging targets of Renewable Energy Sources (RES) penetration in electricity production must be considerably increased in respect to the current situation. In this regard, Italy planned the complete phase-out of coal-fired energy production by 2025 [2], [3], relying more on natural gas fueled power plants (although unexpected socio-political events may result in delaying such plan). Furthermore, according to the Italian Transmission System Operator (TSO, i.e. Terna) data [4], in January 2023, requests for connection to the high-voltage grid of new generation plants from renewable sources reached approximately 340 GW, with up to 37% from solar sources and nearly 54% from wind sources (on-shore and off-shore), a value of about 5 times Italy's 2030 targets. New RES installations have a twofold impact on the Italian transmission network: they reduce the carbon footprint of electric energy production, while increasing the inequality in production distribution across the country. The latter is due to the geographic features of the Italian peninsula. Indeed, the southern part offers much better conditions for RES exploitation than the norther one, due to higher solar irradiation and better wind speed

distribution. Being the industrial energy biggest consumers mostly located in the north, the increasing presence of RES in the south leads to an increased electric power flow from south to north, requiring an improvement in the Italian dorsal power lines.

However, the current energy revolution has an impact on the electrical system. Adjustments in the status of the power grid are already creating considerable changes in management activities. The main technical distinction between RESs systems and thermoelectric power plants is that the formers are interfaced to the network via static components (for instance photovoltaic inverters), whereas the latter employ rotating machines. RES installations, by definition, have non-programmable production profiles, implying that the electricity produced by such installations does not follow the dynamics of energy consumption needs, but rather the dynamics of individual energy sources (for example, photovoltaic production is maximum in the middle of the day and null at night). These characteristics generate the following impacts in network management: the reduction of the number of generation resources able to provide frequency regulation services (active power regulation); reduction of the margin of adequacy in order to cover the load peaks, that can happen in hours with low production of RES; increase of the periods of over-generation in the central hours of the day (production greater than the requirement), which may lead to cuts in the produced energy if the system is not equipped with adequate storage or reserve capacity; increase of steepness of the evening ramp of the residual load, caused by the drastic and sudden reduction of solar production in the evening hours, for which a rapid increase in production from flexible systems is necessary; rise in reserve is required due to increasing non-programmable resources prevalence and randomness. Moreover, due to the renewables production intrinsic variability, the power system's operating point and power flow frequently change, leading to an increase in the number of network configuration changes (e.g. connection and disconnection of power lines) in respect to the past.

All the above-mentioned changes are affecting the transmission system, drifting its structure and behavior away from the ones considered when its control systems were designed. Among the latter, the voltage control system is one of the most affected.

# 1. Power Systems' Voltage Control

The variation of voltage amplitude at which consumers are supplied is one of the factors defining the quality of service in a power generation, transmission, and distribution system. When supplied with nominal voltage, consumers operate and maintain continuity at their best, while any voltage variation from its nominal value may impair performance. For power system components (generators, transformers and lines) too, voltages should be kept within a small range of variability around their nominal value.

Even though voltage variations are a consequence of both disturbances (such as changes in loads, particularly in terms of reactive power) and control actions on reactive power sources (synchronous machines, condensers, reactors, compensators, etc.), it is challenging to keep such variations within sufficiently narrow limits.

*Voltage control* is defined as the set of actions that are carried out in the various part of the system (power plants, transmission network, sub-transmission network, etc.) in order to keep the voltage in all network nodes within values that do not considerably differ from the nominal ones and that ensure the good operation of loads and system components [5]. Proof on reactive power - voltage correlation is provided in Appendix A.

## 1.1. History of Automatic Voltage Control

The first voltage control systems were based on the "manual" control approach, which was widely utilized around the world in the 90's. This means that all possible participants in the voltage regulation, such as the units reactive power dispatching, the power plant high side voltage scheduling, as well as the control switching of capacitor banks, shunt reactors and the use of static var compensators, were controlled by hand. However, it soon became clear that this traditional way to face the network voltage control problems was often considered unsatisfactory because [6]: i) the reactive power dispatching was usually based on forecasting studies that differ from the more dynamic real situation; ii) the dispatching/scheduling was carried out in accordance either with specified specifications or with the system operator's request when it realized it was urgently necessary, leading to an inappropriate control action; iii) in general, there was a lack of coordination among the many control operations "usually" performed by plant and substation operators, thus there was no feasible way to achieve simultaneous and optimized control actions; iv) control interventions were generally out of sync with the dynamic events occurring in the network; this clearly led to the necessary to install an automatic voltage control system.

The need to increase voltage control facilities in the transmission network had always been recognized by network operators, and several methodologies and projects had been developed around the world. In Europe, during the last years of the 90's, hierarchical systems based on network area subdivision and automatic coordination of reactive power resources were initially investigated for network voltage control. These innovative solutions, called Coordinated Voltage Regulation (CVR) or Primary, Secondary and Tertiary Voltage Control (PVC, SVC and TVC), depending on their hierarchical level, were studied in Italy [7], [8], France [9], [10], Belgium [11], [12] and Spain [13]. As a consequence of organizational changes of European utilities and the ensuing liberalization of energy markets [14], hierarchical voltage control systems are becoming more valued and reinforced. Furthermore, system operators recognize that SVC and TVC simplify automatic management of overall transmission network voltages while

also rewarding the efforts of diverse contributors to voltage auxiliary service. From a worldwide perspective, interest in SVC and TVC [15] or simpler power plant alternatives, such as high-side voltage control, was developed in North America in the same period. Contemporary, a wide area voltage control was under development at Bonneville Power Administration, based on the coordination of generator or load tripping, Static VAR Compensators and Thyristor Controlled Series Capacitor (TCSC) modulation, power plant high-side voltage scheduling, and On Load Tap Changer (OLTC) [16]. SVC ideas are also being considered in Brazil [17], where voltage control is being proposed for critical distribution zones as well, based on a methodology that serves as a framework for OLTC assessment and coordination [18].

Progress and trends in transmission network voltage control necessitated considerable development and innovation at the turn of the millennium, requiring the employment of simple, effective, automatic control systems administered and supervised directly by transmission system operators. An in-depth cost-benefit analysis was carried out from the Italian automatic voltage control that support such an improvement [19]. Furthermore, as voltage regulation is essentially a local issue, viable solutions had to take into account automatic coordination of local reactive power resources, notably generators and compensators, but also shunt capacitors and reactors, OLTCs, static voltage compensators, and STATCOMs. As a result, the aims of voltage control in terms of quality and security improvements in network operation could be achieved through a decentralized voltage control system, by implementing local coordination in each area/region of the power system.

The main reasons that had supported coordinated "automatic" real-time voltage regulation at the beginning of the millennium are summarized as follows:

- in terms of reactive power reserves maintained available by generating units for coping with emergency conditions, the security of power system operation is increased;
- the overall transmission network's quality of operation is better due to less variance around the set voltage profile;

- the power system's transfer capability has been boosted, with higher active power levels transmissible and reduced voltage instability and collapse threats;
- the efficiency of power system operation is improved by the reduction of active losses, decrease of reactive flows, and improved exploitation of reactive resources;
- in terms of functional needs and performance monitoring criteria, the controllability and measurability of voltage ancillary service is simplified.

## 1.2. Basics of Hierarchical Voltage Control

The key concepts of hierarchical voltage control are presented in order to comprehend the rationale behind the structure, performance, and benefits of the current control system. Firstly, automatic real-time control of hundreds of transmission bus voltages is challenging, critical, and unreliable, making it unrealistic and uneconomical. Thus, A practical voltage control system should take into account only the dominant buses (a tiny amount), allowing for a suboptimal but viable and reliable control solution. The dominant buses are called *pilot nodes* (PNs) and their main feature is that they have high short circuit power, leading to a strong influence on the other buses' voltages. As a result, it is helpful to define a group of nodes whose voltage is significantly influenced by PN voltage fluctuations. This group of buses, which has voltages close to the PN and to each other, is called *control area* of that given PN. The reactive power of power plants is obviously the key resource available in the field, as it is low-cost and easy to operate for network voltage control. Thus, the control area of each pilot node shall contain power plants that can meet the demand for reactive power. With these premises, it can be defined PVR as the first layer of a hierarchical voltage control, whose responsibility it is to keep voltage within constraints directly at power plant's output bus. The Automatic Voltage Regulator (AVR) is the regulator appointed to this task, which is installed on the power plants' synchronous generators and acts with an equivalent time constant of nearly 1 second (for power electronics interfaced generators, the same task is performed by the converter's voltage control loop). SVC is the middle layer, which coordinates many generators and sources to keep the voltage of a set PNs at a given value. By

configuring the SVR dynamic so that it presents an equivalent time constant of tens of seconds, the dynamic decoupling from the PVC is achieved.

With regard to TVC, the core concept originated from the need to increase the system's operating security and efficiency through centralized coordination of the decentralized SVC structure. The voltage set-points for the PNs must be properly updated and coordinated with dynamics slower than SVC, taking into account the actual grid condition as a whole and avoiding unnecessary and incongruent inter-area control efforts. Moreover, PNs' set-points must be optimized to reduce grid losses while still maintaining control margin. TVC is hence the last and upper layer that guarantees the proper determination of PNs voltage set-points as input of the SVC considering all the aforementioned constraints. The hierarchical voltage regulation scheme is represented in Figure 1 as it was presented in [6].

A more detailed explanation of the three layers (PVC, SVC, and TVC) that comprise the power system's hierarchical voltage regulation is provided in the following paragraphs.

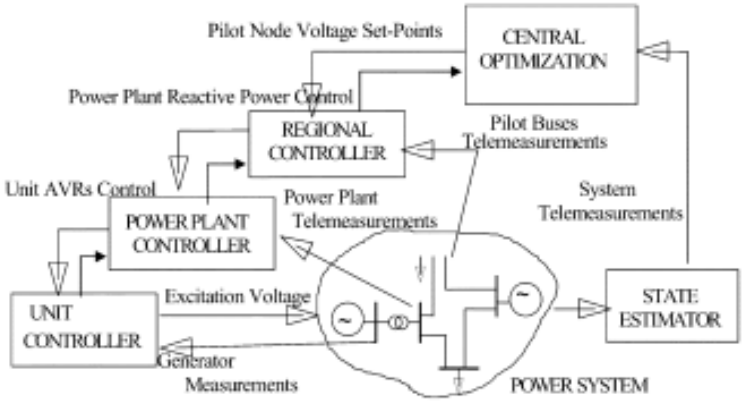


Figure 1 - Hierarchical structure for transmission network voltage control [6] .

## 1.3. Primary Voltage Control

To understand the usefulness of PVC through generators, let us refer to the simple case of a power plant feeding a load through a line with a reactance $x_L$, as shown in Figure 2.

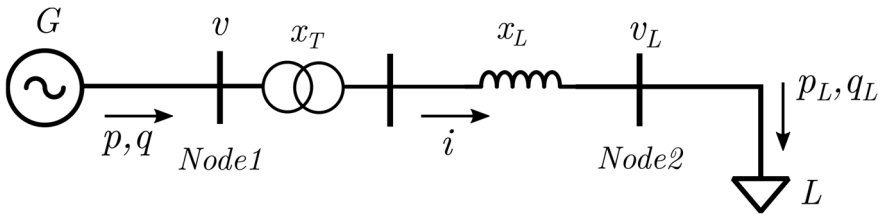


Figure 2 - Model of a generator (G) supplying a load (L)

With the previous adopted approximations, the voltage drop between the terminals of the generator (node 1) and those of the load (node 2) is expressed by equation (1.1):

$$\Delta v = v - v_L = x_e q_L \tag{1.1}$$

in *p.u.*, from which:

$$v_L = v - x_e q_L \tag{1.2}$$

Where $q_L$ is the power absorbed by the load and $x_e$ the total reactance interposed between the generator and the load:

$$x_e = x_T + x_L \tag{1.3}$$

Equation (1.1) shows that, if the voltage $v$ is kept constant, an increase $\Delta q_L$ of reactive load decreases the voltage at the load terminals; this decrease is given by

$$\Delta v_L = -x_e \Delta q_L \tag{1.4}$$

Thus, the greater $x_e$, i.e. the distance of the load from the point where the voltage is held constant, the greater the magnitude of the drop. In this regard, it is worth mentioning that if the generator did not have voltage control, the steady-state changes of

voltage $v_L$ caused by load variations would be greater than in the case of a constant $\boldsymbol{v}$. Indeed, failing such control, the voltage remaining constant upon the variation of operating conditions is no longer $\boldsymbol{v}$, but the excitation voltage $v_f$. Thus, the considerations previously made on eq. (1.1) can be applied again, replacing $v$ with $v_f$ and $x_e$ with $x_i+x_e$, since $x_i$ is the internal reactance of the alternator. If the load is assumed to be purely reactive (zero real power generation) for the sake of simplicity, the excitation voltage is given by:

$$\boldsymbol{v_f = v + x_d i} \tag{1.5}$$

Since $x_d$ may be much higher than $x_e$, the absence of voltage control generator may significantly deteriorate the capability of the generator to support the voltage in the load node.

As is clearly shown by eq.(1.4), when the reactive load (i.e. the reactive power delivered by the alternator) increases, the excitation voltage (or current) should be increased in order to keep the terminal voltage constant. If the excitation stayed constant, any increase in reactive power absorbed by the load, and hence in reactive power delivered by the machine, would reduce the terminal voltage. Furthermore, in order to ensure good load voltage levels, the voltage $v$ at the machine terminals should be kept sufficiently high (e.g. $v \simeq 1.1$ *p.u.*). The generator is operating in the so-called *overexcitation mode*. Instead, with low loads, due to low real power flows across HV transmission lines (power less than natural), the lines generate reactive power. In other terms, the load $\boldsymbol{q_L}$ becomes capacitive and the reactive power flow on the $x_e$ inverts and also the voltage drops inverts. Such that, the voltage is higher on the load node than at the machine terminals. Under these circumstances, the generator should absorb reactive power, i.e. operates in the *underexcitation mode*. To provide adequate load voltage levels, the voltage v at the machine terminals should be kept below its nominal value (for instance, $v \simeq 0.9$ *p.u.*). The excitation control of generators across the transmission network is provided by the AVR, one for each generator. In Figure 3, the role of the AVR is shown within the basic scheme of the PVC.

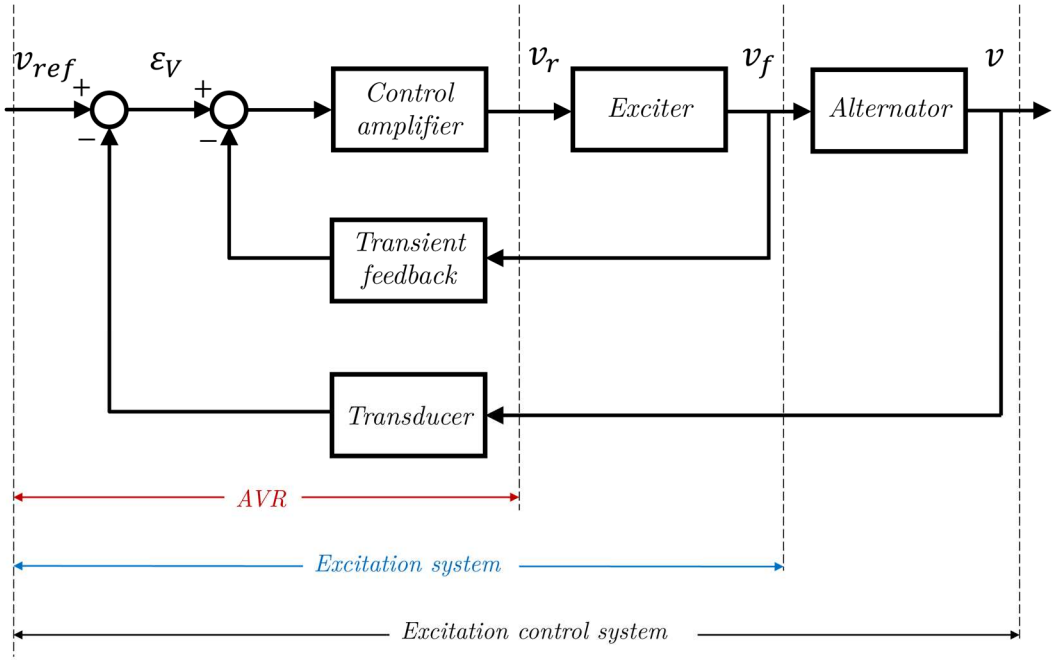


Figure 3 - General block scheme of the excitation control system or PVR.

## 1.4. Secondary Voltage Control

The aim of the SVC is to keep constant the voltages of PNs, upon load variations and perturbations in the system. Voltages in HV nodes are mainly affected by reactive power flows and several sources of reactive power are present in power systems: generators, shunt capacitors and reactors, static VAR systems. Once the appropriate operating voltages of the HV nodes is determined solving optimal power flow problems, an automatic system is desired acting on reactive power sources, to maintain such voltages constant despite the perturbations in the system. A centralized control, reading all selected HV node voltages and acting simultaneously on all reactive power sources in the system to maintain the voltages in those nodes constant, has always been considered unfeasible. The main reasons against a centralized control are the complexity of the transmission data system, the computing time for a central unit to cover all the system, and the reliability of a centralized architecture. Node voltages variations and reactive power variations of the linearized power system can be expressed with a linear matrix relation [5]:

$$[\Delta v] = [S][\Delta q] \tag{1.6}$$

where $[S]$ is called the *inverse-sensitivity matrix* because it is the inverse of the so-called *sensitivity matrix* $[J]$:

$$[S] = [J]^{-1} \tag{1.7}$$

$$[\Delta q] = [J][\Delta v] \tag{1.8}$$

The matrix $[S]$, and all the other matrices representing the transmission network (e.g. $[J]$) can be represented with sub-matrices considering different types of buses. If the network nodes are distinguished into $n$ generator nodes (G) and $N$ load nodes (L), the eq. (1.6) may be expressed by two matrix equations:

$$[\Delta v_L] = [S_{LG}][\Delta q_G] + [S_{LL}][\Delta q_L] \tag{1.9}$$

$$[\Delta v_G] = [S_{GG}][\Delta q_G] + [S_{GL}][\Delta q_L] \tag{1.10}$$

where:

$[\Delta v_G]$, $[\Delta q_G] \in \mathbb{R}^n$ are the vectors of the variations of reactive powers injected into the generation nodes (which are the MV nodes of each power plants) and their voltages;

$[\Delta v_L]$, $[\Delta q_L] \in \mathbb{R}^N$ are the vectors of the variations of reactive powers injected into all other nodes of the network (which are the HV nodes of power plants, lead nodes, pure transit nodes) and their voltages.

The controllers of the SVC layer consist of the Regional Secondary Voltage Regulators (RSVR or simply SVR) and the reactive power station regulators (called SARTs in the Italian Grid). The SVR controls the voltage of PNs through an integral action while the SARTs apparatus actuates the reactive power level required by the regional controller acting on the AVRs. The SVR receives its PN's voltage values and compares them to the reference values set by the TVC before sending a reactive level signal to each of its area's SART. The reference of reactive regulators is the reactive level (a scalar quantity $\mathsf{q}$ in the range of $-1 \leq q \leq 1$ multiplied by the reactive power limit (depending on the size of the generators and their operating point, i.e. depending on the capability curves):

$$Q_{ref} = livq * Q_{lim} \tag{1.11}$$

where $Q_{ref}$ is the reactive power requested to the generator, $Q_{lim}$ is the reactive power limit of the generator and *livq* is the reactive level transmitted by the SVR.

In Figure 4, the block diagram of the SVC applied to a transmission network with PVC is represented. The vectors for generators are further split considering also the power plants that do not participate at the SVC but only in PVC and are identified as subscript (GP), while the ones that participate to both layers are identified with subscript (GS). Also, the vectors for loads are further divided into sub-vectors, pointing the PNs among the common load buses with the subscript (p).

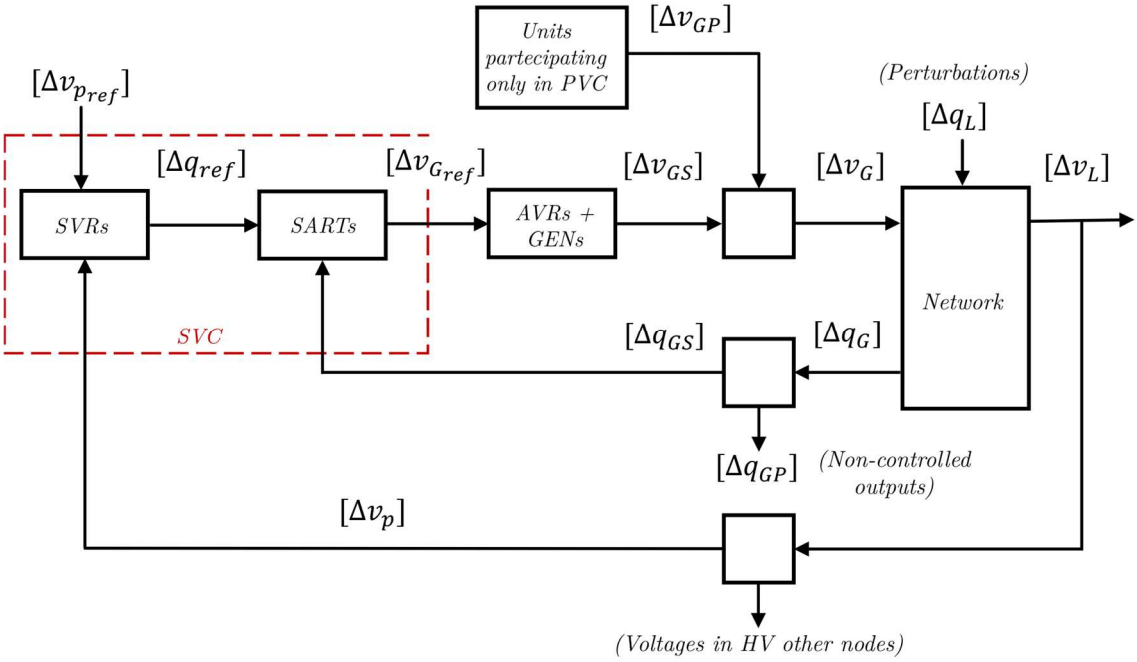


Figure 4 - Block diagram of SVC and PVC applied to a transmission network.

## 1.5. Tertiary Voltage Control

TVC's goal is to find the optimum values for the vector $[\Delta v_{pref}]$ of secondary control PN voltage references while meeting cost-effectiveness and operating security standards. This control is made at the central level by the Central Dispatcher. The related time constant must be greater than the SVC one, in order to achieve a good decoupling from secondary control. In other words, this control consists of a slow correction of $[\Delta v_{pref}]$. The Tertiary Voltage Regulator (TVR), which is the controller into

the TVC layer, works in real-time using the PNs' current voltages and the reactive power levels in the various areas vs the last forecast (short term: one day ahead; very short term: 15 minutes - 1 hour ahead) in terms of optimum voltage profiles. Owing to the slowness of this control, we may hypothesize that secondary control is under steady-state conditions, so that the actual PN voltages are practically the on-line actual pilot node reference voltages $[\Delta v^{a}_{pref}]$; following the nomenclature, the vector $\Delta v^{f}_{pref}$ represents the off-line forecasted PN voltages reference. More precisely, the TVR minimizes an objective function of the following type [5]:

$$f = \left[v_p^a - v_{pref}^f\right]^T [A^2]\left[v_p^a - v_{pref}^f\right] + \left[L_q^a - L_q^f\right]^T [B^2]\left[L_q^a - L_q^f\right] \tag{1.12}$$

in which $[A]$ and $[B]$ are suitable diagonal matrices, which weight the deviations of voltages in the PN and reactive power levels in the area from the optimum forecast values. While $[L_q{}^a]$ and $[L_q{}^f]$ are the vector of reactive level variation (sent by the SVR) in each area respectively actual and forecasted. This objective function implements an optimum trade-off between the need for obtaining the desired voltage profile and the need of the control limits ($[L_q]$ sufficiently far from the limit valued $\pm 1$). Thanks to the $[Q]$ sensitivity matrix (eq. (1.12)) relating the reactive power level variation to the voltage variations of the PNs of the areas

$$\left[\Delta v_p\right] = [Q][\Delta L_q] \tag{1.13}$$

the solution of the optimization problem can be obtained directly in terms of

$$\left[\Delta v_p\right] = \left[\Delta v_{pref}\right] \tag{1.14}$$

which is the only unknown variable in the eq. (1.12). It should be emphasized that the solution

$$\left[\Delta v_p\right] = \left[\Delta v_{pref}^0\right] \tag{1.15}$$

would lead to the optimum operating point in a single step of control action. Nevertheless, taking into account the time constant $T_t$ of the TVC loop (few minutes), it seems appropriate, at every step of the control action, to apply a variation:

$$[\Delta v'_{pref}] = \alpha\,[\Delta v^0_{pref}] \tag{1.16}$$

$$0 \le \alpha \le 1 \tag{1.17}$$

or to exponentially reduce voltage deviation to zero. So, the constant $\alpha$, toghether with the length $\tau$ of each control step, determinates $T_t$ as follows:

$$T_t = -\frac{\tau}{ln\,(1-\alpha)} \tag{1.18}$$

## 1.6. Remarks on Power Systems Voltage Control

In conclusion, Figure 5 shows the PVC, the SVC and the TVC of a power system that are carried out by power plants, where $h$ is the generic power plant of the generic area $i$ having $n_i$ power plants. It should be noted that a power plant is to be included in SVC if its apparent power exceeds 100 MVA.

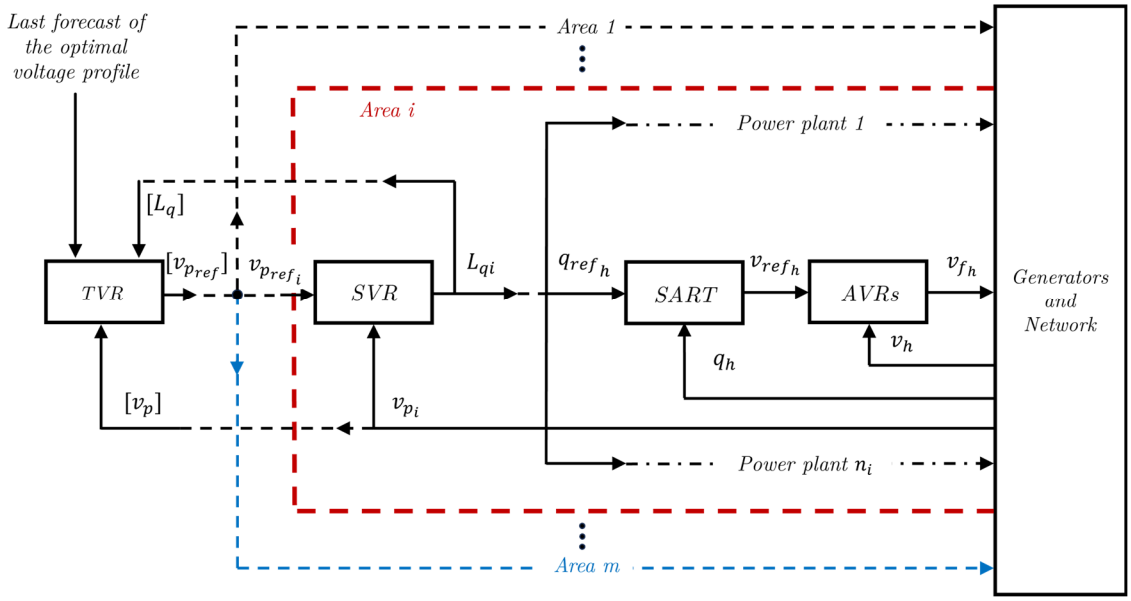


Figure 5 - Block diagram of PVC, SVC and TVC applied to a transmission network

# 2. Critical Points on Current Italian Voltage Control

Currently, the Italian voltage control is articulated on three hierarchical levels that are dynamically decoupled [5] as explained in the previous Chapter. The faster one is the PVC, whose responsibility it is to keep voltage within constraints directly at power plant's output bus. The AVR is the controller assigned to this task, which is placed on the synchronous generators of power plants and operates with an analogous time constant of roughly one second (the same task is done by the converter's voltage control loop on power electronics interfaced generators). SVC is the middle layer that coordinates multiple generators and sources to maintain PN voltage constant. The dynamic decoupling with the PVC is ensured by configuring the SVC dynamic in such a way that an equal time constant of tens of seconds is presented. The final level is a non-dynamic one, namely the TVC, in which the TVR solves an Ideal Reactive Power Flow problem to generate the optimal set of voltage references for SVC-controlled nodes on a regular basis. A diagram of the voltage control hierarchical system is shown in Figure 6 [20], depicting in detail one region (i.e., Region A) containing two areas (namely AREA 1 and AREA 2). A *region* is a group of control areas that are under the surveillance of a

single Terna (the Italian Transmission System Operator, TSO) control and monitoring center due to geographical reasons.

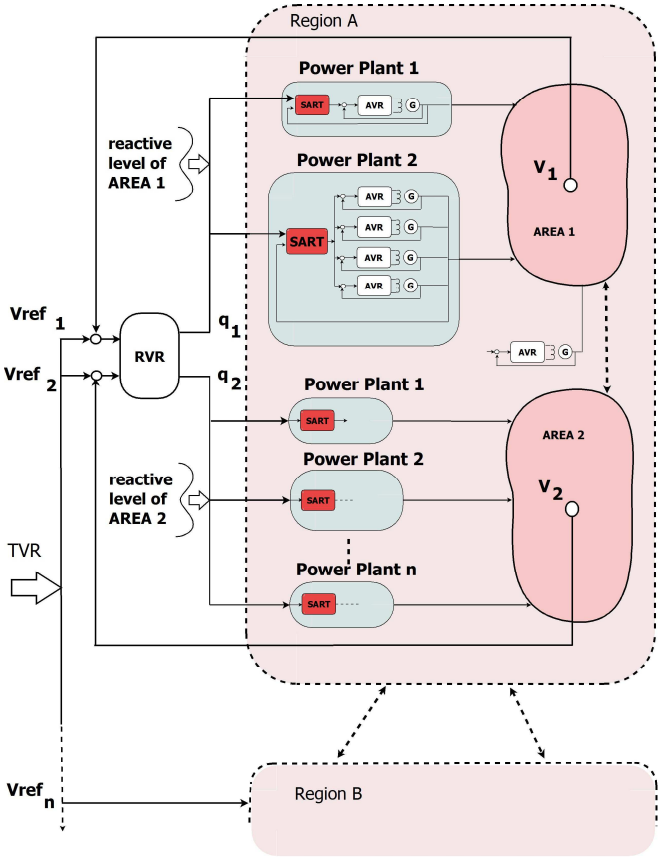


Figure 6 - Schematic diagram of the Italian hierarchical voltage control system.

As previously stated, this multi-layered voltage regulation architecture was designed for a power system that has been considerably altered over time. The actual wide area voltage control architecture, mainly designed in 90's, suffers some limitations due to the use of those years' technology (i.e., communication and computing performances). In detail, the historical approach was purely hierarchical to guarantee, level by level, a dynamic decoupling with a certain degree of stability. Such approach was typical of the old monopolistic approach: all the power stations were owned by only one player, so the technology, performances, parameters, and generator selection were always under the owner control. After market introduction, such paradigm results not valid anymore. Connected generators depend on the market, short circuit power is very variable, and actuators are quite different with parameters that can vary depending on the continuous

variation in needs and optimizations at power station level. In addition, control schemes were designed to manage synchronous machines having all the same performances, and now must face completely different dynamic and reactions of inverter-based renewables (RES: Renewable Energy Sources), VSC links, STATCOMs, regulating HVDC, and so on. Finally, the actual grid is characterized by continuous changes of topology (and consequently impedance matrix of system) and active/reactive flows, while the fundamental hypothesis of the legacy control systems was their time invariance. As a result, in some grid configurations and operating points, the current voltage regulation architecture begins to operate sub-optimally, or even stops working correctly. On the transmission system, oscillatory events and poor voltage loop stability have already been noticed. As a result, a new voltage regulation architecture capable of managing the increased unpredictability in power system operating conditions and configurations must be researched and specified, as well as allowing for the proper integration of new Reactive Power Resources (RPRs) into the regulating pool. Being PVC related with local voltage control, it should be ruled out for solving grid-wide control issues. On the other side, TVC is an optimization layer operating on long timeframes, which is not capable of affecting system dynamics (provided that the chosen set of voltage references are feasible for the applied system configuration). Thus, the SVC is the regulation layer that must be considered for solving the presented issues (both actual and future).

Therefore, the goal of this Chapter is to study, test and stress the current Italian SVC in order to better understand the issues related to such a network evolution which is quickly happening and how to address it. Two in-depth studies on current Italian SVC are described below: the first is about the technique for grouping nodes into control areas and assigning them PNs, while the second is about voltage stability as a result of a network event that actually occurred. Finally, additional considerations about short circuit power following network changes and its consequent impact on SVC are offered.

## 2.1. Issues related to the Area-PN SVC rationale

This study considers the existing methods for the determination of the voltage control areas (i.e. the *zoning* process) and their PN, applicable to the Italian transmission system. Among the methods available in literature [21], two have been selected and implemented. Both the selected procedures are based on the evaluation of a set of data about the system in study.

The first data to be retrieved is the short circuit power of all the nodes. This can be calculated as:

$$S_{CC_i} = V_i^2 \cdot Y_{ii} \tag{2.1}$$

where $Y_{ii}$ is the element on the system's admittance matrix diagonal and $V_i$ is the $i^{th}$ node's voltage.

The First Procedure (FP) [8] is the algorithm that was applied to obtain the first division into areas and the first choice of pilot nodes in the Italian transmission network. The approach begins with the identification of pilot node candidates based on their short circuit power. Then, the node with the highest $S_{CCi}$ is selected as a pilot node, and the area is created by evaluating the coupling between the pilot node and the other ones. The evaluation is done by means of the sensitivity matrix of the voltage in relation to the reactive power, as in the eq. (1.7):

The matrix $[J]$ can be determined directly or by using the $[S]$ sensitivity matrix of the node's reactive power relation to the node's voltage, which is acquired via a power flow evaluation. In the latter instance, the $[S]$ can be determined using the eq. (1.5) starting from a subset of the system's whole Jacobian matrix.

If the $S_{i,j}$ element value, which expresses the sensitivity of $i^{th}$ node voltage in respect to $k^{th}$ pilot node reactive power, is higher than a given control variable (i.e. $\beta$), then the $i^{th}$ node is added to the $k^{th}$ pilot node's area. When there are no more nodes with sufficient coupling to the pilot node, another pilot node is chosen (the one with the

highest $S_{CCi}$ among the remaining nodes), and the procedure is restarted. The $\beta$ is the only variable affecting the areas definition in this procedure.

The Second Procedure (SP) is clustering based [22], [23]. In particular, the nodes are grouped according to a similarity parameter to determine a given number of clusters (i.e. $R$), which are then used to build the areas. The parameter chosen by the Authors is the electrical distance between two nodes (i.e. matrix $[D]$), which can be calculated as:

$$D_{ij} = D_{ji} = -\log\left(\alpha_{ij} \cdot \alpha_{ji}\right) \tag{2.2}$$

where $\alpha_{ij}$ is called *attenuation* between node $i$ and node $j$. The attenuation coefficient is calculated from the Jacobian matrix, using the components related to the nodes in study:

$$\alpha_{ij} = \left(\frac{\partial V_i}{\partial Q_j}\right) \Big/ \left(\frac{\partial V_j}{\partial Q_j}\right) \tag{2.3}$$

The collection of the electrical distances between all the network nodes constitute the electrical distance matrix $[D]$. The definition of $D_{ij}$ univocally relates an electrical distance value to a couple of nodes, which means that each element of $[D]$ contains both the information about the nodes coupling and the specific two nodes involved. The pairs of nodes with the shortest distance are chosen as nucleation starting points, and more nodes are connected to them in an increasing distance sequence. The procedure continues until all of the nodes have been processed, resulting in a certain set of areas based on the number of starting nodes. To maintain the same criterion used in FP, the node with the highest $[S_{CC}]$ component in each area is chosen as the pilot one. However, different options are available in this regard. As an example, in [24] the pilot node is selected as the one having the lowest aggregate distance in respect to all the other nodes in the area.

In SP, the area determination is affected only by the number of clusters $R$, which is the control variable. Indeed, the first cluster collects elements whose value ranges from zero to $1/R$; the second collects elements with a value that is between $1/R$ and $2/R$; and so on until reaching the last cluster that contain the distances between $(R\text{-}1)/R$ and $R/R$. This means that an increased precision can be achieved with a high $R$, but at the

same time the likelihood of having a single couple of nodes in the first non-empty cluster is increased, resulting in a single area definition. To avoid such an issue, another control variable has been introduced, which is the population limit (i.e. $T$). The population limit $T$ defines the number of clusters with low electrical distances that are merged together to define the first set of nuclei for the areas' determination.

### 2.1.1. Procedures' implementation

The zoning procedures have been implemented in Python programming language, leading to the creation of two scripts that automatically determine the areas and the pilot nodes for a given power grid. The required input is the network admittance matrix $[Y]$, and the Jacobian sensitivity matrix $[J]$. To obtain the data for a generic power system, it has been chosen to use a software able to perform load flow calculations, i.e. PSAT [25]. PSAT is a Matlab plugin, thus allowing to extract the required data from the workspace through proper Matlab scripts. The procedure of Figure 7 shows the approach used in this work.

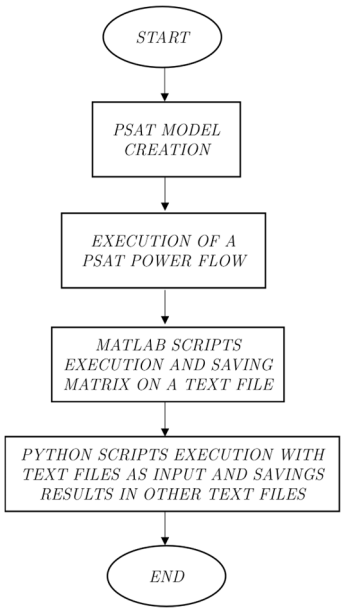


Figure 7 - Study implementation approach

### 2.1.2. First procedure

The algorithm implemented in Python for the FP is shown in Figure 8. In the following are analyzed the most significant steps, identified by the red number in the figure:

1) "[$Y$] and [$J$] loading": input data is loaded from text files.

2) "Matrices calculation": in this step the following operations are performed:

- calculation of [$S_{CC}$] vector from the system admittance matrix [$Y$];
- calculation of [$J$] from the [$S$] matrix.

3) "Definition of $\beta$ coefficient": the user is required to choose the $\beta$ control variable, in the range from 0 to 1.

4) "$k^{th}$ pilot node selection": the node with the largest short circuit power is selected as a pilot node, here depicted with index $k$.

5) "[$S$] relativization": Given the $k^{th}$ pilot node, the [$S$] matrix is relativized by dividing its components by the element $S_{k,k}$. This allows to obtain a set of indexes able to represent the strength of the nodes in respect to the selected pilot node, collected in the [$S'$] matrix.

6) "[$S'$] components selection": given the $k^{th}$ pilot node, the related column of the relativized [$S'$] matrix is selected. Indeed, the elements on the $k^{th}$ column (i.e. $S_{i,k}'$) depict the influence of the pilot node on the other nodes (i.e. the variation of the nodes voltage against pilot node's reactive power variation).

7) "Check 1": all the components of the $k^{th}$ column of [$S'$] are compared with the $\beta$ coefficient, excluding the one on the matrix diagonal (being it related to the pilot node influence on himself). All the $i$ nodes having component $S_{i,k}' > \beta$ are added to the area of the $k^{th}$ pilot node. Indeed, these are the nodes that will have the highest variation in their voltage after a reactive power control action is applied to the pilot node.

8) "Nodes removal": all the elements of the $i^{th}$ row and column of $[S']$ and $[S]$, as well as the $i^{th}$ components of the $[S_{CC}]$ vector, are set to zero. This allows removing the nodes that already belong to an area from the next zone determination procedure.

9) "Check 2": the presence of nodes still to be analyzed in the $i^{th}$ column of $[S']$ is checked, to assess if the coupling with the given pilot node has been evaluated for all the network nodes.

10) "Check 3": the presence of nodes not assigned to any area is evaluated, to verify if the process is finished or not.

11) "Area grouping": once the zoning procedure is finished, an additional step is performed to prevent the presence of very small areas (less than three nodes). This is achieved by merging each small area to a bigger one, selected as the one presenting the highest coupling (i.e. the one with the largest $[S]$ component between the small area nodes and the bigger area ones).

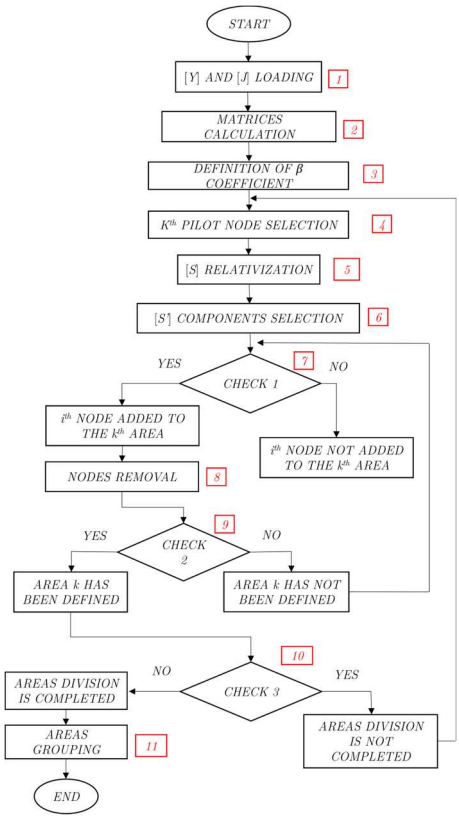


Figure 8 - Implemented algorithm for the First Procedure

### 2.1.3. Second procedure

The algorithm used for the SP implementation is depicted in Figure 9. The most important steps are presented in the following, when differing from the previous procedure ones:

1) "Matrices calculation": the difference in respect to the FP is given by the use of the electrical distances:

- calculation of electrical distances matrix $[D]$;
- relativization of $[D]$, by dividing each $[D]$'s component by the maximum one, to obtain values between 0 and 1 for all its elements (this simplifies the following steps).

2) "Definition of $R$ and $T$": the user defines the number of clusters $R$ and the population limit $T$.

3) "Ordered clusters filling": each element of the relativized $[D]$ matrix is classified into a cluster, leading to the creation of sets of electrical distances, ordered from the lowest (first cluster) to the highest (last cluster) one.

4) "First non-empty cluster selection": the first non-empty cluster is identified and selected as the starting point for the following process. This step is needed due to the non-uniform distribution of electrical distances in real systems. In fact, since the clusters are linearly spaced, the first ones (electrical distances close to zero) may result empty.

5) "Check 1": the presence of nodes not assigned to an area is checked. During the first $T$ iterations, this check allows to identify the presence of nodes that are to be used as nuclei for the areas' determination. Then, this check verifies if there are nodes that are still to be added to the already existing areas.

6) "Check 2": the number of iterations is compared with $T$, to select the proper population method between the one used to define the nuclei (method 1, if iteration number $< T$) and the one used to build the areas (method 2, else).

7) "Method 1 population": this method builds the nuclei for the areas, by merging in a single set all the electrical distances having the same node at one of its ends.

8) "Method 2 population": this method builds the areas over the nuclei, by adding to the existing areas new electrical distances that have a node in common with one of the already present elements. This is done once for each new element coming from the cluster in analysis, selecting the area that has the lowest distance as the recipient. Differently from the previous method, now the new element is removed from the analysis after its first assignation to an area. This allows enlarging existing areas, but not merging two of them together by means of a distance having one node in one area and one in another.

9) "Choice of the pilot node": one pilot node for each area is selected, by choosing the node with the highest $[S_{CC}]$ component.

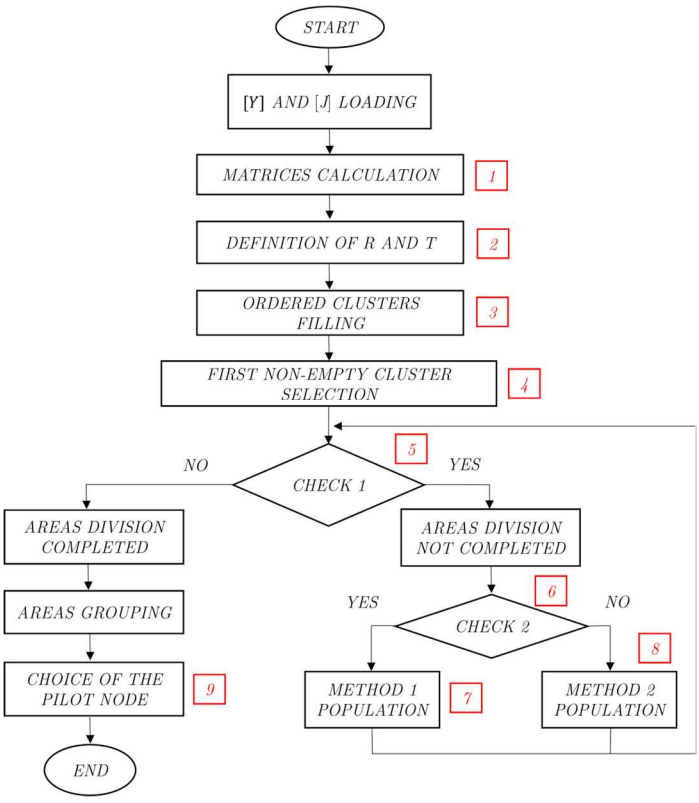


Figure 9 - Implemented algorithm for the Second Procedure

### 2.1.4. Network case study

To assess the effect of the power system structure and its parameters on the results of the zoning procedure, the IEEE 39 bus test network has been chosen as the case study. The 39 buses, 10 generators, and 18 loads network model has been built in the PSAT plugin for Matlab (Figure 10). By using the load flow capabilities of PSAT (the voltage profile of one of the analyzed cases is shown in Figure 11), it has been possible to automatically calculate the power system admittance matrix, as well as the Jacobian one. Then, by using some tailor-made Matlab code, the matrices have been extracted from the Matlab workspace and saved in the format needed by the developed Python scripts. In regards to the Case Study, in Figure 10 it is possible to examine the PSAT model, where the circles represent the generators (modeled as constant power, constant voltage sources), the square represents the slack bus (which substitute one of the generators in the test network), the triangles represent the loads, the lines are depicted as rectangular boxes with the $\pi$ symbol, and the transformers are represented with their usual symbol. The bus numbering follows a convention defined by the authors. In particular, it has been chosen to use numbers starting with one for the common buses, numbers starting with two for the generator buses, and the slack bus has a number starting with three.

The first set of tests has been aimed at finding the set of control variables that allows attaining similar results for both the procedures. Then, for one significant case the effects of the power system parameters have been examined.

#### 2.1.4.1. *Definition of control variables for the study*

The two zoning procedures are characterized by some control variables, which need to be provided by the user. In fact, for FP the control variable is $\beta$, while for SP the variables are $R$ (number of clusters) and $T$ (population limit). To limit the possible variable combinations in the SP, it has been decided to fix $R$ at 100, and thus to vary only $T$. In Table I are shown the most significant cases, the applied control variables, the

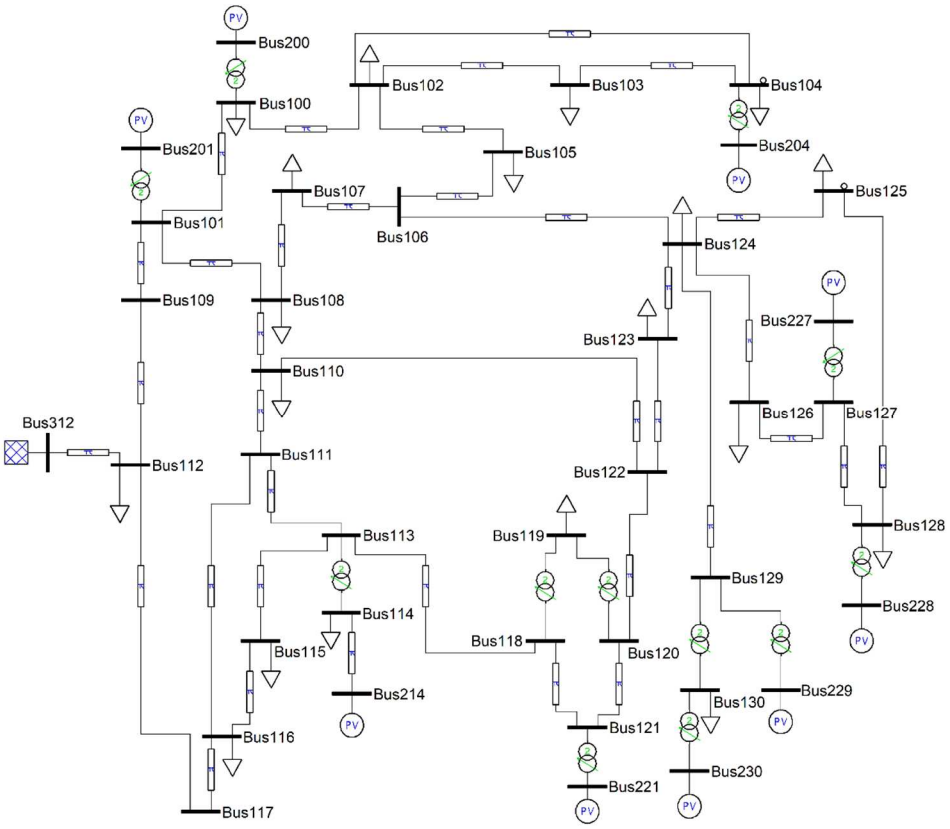


Figure 10 - PSAT model of IEEE 39 Bus Test Network

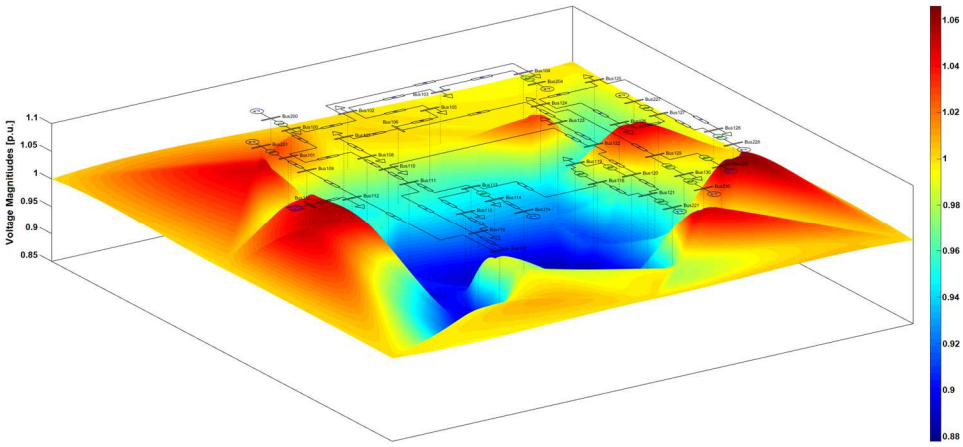


Figure 11 - Voltage profile resulting from PSAT's power flow of the case study Test Network

number of areas resulting from the procedures application, and the figure in which the specific area division is depicted.

By comparing the results obtained with FP (Figure 12 and Figure 13) and SP (Figure 14 and Figure 15), it is possible to see how the two procedures, while working on the same set of data and leading to the same number of areas, give different results in terms of areas boundaries. In particular, it is possible to see how the FP has some issues

in correctly determining the areas in case 1.1. Indeed, in Figure 12, it is clear to see that the area 3 pilot node (NP in the figure) is not directly connected to the rest of the area nodes, but rather through a node from area 2. The FP algorithm causes such inaccurate boundary definitions by starting from a specific pilot node and prioritizing bus assignment to him before studying the next pilot node. Because the algorithm does not know which pilot node will be the next pilot node, it is not possible to determine if a bus is more linked with the future pilot node rather than the one under consideration. By analyzing Figure 12, it is clear that bus 102 must have a good coupling with bus 100 (the area 3 pilot node), because it is connected to him by a single line. Conversely, the connection among bus 102 and area 2 pilot node (bus 129) is worse, despite having still a coupling that is higher that the defined $\beta$, due to the number of different lines between them. Such a result is also visible by analyzing the system's admittance matrix (here not shown for space reasons). Bus 102, on the other hand, is assigned to bus 129 (region 2 pilot node) merely because the algorithm analyzes such a node before bus 100. (area 3 pilot node). This conclusion is unlikely to have been noticeable in a different network with longer lines (and hence more decoupling between buses). The SP, on the other hand, does not exhibit such an inaccuracy since the clustering procedure allows its algorithm to compare all coupling across nodes with identical electrical distances. A bus is added to the region to which it is primarily connected in this manner, without the use of a hierarchical allocation. The definition of the node with the highest $S_{CC}$ as pilot node in both procedures led to similar results in this regard. It is relevant to notice that the areas are numbered in a descending order of pilot nodes' $S_{CC}$ (area 1 pilot node's $S_{CC}$ > area 2 pilot node's $S_{CC}$ > …).

For the following studies, the parameters leading to the determination of three areas for both procedures have been selected as "base cases". In particular, these are case 1.1 ($\beta = 0.09$) for FP and 2.1 ($R = 100,\ T = 4$) for SP.

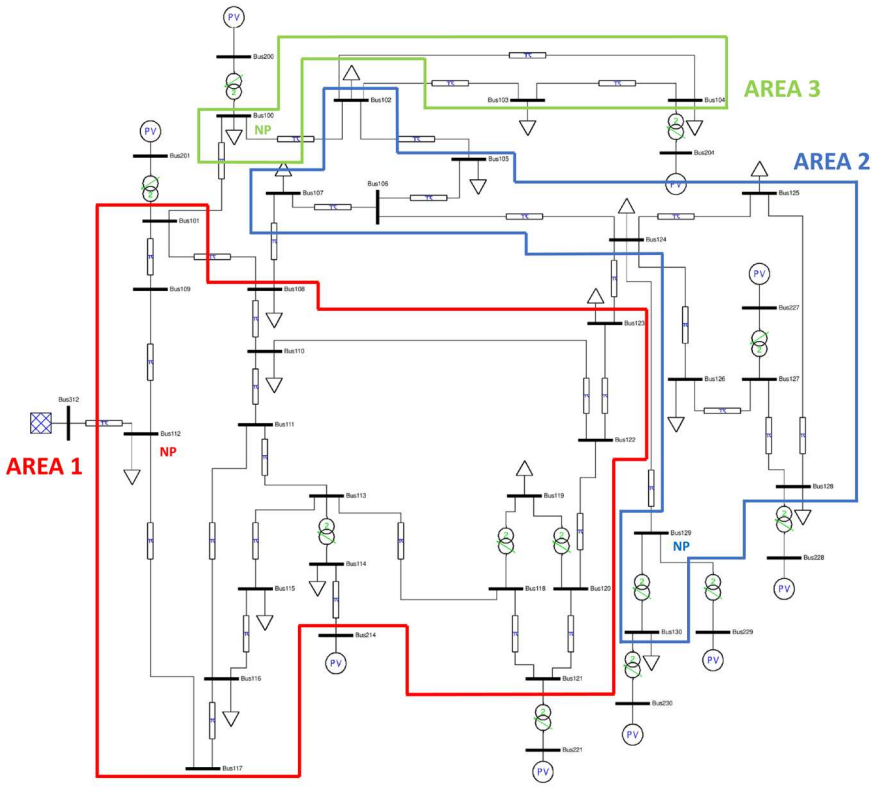


Figure 12 - IEEE 39 Bus Test Network area subdivision, case 1.1

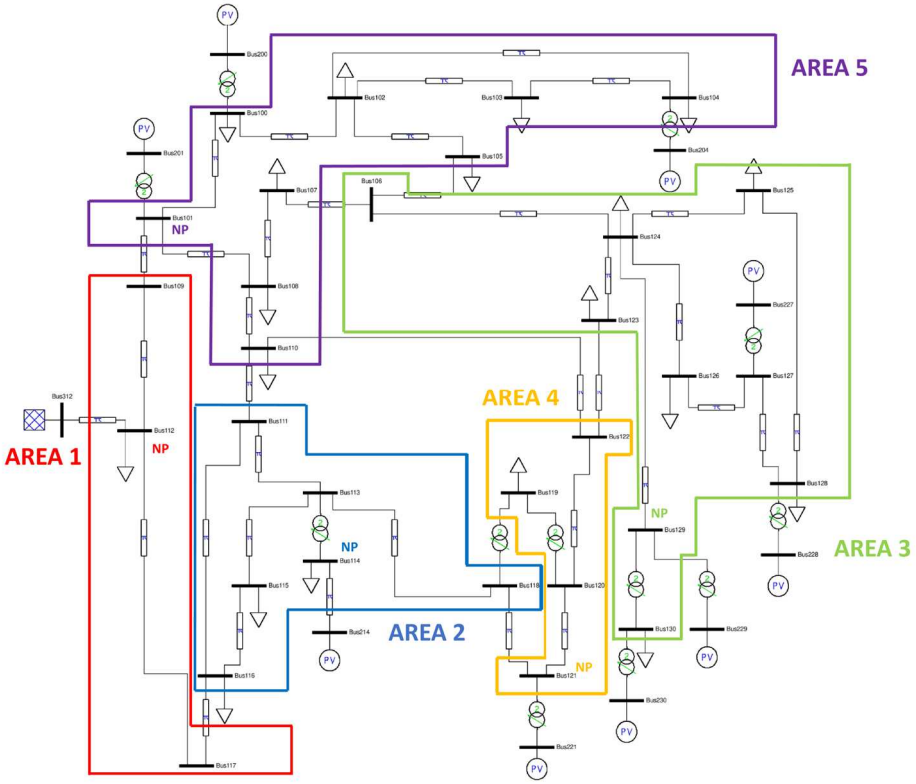


Figure 13 - IEEE 39 Bus Test Network area subdivision, case 1.2

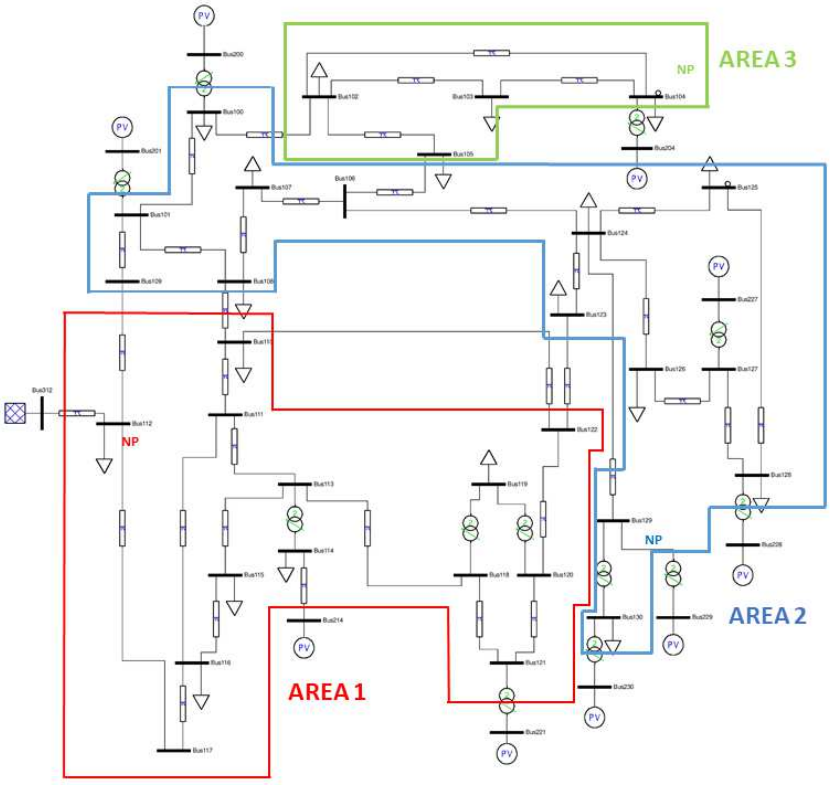


Figure 14 - IEEE 39 Bus Test Network area subdivision, case 2.1

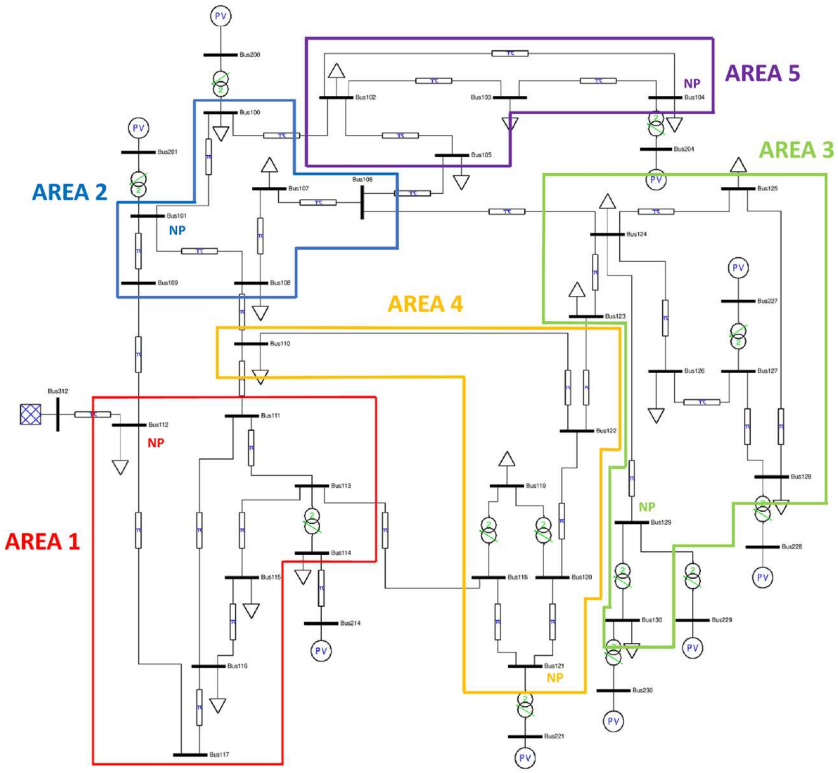


Figure 15 - IEEE 39 Bus Test Network area subdivision, case 2.2

#### 2.1.4.2. *Assessment of working point variation effect*

Additional studies on the base cases have been conducted to analyze the influence of a change in the power system functioning point on the areas' determination. The generator's active power assignment has been changed, causing power flows on the system to change. A scenario with no active power (save for the presence of losses on the system) as well as a case with a significant increase in reactive power of the loads have also been investigated. In all of the preceding situations, no modifications in the definition of the areas were discovered. As a result, it is reasonable to deduce that the regions subdivision is resistant to working point fluctuations. This has obviously been checked for plausible working points. Such a result was expected, since the limitation in voltages' variations in turn imply a limitation in the changes that can be found in the $[S]$ and $[D]$ matrices.

#### 2.1.4.3. *Assessment of network configuration change effect*

To test the effect on the area definition of changes in the network configuration, it has been chosen to add or remove power lines between system buses. This has a direct effect on the admittance matrix $[Y]$, while the effect on the sensitivity matrix $[S]$ depends on the changes in reactive power flows on the lines (with the same loads and generators).

To this aim, three variations have been tested on the base case:

- Removing the line between bus 113 and bus 118;
- Adding a line between bus 104 and bus 125;
- Both of the above two modifications.

In all the examined cases, the change in the network structure leads to changes in the areas. For space reasons, only the latter case (both modifications to the network structure) is here shown (Figure 16 and Figure 17 for FP and SP respectively).

The FP leads to the same number of areas of case 1.1. The most evident change is the merging of the former area 2 and area 3 in a single area (area 3 in Figure 16). At the same time, a new area 2 is formed, starting from a new pilot node (the bus 114),

which was previously included in area 1. Once again, the FP leads to an inaccurate definition of the area boundaries. For what concerns the SP, the use of the case 2.1 control variables in the new configuration leads to six areas, in respect to the original three. To attain again three areas (Figure 17), the population limit $S$ had to be increased up to 7. By comparing Figure 17 and Figure 14, the changes resulting from the network structure change can be appreciated.

Specifically, the former area 3 (buses 102, 103, 104, and 105) has been included into area 2, thanks to the new link between bus 104 and bus 125. The change in the reactive power flows due to both the new link and the removal of the line between bus 113 and bus 118, leads to the creation of a new area 3, composed by bus 100, 101, and 109. This highlights a significant reduction in the reactive power contribution of the generators connected to bus 100 and 101 to the area 2 loads in the new configuration, in respect to the former one.

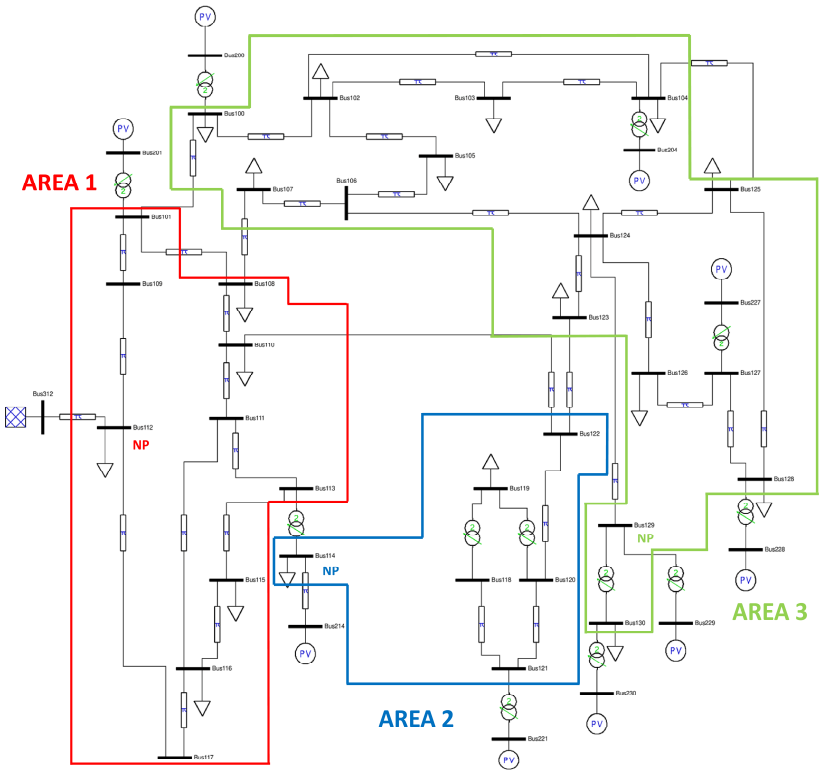


Figure 16 - IEEE 39 Bus Test Network area subdivision, change in network configuration

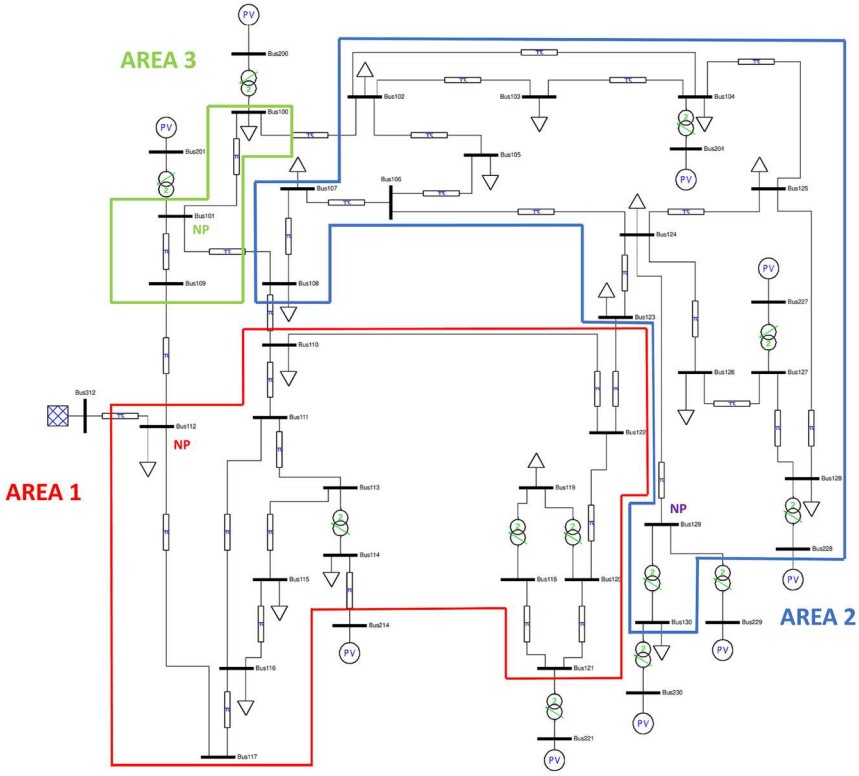


Figure 17 - IEEE 39 Bus Test Network area subdivision, change in network configuration

### 2.1.5. Remarks

In this research study, two different procedures for the determination of the voltage control areas and their PN have been used, with the aim of analyzing the effects of the changes in power system parameters. When the system operating point is possible, it turns out that a significant lack of sensibility can be highlighted in terms of the operating point effect for both techniques applied (i.e. voltage at buses inside the standard transmission system limits). A change in network configuration, on the other hand, produces significant changes in the voltage control areas that result (i.e. adding and/or removing power lines). It is also worth noting that the First Procedure occasionally produces inaccurate area boundary determination due to an inherent limitation of its algorithm that prioritizes bus assignment to the highest SCC nodes, whereas in the same cases, the Second Procedure appears promising and appears capable of correctly managing the boundaries' definition via the clustering approach. This leads to the fact that if network layout changes become more frequent and/or more

substantial, the allocation of PNs and their control areas must also be able to follow this change (avoiding the control of wrong couples of PN - group of regulating power plants). As a result, the SVR must be able to adapt to network changes in order to track the movements of control areas (and regulating power plants) and their PNs.

## 2.2. Voltage Instability Issues

As regards voltage instability issues, Terna, the Italian TSO (Transmission System Operator), recorded a voltage oscillatory network event following a sudden shutdown of a production plant under adverse conditions of the network. An equivalent network model of the network under discussion (Figure 18) was developed in order to properly investigate the phenomenon and evaluate whether it can be attributed to the actual SVR.

As shown in Figure 18, the network part under study is made up of three power plants, two of which (Power Plant 1 and Power Plant 2) insist on the same node (Node 1) via two equivalent reactances ($x_1$ and $x_2$, which account for power plant transformers and short HV lines), and one (Power plant 3) insists on a node (Node 2) through another equivalent reactance ($x_3$). The Nodes 1 and 2 are coupled via reactance ($x_a$) that models the HV line between them. The whole scheme is connected to the rest of the Italian grid (which may be assumed as an infinite short circuit power point) through the last equivalent reactance ($x_b$). The Power Plant 3 was affected by the sudden shutdown, which resulted in the development of a steady voltage oscillation with a period of around 30 s on the Node 2 voltage, which has a nominal voltage of 380 kV. Before the event, the system was in an underload condition, and power plants were absorbing reactive power to compensate for the line's reactive power production. Furthermore, in order to limit the amount of capacitive reactive power required to compensate, some lines were left open, resulting in a significant reduction in the level of the area interconnection. As a result, the disturbance produced by the disconnection of the Power Plant 3 occurred in an unfavourable network configuration.

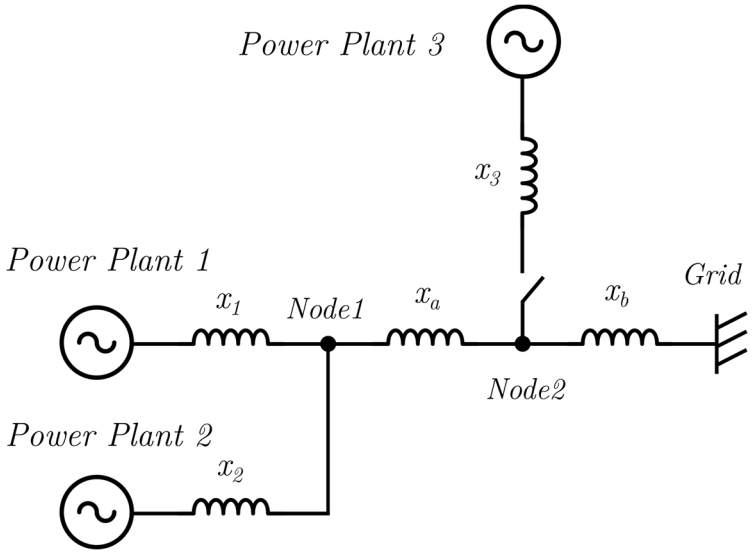


Figure 18 - Equivalent network model of the under-investigation grid part due to the oscillatory event

### 2.2.1. The System's mathematical model

Based on the real data and information provided by Terna, a mathematical model of the system under investigation has been developed to examine the event. The model is made up of a dynamic part generated in the Matlab-Simulink environment, as described below, and a Matlab script for setting system parameters, programming simulations, and showing the results.

Figure 19 shows the general view of the mathematical model of the entire adjustment chain in Simulink. They are modelled the primary and secondary voltage control loop (blocks SVR, SART and AVR), the systems of measure and remote control necessary to the secondary control (blocks "Measure Δv_p to SVR" and "Command SVR to SART" respectively), the portion of network under investigation of Figure 18 (block "Network").

The model takes as reference the operating condition immediately precedence to the event (which are described above) and evaluates the variations around them, using the relative values (inserting where necessary the appropriate base changes). Nevertheless, for clarity and simplicity of representation, it was decided to use the physical values in all the results shown in the following sections.

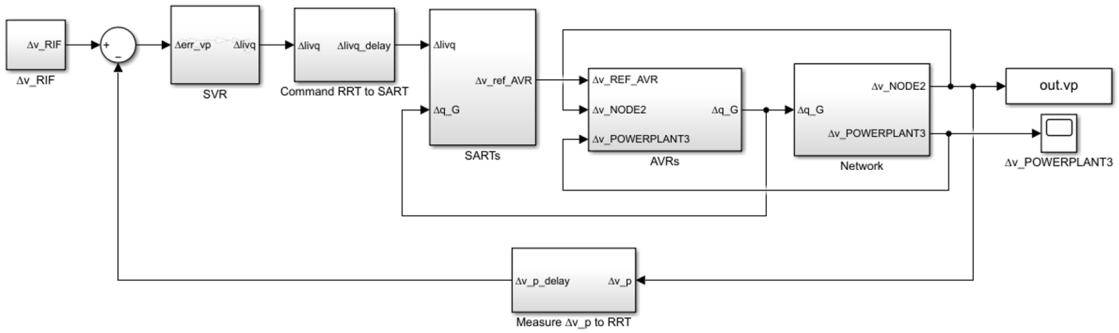


Figure 19 - Matlab-Simulink network mathematical model of the under-investigation grid part

The models of the individual components are described in detail below, where the Δ symbol is omitted to allow a better legibility.

#### 2.2.1.1. *Structure and parameters of SVR model*

The SVR in this case consists of a single PI regulator, which measures the voltage of the Node 2 and applies a control action by means of the *livq* signal on the power plants under study (Figure 18). The regulator shall be represented using the model shown in [5] namely:

$$livq = \left(K_S + \frac{1}{sT_S}\right) * Qlim_{area} * err\_vp \tag{2.4}$$

where: *livq* is the remote-control signal sent to the power plants, *err_vp* is the difference between the voltage reference of the PN (Node 2) and the measurement of the same, *Ks* is the gain of the proportional part of the controller, *Ts* is the time constant of the regulator's integral part, $Qlim_{area}$ is the reactive power limit of the tested area.

In order to derive the parameters $K_S$ and $T_S$ to be set in the model, the PN voltage measure and *livq* signal of area effected by the event have been used. In particular, assuming the use of a PI regulator in the form:

$$livq = \left(K_P + K_I * \frac{1}{s}\right) * err\_vp \tag{2.5}$$

subjected to a sampled input signal (err_vp piecewise-constant), it is immediate to derive that:

- $K_P$ is the ratio of the *livq* step variation to the err_vp step variation;
- $K_I$ is the ratio between the slope of the ramp of *livq* and the step variation of err_vp;

The measures provided by Terna show that:

- $K_I = \left(livq_{ramp} \,/\, \Delta t_{ramp}\right) / \, err\_vp = 0.66$ [s]
- $K_P = livq_{step} \,/\, err\_vp = 16$ [p.u./p.u.]

Assuming a $Qlim_{area}$ equal to 0.5 (the regulating plants in the area during the event were in an operating condition with very low active power), the following parameters result:

- $K_S = K_P \,/\, Qlim_{area} = 16 \,/\, 0{,}5 = 32$ [p.u./p.u.]
- $T_S = Qlim_{area} \,/\, K_I = 0.5 \,/\, 0.66 = 0.7575$ [s]

2.2.1.2. *Power plants' model*

The two power plants that were connected to the network in Figure 18 area during the event, namely Power Plant 1 and 2, present models with equal structure but different parameters. Power Plant 3 instead originates the event, by disconnecting itself from the network. The various elements in the model have been grouped according to the standard classification of voltage regulation levels rather than geographical location. Therefore, the Simulink model contains the sub-models SARTs and AVRs, in which the SART and the AVR of the plants are collected, respectively.

The single power plant is represented by a single equivalent generator, with a constant gain of 1 voltage p.u. in order to neglect the faster dynamics inherent in the generator. The plant's capability curve is represented by a reactive limit *Qlim* at the input of the single plant's SART, calculated as the mean value of the reactive limits of the different generators active in the plant at the moment preceding the event.

As shown in Figure 19, the network model requires the reactive power exchanged by the individual power plants with the network. Therefore, the following calculation is present in the power plant model:

$$\Delta q_G = \frac{1}{x_{trasf} + x_{line}} * (\Delta v_{MV} - \Delta v_{HV}) \tag{2.6}$$

where $x_{trasf}$ is the equivalent reactance of power plant lift transformers, and $x_{line}$ is the reactance of the line connecting the single power plant to the PN (Node 2), $\Delta q_G$ is the variation of reactive power exchanged by the single power plant with the network, $\Delta v_{MV}$ is voltage variation at the terminals of the equivalent generator modeling the single central, $\Delta v_{HV}$ is the variation of the tension of the NP (Node 2).

AVRs are modelled with a first order transfer function, with time constant $t_{AVR}$, using the voltage reference as input $v_{ref}$ and provides output voltage to machine clamps $v_{MT}$ (since the synchronous machine is assumed to have a unitary gain). The voltage reference signal is generated within the AVR model by means of the calibrator, which receives pulses of "increase" or "decrease" reference from the SART. The calibrator by its nature acts as an integrator, a behaviour exploited by the SART (the reactive power regulator integrated in the SART is devoid of integral action, as it uses that of the calibrator).

The SART model consists of the dynamic part of the SART system currently installed in the Power Plant 2 (developed by the authors of [20]) . The model consists of an appropriate value gain (dependent on the integral cycle time constant and the parameters of the plant) which multiplies the reactive power error of the power plant. This signal is processed by means of a block of PWM that generates the signals of "increase" and "decrease" reference to be sent to the calibrator of the AVR, signals that constitute the output of the SART itself. The model uses the absolute values, represented in p.u. of the values base for the single central one, for which the opportune necessary transformations are present. This type of SART is maintained throughout the study, but some preliminary simulations suggest that the results shown below are largely

comparable (from the point of view of the effect of the parameters on system damping) even if you use the model of a SART system that is capable of acting directly on the voltage node of the AVR (and not via calibrator). In particular, Figure 20 shows the comparison between the results in terms of PN voltage in the presence of a limit cycle, for the two types of SART. The width of the limit cycle is greater for the d SART without calibrator. This is due to the presence in the SART with calibrator control of the PWM function, which limits the excursion of the control signal.

A limitation on the excursion of the voltage reference (in amplitude and speed of variation) is not present in the SART with direct control signal model used for this test, leading to the differences shown in the figure. Nevertheless, the system demonstrates similar (unstable) behaviour with both SART models, when the parameters are equal.

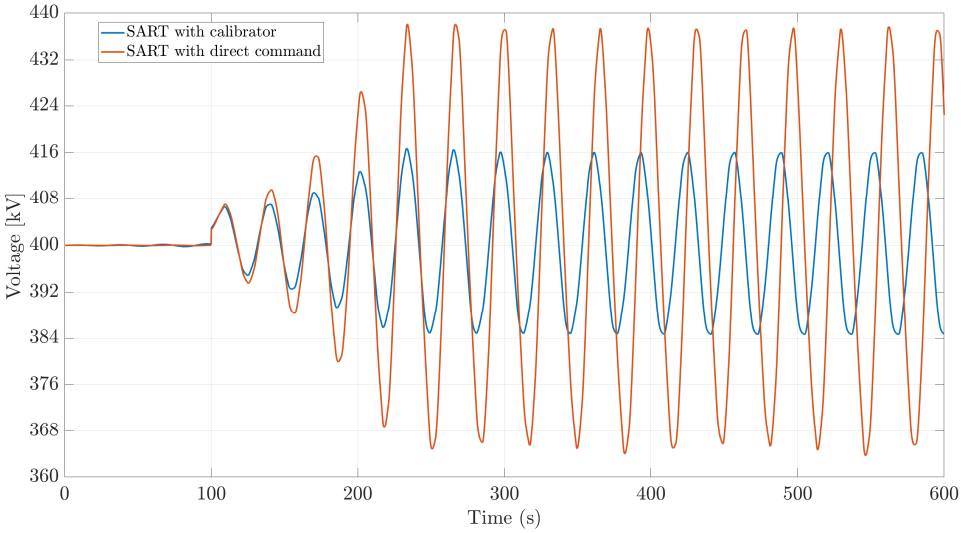


Figure 20 - NP's Voltage in the presence of a limit cycle, comparison between SART with calibrator control (blue) and SART with direct control on the voltage node of the AVR (red)

### 2.2.1.3. *Network Model*

Under the operational conditions in which the event happened, the portion of the network under examination has the longitudinal structure depicted in Figure 18. It is evident that the power plants linked to the network are very coupled with each other and with the PN (Node 2) (lines with impedances in the tens of ohms), but very decoupled (lines with impedances in the tens of ohms) from the nearest node (Grid).

Due to the general network's unique properties, the reactors of the lines connecting the two plants and the PN can be incorporated into the models of the individual plants. As a result, the network is made up of the single impedance that connects Node 2 to the Grid Node (sum of the impedances between the Node 2 and Node 3, and between the latter and the Gird Node). Furthermore, measurements taken during the event demonstrate that the synchronous compensators deployed in the closest control area (which is represented by the Grid Node) show negligible reactive power changes. This demonstrates that the event had no effect on this area, allowing it to be regarded as an infinite short circuit power node ($\Delta v_{Grid} = 0$).

Finally, as is typically the case at the transmission level, the lines are purely reactive and it is thus possible to ignore their resistance.

As a result, it is possible to calculate voltage variations in the Node 2 as:

$$\Delta v_{Node2} = (\Delta q_{GPowerPlant1} + \Delta q_{GPowerPlant2}) * x_{Node2-Grid} \tag{2.7}$$

The network model uses p.u. base values $V_b$=400 kV and $A_b$=100 kVA, so all input and output variables are expressed using these base values (the transformations in per unit with different bases are carried out, when necessary, in the individual models that require them).

#### 2.2.1.4. *Sampling and measurement delay and remote control*

The mathematical model also includes the measurement systems (channel BK - backward) and remote control (channel FW - forward) necessary for the secondary control, limited to the functions of measuring the voltage of the pilot node and its reception, and the generation of the *livq* signal and its transmission. These are sampled signals that are sent via proper communication channels and processed once received. The basic idea is the same for both functions and is accomplished by a zero-order hold block for sampling that is connected in series with a transport delay that implements the delay. Sampling for both channels is set according to the data characteristics of the current system, namely 4s for the measurement of the PN voltage and 2s for the

generation of the *livq* control. As for delays, it is necessary to distinguish between the two channels. The measurement delay (BK) refers to the time between a change in the voltage in the pilot node and the application of the error signal due to it at the PI input of the RRT. Its set value is 0.2 s. The remote control delay (FW) is the period that elapses between a change in the *livq* signal output from the SVR PI and the application of the change to the input reactive power reference to the control groups' reactive power regulators. As a result, this delay encompasses both the communication latency between Terna and the individual power plants and the power plants' internal delays (for example, RTU processing, internal data network communication, SART processing, any check of the central automation, etc.). Because no measures are available, this delay has been assumed.

### 2.2.2. Model parameters and event simulation

The parameters used in the model for the reproduction of the current oscillatory event in the area of Fig. derive from the system data and the considerations expressed in the previous paragraphs. The main values used in the simulations are summarised below:

- PI regulator of SVR:
  - $K_S = 32$ p.u./p.u.
  - $T_S = 0{,}7575$ s
  - $Qlim_{area} = 0{,}5$
- Sampling times of measurement and remote control channel:
  - remote control channel FW (*livq* signal) = 2 s
  - measurement BK (PN voltage) = 4 s
- Delays in measurement and remote control channels:
  - remote control channel FW (from PI SVR output to SART) = 5 s
  - measurement BK = 0.2 s
- AVRs time constant:
  - for both Power plant 1 and 2 $t_{AVR} = 1.3$ s
- Power plants reactive power regulators' time constants:

- Power plant 1, with synchronous comensators $t_{RPRG-1} = 5$ s
- Power plant 2, with conventional units $t_{RPRG-2} = 8$ s

- Power plants reactive power capability:
  - Power plant 1 $Qlim_1 = 0{,}512$
  - Power plant 2 $Qlim_2 = 0{,}45$

The disturbance applied to the event simulation system is a 1.5% voltage step on the PN (Node 2). This model models the effect of the disconnection of the Power plant 3, as can be recorded from the Terna's measurements of the event.

The event modelling, using the above-mentioned model, reveals the trend of PN's voltage prior to the application of the disturbance (Figure 21). It is clear how, in the simulated system, an oscillation of continual voltage in the Node 2 is created by the introduction of the disturbance at t = 100 s. Indeed, the system enters a limit cycle with a period of around 32 s and an amplitude equal to 8% of the nominal voltage. The model's simplifying hypotheses do not allow for the reproduction of the precise waveform detected during the event, but they do show the potential start of a non-damped oscillatory response with a period almost identical to that of the event.

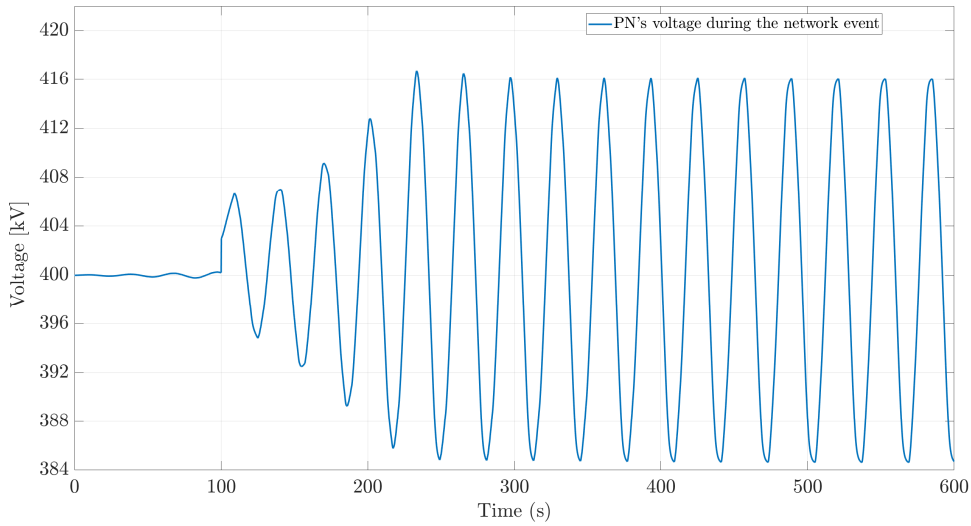


Figure 21 – PN's voltage simulation during the network event

#### 2.2.2.1. *Effect of parameters on reactive voltage oscillation damping*

The effect of the main parameters of the secondary regulation system on the oscillations damping in the NP voltage is of interest in order to draw some conclusions about the possibilities of improving the current control architecture with respect to the described phenomenology.

Sampling times

The effect of the sampling times of the measurement and remote control chains on the damping of voltage fluctuations in the NP is evaluated.

The action on the sampling alone of the system of measuring the tension of the node pilot, while leaving the rest of the system untouched, increases damping only transiently: this effect is inadequate to prevent the development of a limit. This is demonstrated by the results of Figure 22, which compares the existing system (blue curve) to one with PMU (red curve). The latter is represented by a sampling time of 0.02 s. The usage of the PMU benefits the remainder of the control system, but it is insufficient to prevent the unstable condition.

The action on the sampling only (with the same sampling time BK = 4s) of the remote-control signal sending system (i.e. "sampl. FW") is even less effective on equal terms with the rest of the control system. Indeed, as seen in Figure 23, the transient increase in damping is so small that it is negligible. The combined and simultaneous reduction of both sampling times has a significant effect on the damping of oscillations, as shown in Figure 24. Even if reducing both sample times to 1s results in a positive damping system, it is still insufficient as a design criterion. The results also demonstrate that the damping increase for sampling durations shorter than one second is almost minimal, indicating that additional levers are required to improve the secondary voltage regulator's current performance.

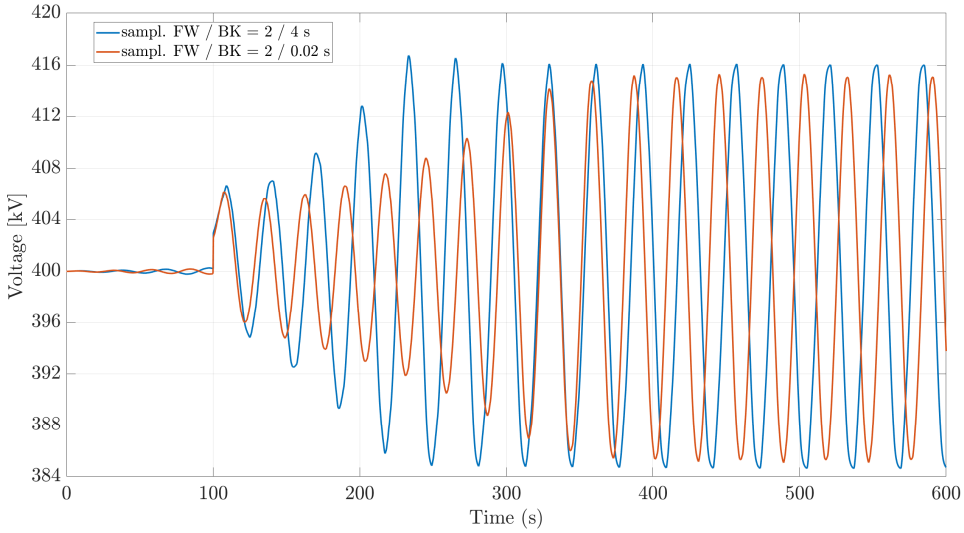


Figure 22 – PN's voltage, comparison between current system and PMU system

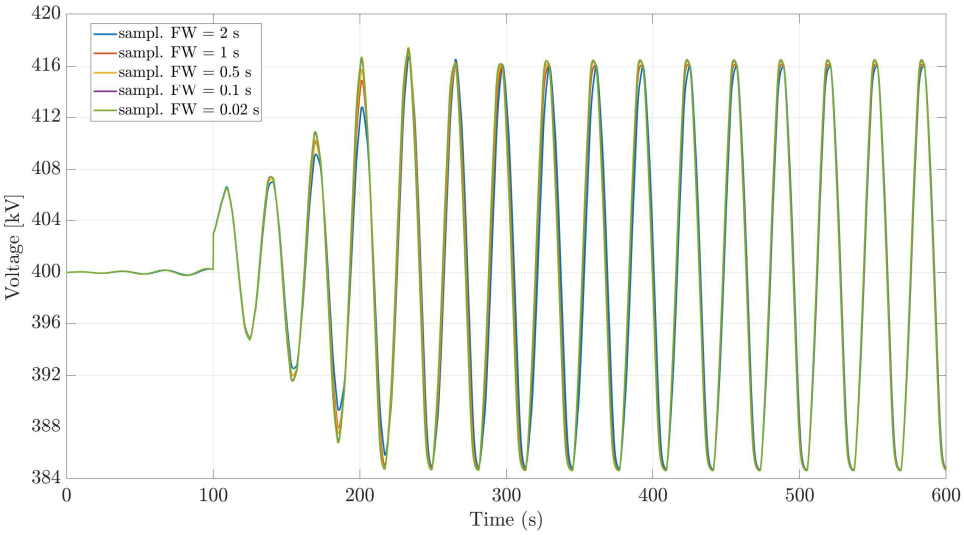


Figure 23 – PN's voltage, effect of the change in sampling time of the remote-control signal

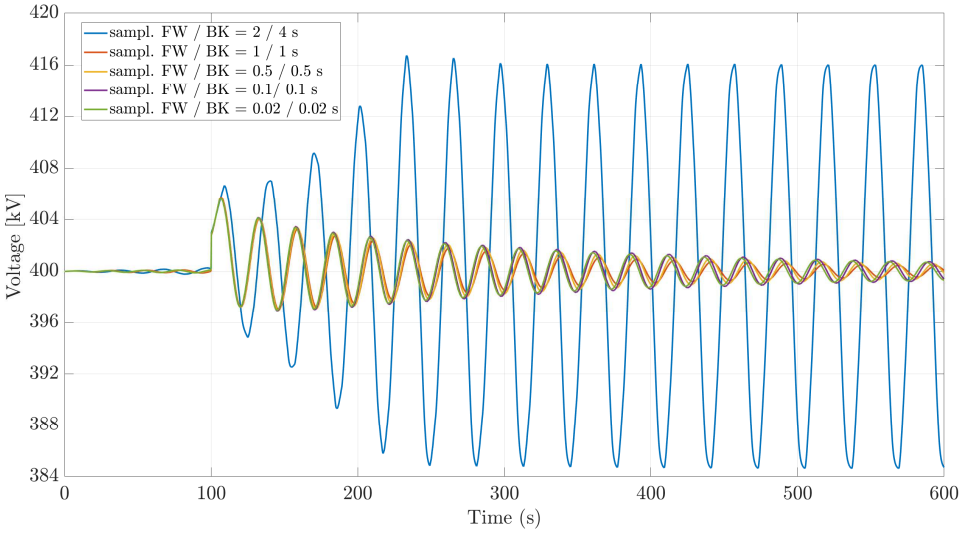


Figure 24 – PN's voltage, effect of the combined variation in sampling time of measurement and remote-control signals

Delay in the remote-control chain

The damping of voltage fluctuations in the NP is examined in relation to the delay in the remote-control chain. This delay refers to the time between a change in the *livq* signal output from the SVR's PI and the application of the change to the reactive input power reference to the control panels' reactive power regulators, and thus includes both the latency of communication between Terna's equipment and individual power plants, as well as internal power plant delays.

Figure 25 shows that as the delay is reduced, the damping increases. With the existing control system's architecture and the parameters explained in paragraph 2.2.2, a limit cycle (green curve) is established in the system under study with a delay more than or equal to 5 seconds. Damping is positive but low for delays between 4 and 3 s (purple and yellow curves), but a properly damped response is highlighted by a delay of less than 2 s (red and blue curves). Even if the system remains in a limit cycle for delays of 5 s or more, the sheer installation of a PMU-based measuring system increases the damping impact of reduced delay times (Figure 25).

When the measurement system with PMU is used in combination with a reduction in the sample time of the remote-control signal to 1 second, damping in voltage

oscillations is significantly increased. In reality, as shown in Figure 27, increasing the delay of remote adjustment up to 6 s is required to produce an oscillating response that is not damped, even if the answers are damping substantially reduced from 4 s up.

Finally, regardless of the sampling times utilized, a 6 s delay in the remote-control chain induces the development of a limit cycle on the PN voltage.

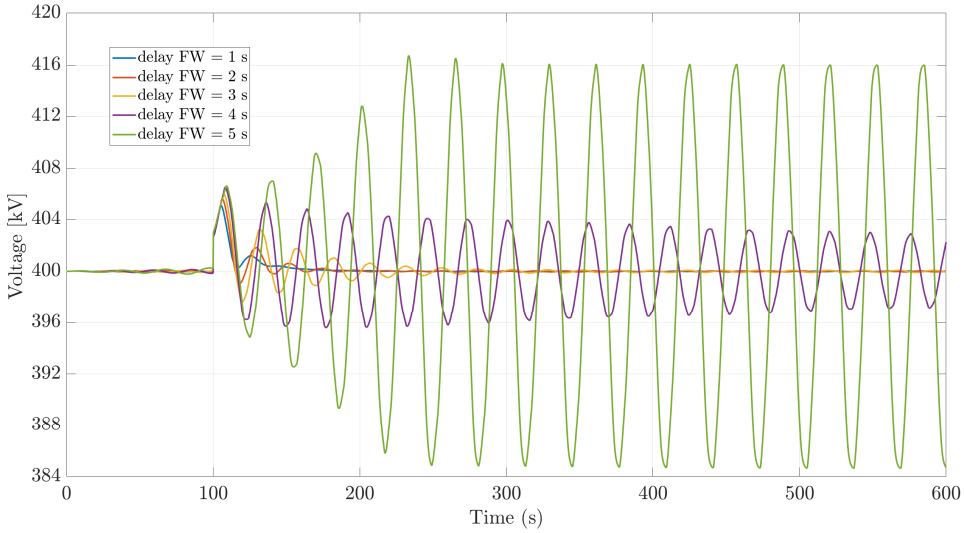


Figure 25 – PN's voltage, effect of change in delay time of the remote-control signal with current system

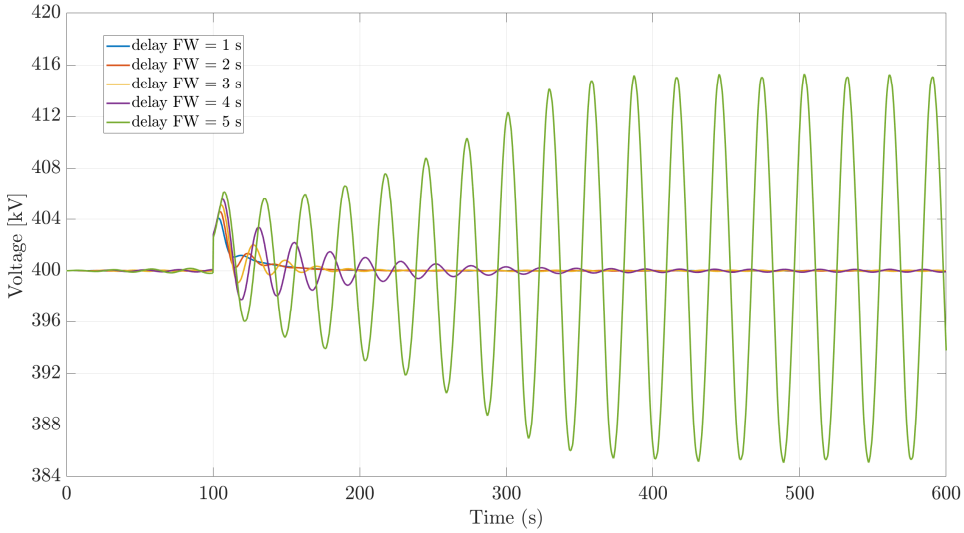


Figure 26 – PN's voltage, effect of change in delay time of the remote-control signal with current system and measurement by PMU

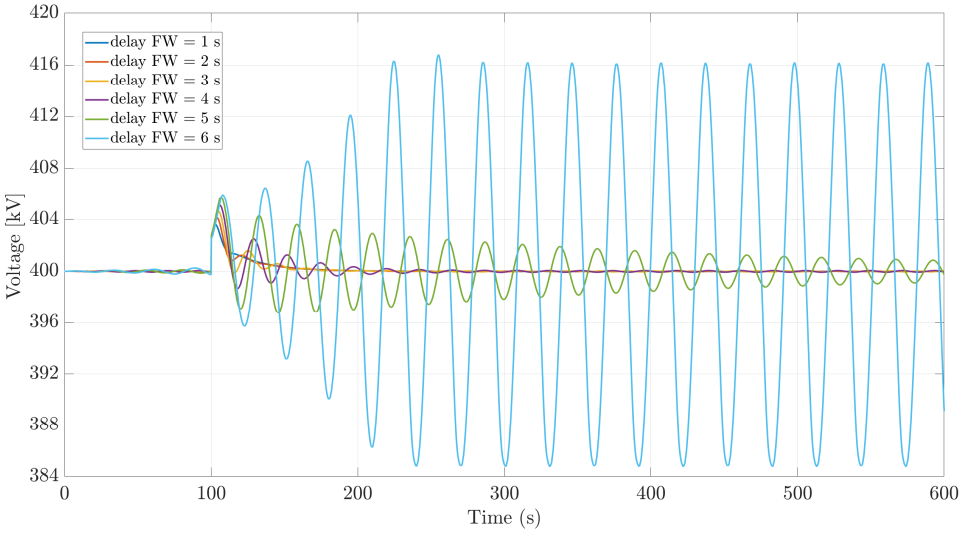


Figure 27 – PN's voltage, effect of change in delay time of the remote-control signal with current system and measurement by PMU and reduction of the sampling time of the remote-control signal to 1 second

SVR parameters

The damping of tension oscillations in the PN is studied in relation to the PI regulator parameters. In particular, the first step will limit the assessment of the influence of proportional gain since it has a direct effect on damping but not on the frequency of oscillations in the context of secondary voltage control [5].

Figure 28 compares the effects of the disturbance on the tension of the PN in the current system (i.e. "base case") and in the current system with the SVR's proportional gain halved (i.e. "base case with Ks/2"). Despite the presence of the remote-control delay of 5 seconds, the damping increases dramatically.

The damping increases even more when the proportional gain SVR is halved in the system, the sampling period for the remote-control signal is reduced to 1 second, and the PMU is used for measurements (Figure 28). This demonstrates how the use of an adaptive SVR type PI (with earnings varying depending on network operating condition) is effective for dampening oscillations in the current case, especially when combined with the interventions on the measurement and remote-control chain highlighted in the previous section.

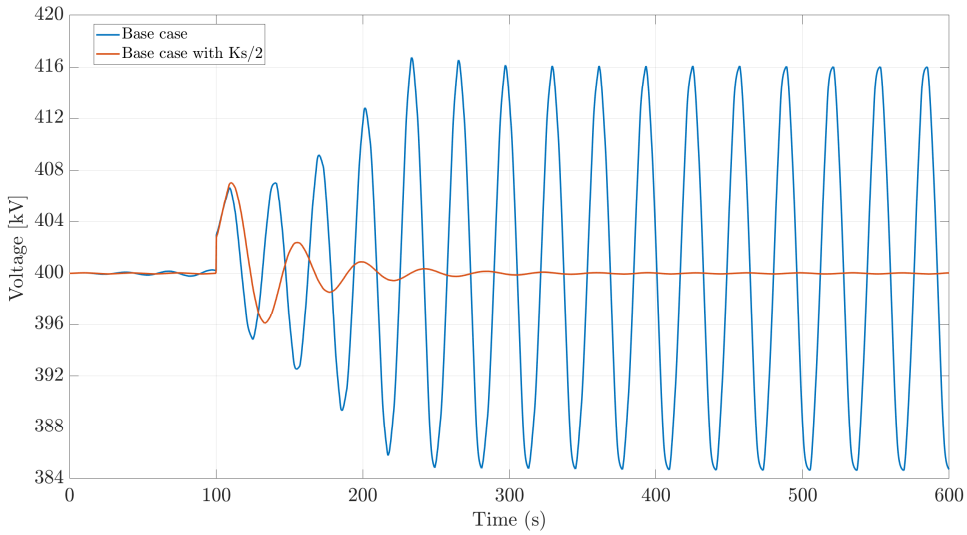


Figure 28 – PN's voltage, comparison between the implemented system and the SVR's PI with proportional gain halved

### 2.2.3. Remarks

This study shows that critical conditions are achieved by combining the following points:

- operating condition of the network (circulating power, central power, line connection, etc.);
- sampling time of the PN voltage measurement signal;
- sampling time of the remote-control signal sent to the regulating power plants;
- delays in the remote-control chain, including delays inherent the regulating power plants;
- RRT controller structure and parameters.

The results also show that reducing delays in the remote-control chain has a highly stabilizing effect. If a limit cycle occurs in the system with a delay greater than or equal to 5 seconds, damping is positive (even if somewhat low) for delays between 4 and 3 seconds, while a sufficiently damped response shows up for a delay of less than 2 s. It should be noted that the delay in the model's remote control chain includes the internal delays to the regulating power plants. Since the latter rely on central equipment (RTU, internal data network, SART architectures, central automation, and so on), this solution

requires the revision of these components as well. Action on simply one of the above aspects (for example, using PMUs only to measure the voltage of the pilot node) is often insufficient to restore system stability; instead, a combined action with other elements should be implemented. Even though the damping is still low and the differences are negligible below the sampling time value of 1 s (it is necessary to act on additional parameters to improve performance), the combined reduction in the sampling time of the measuring and remote regulation branches of the SVR has a significant effect on the oscillations damping (no limit cycle for delay time in the remote control channel up to 5 s is established).

Furthermore, the installation of a measurement system based on PMUs amplifies the damping effect provided by shorter delay times, and this effect becomes significant (limit cycle only for delays greater than or equal to 6 seconds) when PMUs are combined with a 1 second sampling time on the remote-control side. Finally, when combined with shorter sample durations, the adoption of an adaptive RRT type PI regulator is actually effective leading to a substantially enhance on oscillation damping.

## 2.3. Considerations on Short Circuit Power

In order to better understand how short circuit power varies following the network changes, it should be mathematical defined [5]. Assuming that $v^{0}_{Lh}$ is the steady-state node $h$ voltage value before a perturbation of injected power $\Delta q_{Lh.}$ Considering the Thevenin's theorem, this value can be assumed as the voltage value without load in the node $h$, thus the equivalent generator voltage (or the node $h$ voltage with no reactive power variation) as could be seen in Figure 29, where $(X_{CC})_{hh}$ is the diagonal component $h$-$h$ of the short circuit reactance matrix of the network (thus the diagonal component related to the node $h$). The short circuit matrix $X_{CC}$ can be calculated starting from eq. (1.7) and applying some simplifications (complete mathematical demonstration in 11.2.3 of [5]): i) network under reactive power unloaded condition, thus the voltage around which the linearization has been made is equal at *1 p.u.*; ii) consider only reactance, neglecting the resistance part of all lines, as is usually do on a transmission network since

$Re(Z_{ij}) << Im(Z_{ij})$, where $Z_{ij}$ is the line impedance between two given nodes $i$ and $j$. With the latter, a simplified and more practical form of the sensitivity equation can be written:

$$\begin{cases} [\Delta v_L] = [H][\Delta v_G] + [X_{CC}][\Delta q_L] \\ [\Delta q_G] = [C][\Delta v_G] + [D][\Delta q_L] \end{cases} \tag{2.8}$$

where:

$$\begin{cases} [H] = -[B_{LL}]^{-1}[B_{LG}] \\ [X_{CC}] = -[B_{LL}]^{-1} \\ [D] = [B_{GL}][B_{LL}]^{-1} \\ [C] = [B_{GG}] + [B_{GL}][H] \end{cases} \tag{2.9}$$

considering the subdivision in generator nodes (G) and load nodes (L) of the admittance matrix $[Y]$:

$$\begin{bmatrix} Y_{LL} & Y_{LG} \\ Y_{GL} & Y_{GG} \end{bmatrix} = \begin{bmatrix} G_{LL} & G_{LG} \\ G_{GL} & G_{GG} \end{bmatrix} + j \begin{bmatrix} B_{LL} & B_{LG} \\ B_{GL} & B_{GG} \end{bmatrix} \tag{2.10}$$

Thus, under the above mentioned conditions of a given transmission network, which are:

$$\begin{cases} [v_G] = constant \\ \quad \begin{cases} \Delta q_{Lk} = 0 \\ k \neq h \end{cases} \end{cases} \tag{2.11}$$

where $[v_G]$ is the generators voltage array and $\Delta q_{Lk}$ is the reactive power variation of the generic node $k$, it can be deduced that:

$$\Delta v_{Lh} = (X_{CC})_{hh} \Delta q_{Lh} \tag{2.12}$$

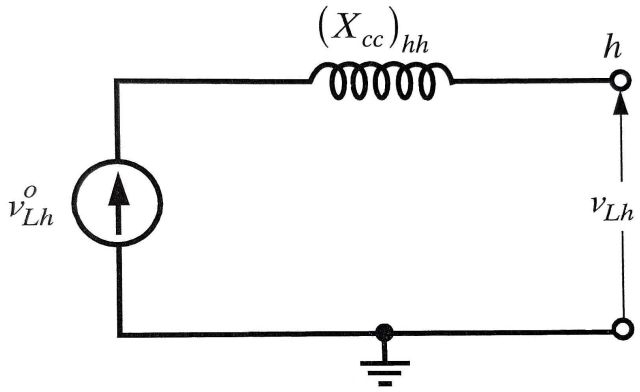


Figure 29 - Equivalent scheme of a generic node $h$ of a transmission system

If the no-load voltage is assumed to be close to the nominal one and thus:

$$v_{Lh}^{0} \cong 1\ p.u. \tag{2.13}$$

we can infer that the inverse of the short circuit reactance of node $h$ is the variation of the reactive power absorbed in node $h$, which zeroes the voltage $v_{Lh}$ (as a three-phase short circuit in node $h$)

$$\frac{1}{(X_{CC})_{hh}} = [\Delta q_{Lh}]_{\Delta v_{Lh}=-1} \tag{2.14}$$

The inverse of the short-circuit reactance of node $h$ in p.u. is defined as *short-circuit power* of node $h$ at constant generators voltage in p.u. and it is identified by $(S_{CC})_h$:

$$(S_{CC})_h = \frac{1}{(X_{CC})_{hh}} \tag{2.15}$$

Therefore, following eq. (2.12)(2.12):

$$\Delta v_{Lh} = \frac{\Delta q_{Lh}}{(S_{CC})_h} \tag{2.16}$$

If the approximation of eq. (2.13) is not applicable, the short-circuit power definition could be written in a more general way:

$$\left(S_{CC}^{0}\right)_h = \frac{v_{Lh}^{0}}{(X_{CC})_{hh}} = v_{Lh}^{0}(S_{CC})_h \tag{2.17}$$

which considers actual operating conditions, which may be different from the nominal ones (e.g. $0.9 \leq v^{0}_{Lh} \leq 1.1\ p.u.$).

It is hence important to be noted that, from eq.(2.16), it can be said:

- If only operating conditions changes, then only $v^{0}_{Lh}$ and thus $(S^{0}_{CC})_h$ varies but not $(S_{CC})_h$;
- If the network structure varies, then both $(X_{CC})_{hh}$ and $v^{0}_{Lh}$ and thus $(S_{CC})_h$ and $(S^{0}_{CC})_h$ will vary.

The reactance $(X_{CC})_{hh}$ or the short-circuit powers $(S_{CC})_h$ has some important features, which stem from their definitions and are helpful in practice. Firstly, the greater

the number of parallel inductive branches connecting one node to ground, the lower the short-circuit reactance, and hence the higher the short-circuit power. Secondly, the fewer parallel inductive branches from one node to ground, the greater its short-circuit reactance, and hence the lower its short-circuit power. Finally, considering equal injected reactive power variation, the nodes with higher short-circuit power will undergo smaller voltage variations, as is evident from eq. (2.16). This is why PNs are chosen as the strongest bus, in terms of short-circuit power, among the buses belonging a given control area.

As a consequence, an important consideration about short-circuit power is related to the generators type present within the network. Indeed, the distribution of short-circuit power may change by introducing distributed generation (RES) when large power plants are switched off. A traditional generator in short conditions shows with its sub-transitory reactance (very low) and therefore with a very high short current (about 5-8 times the nominal), while a renewable source contributes to the short with a current much lower because of the presence of inverters (about 1.5 the nominal). Converting such reasoning into short-circuit power terms, replacing a conventional power plant with one RES-based leads to a decrease in the short circuit power of the HV nodes on which it is connected. Moreover, if the replacement is done with many smaller RES power plant deployed all over the territory the effect is also a deployment of the short-circuit power. This phenomenon is caused by the massive exploitation of RES among the transmission network that slowly drive the conventional power plant to be shut off. As a consequence, the high short-circuit power of certain buses, which could be selected as PNs, is going to be distributed among the other bus, leading to a challenging selection of PNs.

## 2.4. Remarks

The goal of this Chapter was to identify and study issues on current Italian transmission system voltage control due to the massive changes that it is undergoing. The first study on Area-PN selection shows how this rationale could be ineffective in the near future. Certainly, in the event that alterations to the network configuration occur

more frequently or on a larger scale, the assignment of PNs and their associated control areas should be flexible enough to accommodate these shifts. Consequently, the SVR needs to possess the capability to adjust the network modifications, enabling it to monitor the relocations of control areas and their respective PNs. This means that SVR must have an inner parameters adaptivity.

The second study was performed replicating an actually happened event on the network, which was an important voltage oscillation instability due to a sudden disconnection of a conventional regulating power plant. The main issue that emerges from simulations is that delays on the control chain are also highly important from the standpoint of system stability. Thus, a new SVR have to be included in a new architecture which is designed to accommodate faster and smarter measurement devices and communication channels. Moreover, with an increasingly presence of RES, also the powerful photovoltaic and wind farms could be involved in the voltage regulation, which have faster dynamic available and thus the new architecture has to be ready to accommodate them.

Finally, short-circuit power modification on transmission network buses also may result in difficult identification of PNs or, at the very least, a rapid change of them, foreshadowing a future in which RES not only can control voltage but also enter and exit due to weather changes.. As a result, a new SVR capable of regulating the voltage of numerous PNs as well as switching between them may be required, in order to optimize the PN selection in response to transmission network changes.

# 3. Innovative Approaches for Power Systems' Voltage Control

The present Italian SVC is made by a set of Proportional Integral (PI) controllers processing the PNs' voltage error, and then delivering an equal (at area level) reactive power control signal to the regulating power plants (which must be present in each PN area). Such an architecture is simple but is based upon the idea that the physical impedances of the power system can guarantee a complete decoupling among each control channel, effectively turning the entire multiple-input multiple-output (MIMO) system in a set of non-interacting single-input single-output (SISO) ones. While such an approach proved to be effective in the past, this is not true anymore given the above-mentioned changes and issues in the Italian power system. Indeed, the area-PN rationale is becoming more challenging to apply, as the PNs are becoming less dominant (because the RES are distributing the short circuit power throughout the network) and the rapid changes in the network are causing a difficult individuation of control areas and the power plants within them. To face that, a set of new features has been introduced in the SVC voltage regulator. In respect to what has been presented in [6], a decoupling matrix has been introduced on the output control signals (to reduce as much as possible cross-interactions among the PNs pertaining to the same region), as well as a first approach to

adaptivity (by changing the gain of the SVC regulator following power system operative condition). Nevertheless, such features are not calculated in real-time, but rely on a limited amount of static grid snapshots that are evaluated a couple of times a year based on forecasts. This means that only a limited set of load and grid configuration scenarios can be evaluated, which cannot represent all the possible cases that can happen in the modern power system. For instance, in [26] it has been demonstrated through simulation that voltage control areas and PNs would change if a change in the network occurs, which may cause issues for voltage control if the regulator is not updated accordingly.

A potential solution can be the use of a different voltage control area selection method (i.e., the "zoning" process), to ensure the correct decoupling among PNs in all the operative conditions for the power system. In [8] the first Italian network area subdivision is explained. The couplings between buses are evaluated using the voltage versus reactive power sensitivity matrix $\partial V/\partial Q$. Instead, in [24] the parameter applied to evaluate the coupling is given by the so-called electric distance. The graph theory-based zoning approach is also well-represented in the literature [18][19]. Zoning may be also performed applying neural networks [20][21] or fuzzy theory [31]. In addition to zoning, the pilot nodes can be selected using different methods. For instance, the initial choice of Italian PNs was based on their short circuit power [8]. The core concept is that a high-power node can affect the voltages of the surrounding ones (which present lesser power), therefore allowing to control the entire area voltage from a single control point [14]. However, PNs can be also selected using the $\partial V/\partial Q$ sensitivity matrix, which allows to identify the ones whose voltage varies the most following a reactive power injection in the other network nodes. If such node voltage is kept strictly controlled, then it follows that all the other buses should present only smaller voltage variations [32]–[34]. Finally, another way of choosing PN is based on electrical distance [24]. Although the current voltage control system may be further updated for integrating one of the mentioned modern approaches for defining the voltage control areas and related PNs, the required changes will be so extensive to make a complete redesign of the SVC layer an equally appealing option. The logic conclusion is that a modern control strategy must be

conceived from scratch, also integrating adaptivity (being the system more and more time variant and less observable).

Given these premises, the purpose of the research here presented is to investigate new control approaches for the SVC of the electrical transmission network, to improve over the existing one and possibly solve its actual (and future) issues. In this regard, in literature some works can be found. In [35], the authors made a huge study for improving voltage control in China, proposing a solution based on the adaptive computation of the control areas and the selection of their optimal number. In [36] the authors suggest a new concept of voltage control, in which SVC and TVC are computed in the same location and the optimal power flow calculation is factored into subproblems to reduce computation time. Both these works require a complete revision and replacement of the control hardware and software at several levels, which requires a huge organizational and economic effort. In [37] and [38] authors present a new adaptive PMU (Phasor Measuring Unit)-based approach to SVC problem, considering a nonlinear control model under unexpected disturbances. The control concept is based on providing signals that drive the system to successive equilibrium points, keeping each RPR within established voltage boundaries. Another prolific research path regards the application of artificial intelligence concepts to voltage control. In [39] an SVC design based on a genetic algorithm and neural networks for defining the PID controller parameters is presented. The control architecture remains pretty simple (a PID controller), although control parameters are obtained through an optimization process. In [40] is presented a WAMS (Wide Area Monitoring System) -based technique for SVC. In [41] a genetic algorithm is implemented for an SVC, considering only RESs as RPRs. In [42] fuzzy logic is applied to SVC, demonstrating its effectiveness only for small perturbations.

While all the above proposals have elements of interest for this work's aim, they are not completely suitable for the application in the Italian transmission network. Indeed, the Italian TSO set some specific requirements for studying a new secondary voltage control system. Specifically, it is required to exploit as much as possible the improvements made in the transmission system monitoring system (i.e., the installation

in several substations of PMUs), as well as ensure the capability of exploiting all kind of RPSs. Moreover, controllers based on neural networks, genetic algorithms, or fuzzy logic must not be used. This is because the voltage regulation is a safety-critical application, where intelligible control systems are required, providing a well-known behavior in all the possible operating conditions. Simplicity in deployment, ease in human supervision, and fast and simple manual intervention in case of emergency are also sought goals. Therefore, by investigating the control approaches proposed in literature for MIMO systems, and considering the requirements, the Authors selected two possible candidates for designing a new secondary voltage regulator: Decoupling Control and Linear Quadratic Regulator with Integral action (LQRI).

## 3.1. MIMO Systems and MIMO Controllers

The purpose of this paragraph is to provide a summary of MIMO systems and controllers without claiming to be exhaustive; for more information and general theory see [43],[44].

MIMO systems are systems with multiple inputs and multiple outputs. The state-space description of a MIMO system is very similar to the one of a SISO system. For a linear, time invariant MIMO system with $m$ input signals and $p$ output signals, it holds:

$$\begin{aligned} \dot{x(t)} &= [A]x(t) + [B]\,u(t) \\ y(t) &= [C]\,x(t) + [D]\,u(t) \end{aligned} \tag{3.1}$$

where:

$x(t) \in \mathbb{R}^n$, $u \in \mathbb{R}^m$, $y(t) \in \mathbb{R}^p$, $[A] \in \mathbb{R}^{nxn}$, $[B] \in \mathbb{R}^{nxm}$, $[C] \in \mathbb{R}^{pxn}$, $[D] \in \mathbb{R}^{pxm}$.

It should be noted that dimensions of the matrices $[A]$, $[B]$, $[C]$, $[D]$ are very important and they are a key concept to understand problems. The big difference from SISO systems is that *u(t)* and *y(t)* are here vectors and no more just scalars. For this reason $[B]$, $[C]$, $[D]$ are now matrices.

The transfer function matrix $[P]$ of a MIMO system can be computed as follow:

$$[P(s)] = [C](s[\mathbb{I}] - [A])^{-1}[B] + [D] \tag{3.2}$$

where $[\mathbb{I}]$ is the identity matrix and $[P]$ can be definite as:

$$[P(s)] = \begin{bmatrix} P_{11}(s) & \cdots & P_{1m}(s) \\ \vdots & \ddots & \vdots \\ P_{p1}(s) & \dots & P_{pm}(s) \end{bmatrix}, \qquad P_{ij}(s) = \frac{b_{ij}(s)}{a_{ij}(s)} \tag{3.3}$$

where $P_{ij}$ is the transfer function from the $j$-th input to the $i$-th output.

It can be seen that MIMO systems are more complicated than SISO systems and, as a result, their control is more complex as well. In fact, it is very difficult to apply intuitive concepts like loop shaping, that apply to SISO systems, because of the cross couplings/interactions between the inputs and the outputs. This means that systematic methods should be used, in order to achieve good control properties. Two big groups of methods can be defined, which are used nowadays:

- $\mathcal{H}_2$ methods: Optimization problems in time domain which try to minimize the error signal at all relevant frequencies.
- $\mathcal{H}_\infty$ methods: Optimization problems in frequency domain which try to minimize the error signal at all relevant frequencies.

Because the transmission network is a MIMO system that demands reliability and service continuity, but most importantly, operators in Central Control Dispatch must be able to act quickly in the event of an emergency, the SVC cannot be overly sophisticated.

In this thesis the two simplest $\mathcal{H}_2$ approaches are studied and tested, Decoupling Control and LQRI control, avoiding wasting time developing a complex controller that would not be easily implemented in reality.

## 3.2. Decoupling Control

The decoupling control approach is based on the estimation of a reference transfer matrix capable of decoupling the MIMO system's input-output behavior. By means of this

matrix, it becomes possible to control each output variable independently, like in a SISO system. To explain how this approach works, in Figure 30 is depicted a generic MIMO dynamic system [34][35] composed by the controlled system $[G_2]$, the controller $[G_1]$, and a suitable control feedback $[H]$.

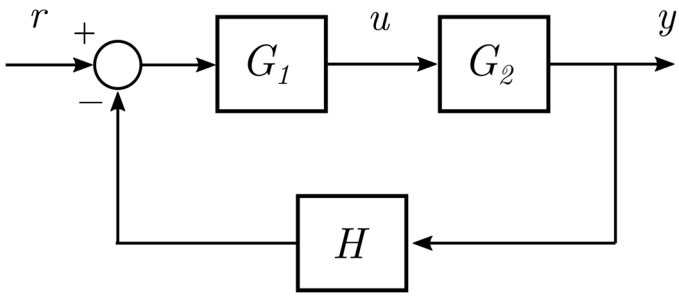


Figure 30 - General scheme of Decoupling Control

The figure shows:

- $u \in \mathbb{R}^m$, array of control signals
- $y \in \mathbb{R}^t$, array of system's output signals
- $r \in \mathbb{R}^t$, array of controller's input signals, which are the references for the control system
- $[H] \in \mathbb{R}^{t \times t}$, transfer function matrix of control feedback transducers (here assumed to be diagonal, i.e., there is no cross-influence between the measurements)
- $[G_2] \in \mathbb{R}^{m \times t}$, transfer function matrix of the dynamic system to be controlled
- $[G_1] \in \mathbb{R}^{t \times m}$, transfer function matrix of the controller.

The $[G_1]$ transfer function matrix must be defined in such a way to obtain the desired decoupling. Once the proper $[G_1]$ is found, each $r$ signal can be used to act on its related output signal $y$ only. In the system in Figure 30 , this can be achieved by defining a suitable diagonal non-singular matrix $[G]$, which contains the desired transfer functions for the single output controllers. To obtain the decoupling, the matrix must be calculated as follows:

$$[G_2(s)][G_1(s)] = [G(s)] \tag{3.4}$$

The non-singularity of $[G]$ implies that $[G_2]$ rank must be $t$. Consequently, to retain complete system controllability it must always result $m \geq t$ (the control signals are at least equal in number to the controlled outputs). Thus, the complete control system transfer function $[G_1]$ can be determined as:

$$[G_1(s)] = [G_2^+(s)][G(s)] \tag{3.5}$$

where $[G_2]^+$ is the Moore-Penrose pseudo-inverse matrix of $[G_2]$ ($[G_2]^+ = [G_2]^{-1}$ only if $m = t$).

Therefore, a controller built using the decoupling approach is constituted by a control matrix $[G]$ which is a matrix of SISO regulators, and a decoupling matrix $[G_2]^+$ that ensures the input-output decoupling for the controlled system.

## 3.3. LQRI Control

The LQRI control approach builds on the LQR one, by introducing a set of integrated variables as additional inputs [47]–[49]. Its notional representation can be seen in Figure 31. The integral feedback can be used to cancel out the steady state error in the output variables, which might be a desired behaviour in some applications.

Being the LQRI based on the LQR, it is necessary to provide a brief background on the latter to explain the former.

To this aim, it is possible to consider a generic time-invariant dynamic system in its standard state-space representation:

$$\begin{cases} \dot{x}(t) = [A]x(t) + [B]u(t) \\ y(t) = [C]x(t) \end{cases} \tag{3.61}$$

where $x(t) \in \mathbb{R}^n$ is the system state, $u(t) \in \mathbb{R}^m$ is the input (control) signal, and $y(t) \in \mathbb{R}^t$ is the system output.

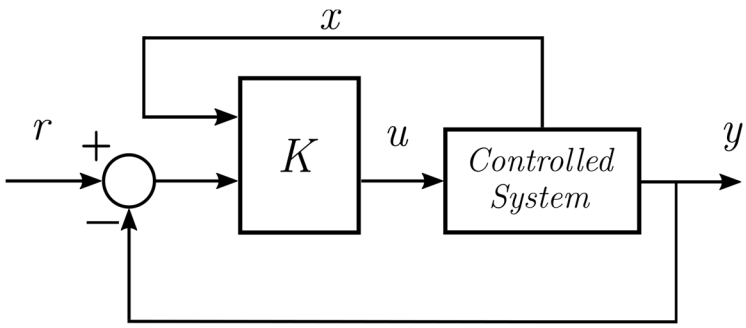


Figure 31 - Notional diagram of an LQR controller applied to a system

The goal of the LQR controller is to define a suitable control signal using a proportional control matrix $[K]$, which minimizes the following quadratic cost function:

$$C(x,u) = \int_0^\infty [x^T(t)[R_{xx}]x(t) + 2x^T(t)[R_{xu}]u(t) + u^T(t)[R_{uu}]u(t)]dt \tag{3.7}$$

where the state is weighted relative to the amount of control action in $u(t)$ through the state weighting matrix $[R_{xx}]$, the control weighting matrix $[R_{uu}]$, and the cross-weighting matrix $[R_{xu}]$. Specific feedbacks can be penalized (with high $R$ values) or promoted (with low $R$ values) using the weighting matrices.

If the following assumptions are also valid:

- the whole state vector $x(t)$ is available for feedback (either measured or estimated)
- the ($[A]$,$[B]$) couple is stabilizable and the ($[A], [R_{xx}^{1/2}]$) couple is detectable
- $[R_{xx}]$, $[R_{xu}]$ and $[R_{uu}]$ are symmetrical and positive definite.

Then:

- the linear quadratic controller is the following unique, optimal, full state linear feedback control law that minimizes the $C$ cost:

$$u(t) = -[K]x(t) \quad \text{with} \quad K = [R_{uu}^{-1}][R_{xu}^T + B^T S] \tag{3.8}$$

- $[S]$ is the unique, symmetrical, positive semidefinite solution of the algebraic Riccati equation ([ ] symbol for matrices is omitted):

$$SA_r + A_r^T S + (R_{xx} - R_{xu}R_{uu}^{-1}R_{xu}^T) - SBR_{uu}^{-1}B^T S = 0$$
$$\text{where } [A_r] = [A - BR_{uu}^{-1}R_{xu}^T]; \tag{3.9}$$

- the closed-loop dynamics can be calculated as:

$$\dot{x}(t) = [A - BK]x(t) \tag{3.10}$$

  and $[K]$ guarantees its asymptotical stability.

There are other elements required to correctly design an LQR controller, but they are outside the scope of this work (refer to [48] for an in-depth mathematical description of the LQR control).

By adding an integral action to the system output variables and using them as an additional input for the above-described LQR controller, the so-called Linear Quadratic Regulator with Integral Action (Figure 32) can be built. The integrated feedback enables the cancellation of the steady-state output variables error. The latter is always present in an LQR controller, being it based on a proportional gain matrix $[K]$. The LQRI can be designed using the above-described LQR theory, by considering a system with an augmented state made by the controlled system state $x(t)$ and the controller integrators' internal states $x_i(t)$, i.e. [50]:

$$x_{augmented}(t) = [x(t),\ x_i(t)] \tag{3.11}$$

With respect to an LQR controller, an LQRI one presents an increased design complexity. In fact, the addition of integrators to the control system increases the number of states of the overall controller plus controlled system ensemble, which also requires an increase in the $[K]$ matrix size and a corresponding increase in computational effort for its determination.

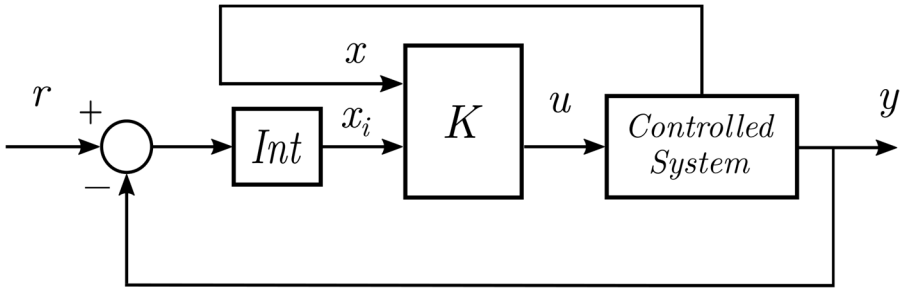


Figure 32 - Notional diagram of an LQRI controller applied to a system (Int = integrator/s)

# 4. New Voltage Control Approaches Implementation in the Italian Transmission Grid

The MIMO systems control approaches depicted in Chapter 3 can be used to build a SVR for a transmission system. In this section, the specific implementation of the above depicted background theory is discussed, detailing five new SVR architectures, which are compared with the actual one. Specifically, while Decoupling Control resulted in a single implementation, four different ones originated from the LQRI approach. In the following, the $\Delta$ symbol is omitted, to improve readability of figures and tables. Due to the use of different SVR control approaches, it has been decided to stop referring to the term PNs from now onwards, and simply refer to the more general term "voltage Control Nodes" (CNs).

The different SVR implementations originate from two variables: the type of the control signal sent to the RPRs by the regulator, and the number of separated controllers. The first can either be a single reactive power control signal sent to all the RPRs in the control area (i.e., a *livq* signal like the one used by the present regulator), or a set of reactive power references calculated for each RPR (i.e., a *qref* signal array).

Regarding the second (that is the number of separated controllers), it is possible to either design a centralized controller that measures and act on the whole case study system, or a set of decentralized controllers each measuring a single CN and acting only on the RPRs that are electrically coupled with it (the RPRs/CNs matching is made using the sensitivity matrix [$S$]).

In Table 1 are listed the actual SVR architecture (A), and the five new ones. The "feedbacks" column specifies the type of feedback signals that are required for the correct operation of each SVR system. While A and B architectures only need the CNs' voltages ($v_{CN}$) as feedback, all the LQRI-based architectures also require the system state *x(t)*. It is relevant to notice that *x(t)* is the mathematical state of each RPR, which in the model is the output signal of the integral part of the reactive power regulators (this is the result of modeling hypotheses well detailed in Chapter 5). In the field implementation, such a state can be suitably substituted with other signals (see paragraph 6.1).

Figure 33 depicts the notional block diagrams of the six SVR architectures given in Table 1. The transmission network is represented by the "GRID" block. The RPRs blocks include the "SARTs" and "AVRs + RPRs" blocks, as well as the reactive power regulation loop, the PVC loop, and the source model. Other blocks, such as PI regulators or particular decoupling/control matrices, are included if the specific control architecture needs them. All of the signals in the block diagrams are time-dependent, although this information is excluded from the pictures for readability. For the same reason, the same type of arrow is utilized in the diagrams to represent both scalar and array signals.

All the SVR architectures have the CNs reference voltages (coming from TVC) as the input and provide at the output suitable control signals. The CNs voltages are obtained through the application of the control signals to the transmission system's model and are used as feedback for the SVR. All the *livq*-based architectures (i.e., A, C, and E) need the RPRs to be properly grouped, in order to control the assigned CNs (using the concept of voltage control areas). Conversely, the use of *qref* signals (in architectures B, D, and F) enables the individual management of the RPRs, applying a finer control action on the power system.

Table 1 - Overview of the SVR architectures

| Architecture | Control approach | Control signals | Controller type | Feedback signals |
|---|---|---|---|---|
| A | PI | *livq* | Centralized | $v_{CN}$ |
| B | Decoupling Control | *qref* | Centralized | $v_{CN}$ |
| C | LQRI | *livq* | Centralized | $v_{CN} + x(t)$ |
| D | LQRI | *qref* | Centralized | $v_{CN} + x(t)$ |
| E | LQRI | *livq* | Decentralized | $v_{CN} + x(t)$ |
| F | LQRI | *qref* | Decentralized | $v_{CN} + x(t)$ |

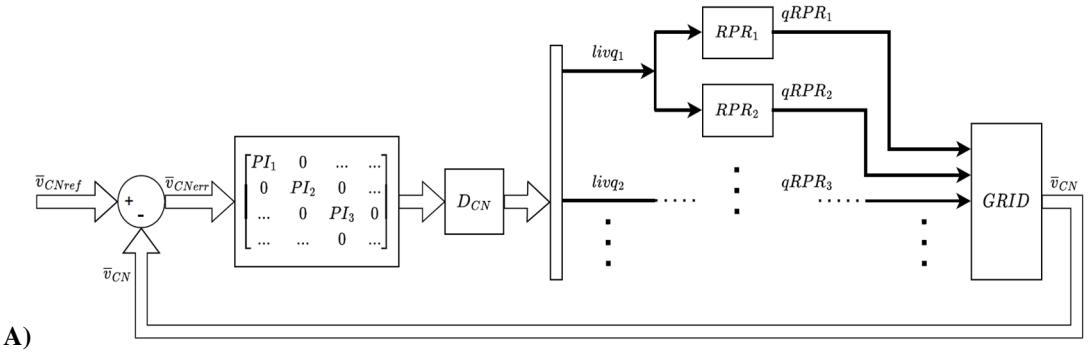


**A)**

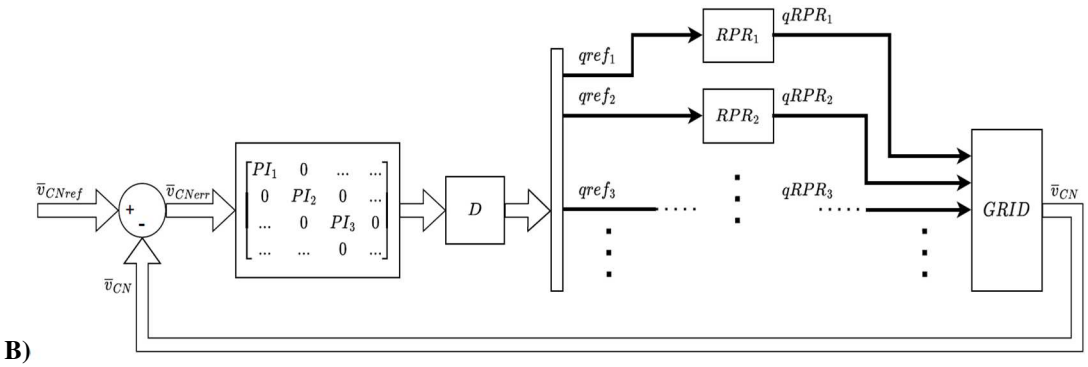


**B)**

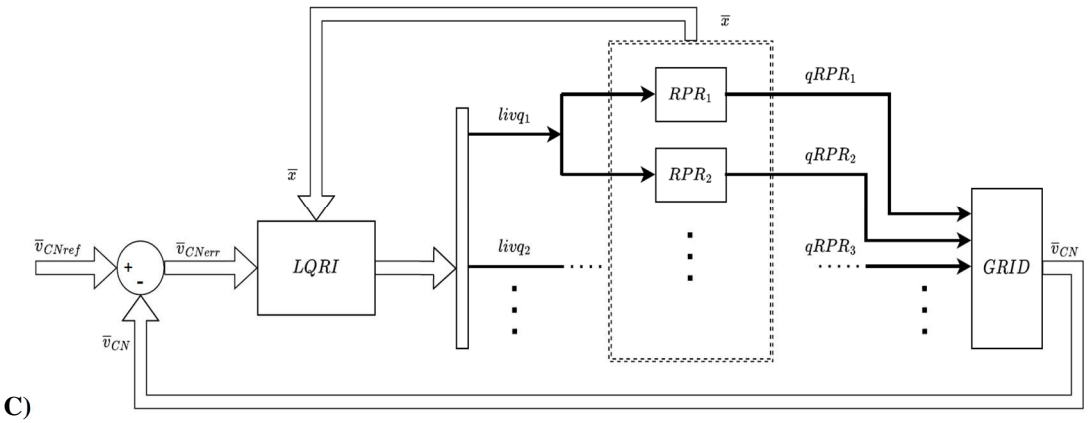


**C)**

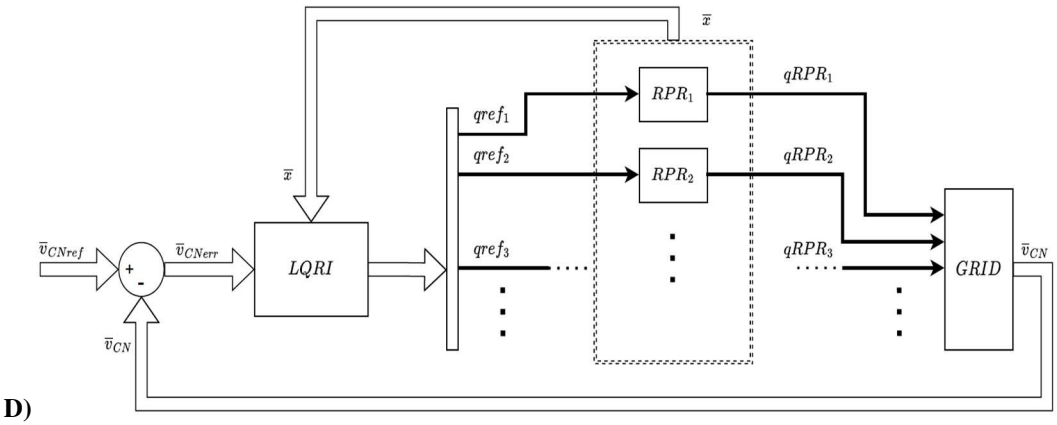


**D)**

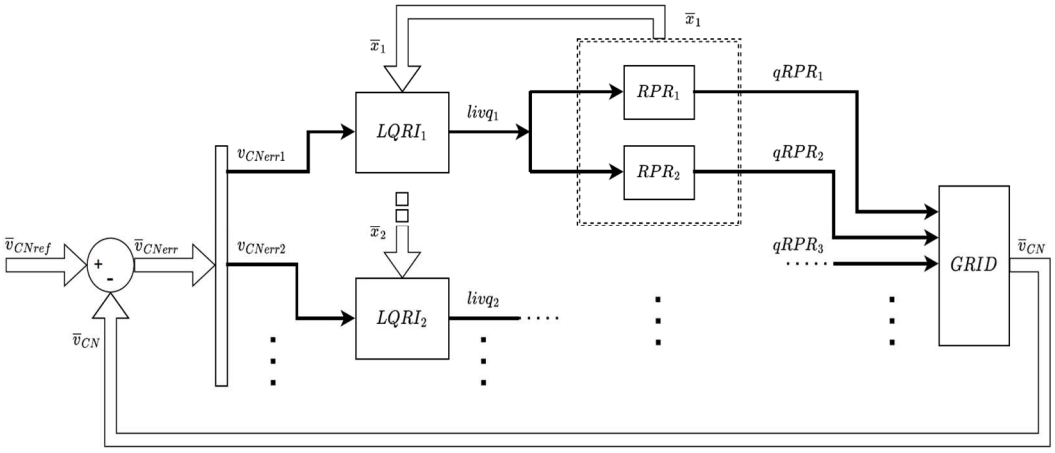


**E)**

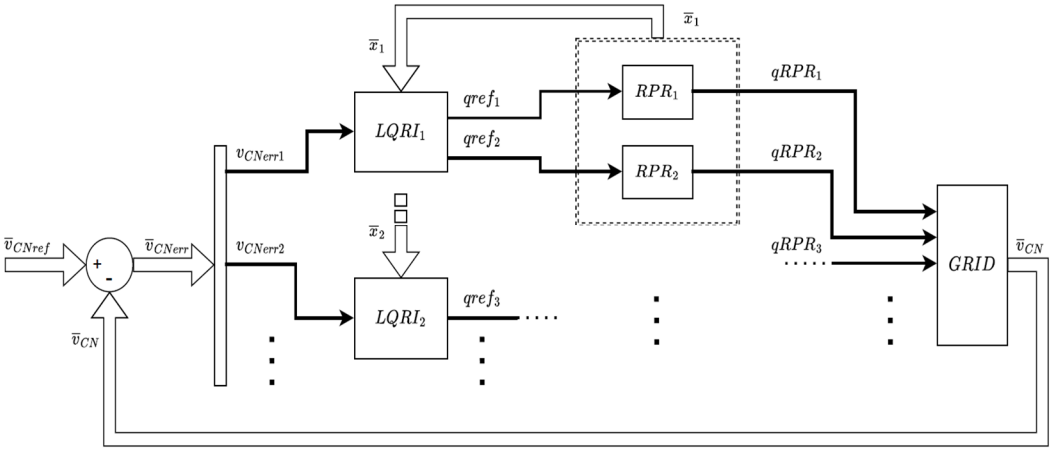


**F)**

Figure 33 - Notional block diagrams of the SVR architectures

## 4.1. Present Italian SVR

In Figure 33-A is depicted the block diagram of the actual Italian SVR, that is, the architecture A, applied to the case study transmission system. A brief description of this architecture has been provided in Chapter 2, and extensive explanation can be found in references [5],[50] and [8]. It is relevant to notice the presence of the matrix $[D_{CN}]$, which decouples the control signals between the different voltage control areas (each endowed with its CN). This can be thought of as a partial implementation of the decoupling control strategy. The A architecture is, in fact, a subset of the latter, in which the *livq* control signal is used and RPR decoupling is left to the physical reactance between their nodes.

## 4.2. Decoupling Control

The block diagram of Figure 33-B shows the Decoupling Control implementation, that is architecture B. Despite still relying on PI voltage controllers for the CNs, this architecture uses the full input-output decoupling matrix (block *D* in the figure) calculated by means of equation (3.5). To briefly explain how to obtain the matrix, it is possible to refer to Figure 30 and Figure 33-B. By comparing them, it is easy to notice that the SVC application in Figure 33-B SVC implies that $u=qref$, $r=v_{CNref}$, $y=v_{CN}$, $[H]=[Id]$ (where $[Id]$ represents the identity matrix), $[G_2]=[S]$ (represented by the GRID block, see the modeling hypotheses in Paragraph 5.2), and $[G_1]$ is the controller transfer function which integrates a diagonal matrix of PI controllers. Therefore, the decoupling matrix can be calculated as follows:

$$[D] = [S]^{+} \tag{4.1}$$

## 4.3. Centralized LQRI with "livq" Control Signals

The block diagram in Figure 33-C represents SVR architecture C, which uses a single centralized LQRI, which sends a set of *livq* control signals to the five voltage control areas. In this configuration, the LQRI substitutes both the PI and decoupling

matrix of the present Italian SVR. However, it requires the additional feedback of the RPRs states *x(t)*. By comparing Figure 32 and Figure 33-C, it is possible to highlight how this architecture has been built based on the notional LQRI controller. Specifically, this implementation is obtained by imposing $r=v_{CNref}$, $y=v_{CN}$, and $u=livq$.

## 4.4. Centralized LQRI with "qref" Control Signals

Figure 33-D depicts the block diagram of the centralized LQRI using eleven *qref* control signals, i.e., architecture D applied to the case study transmission system. The system is like the previous one (architecture C), but the control signal difference requires a complete recalculation of the control matrix [*K*], which also results increased in size. However, controlling each RPR with a dedicated signal enables a finer voltage control action with respect to the use of a single output signal (like in architecture C). Such statement is demonstrated in the next Chapter 5.

## 4.5. Decentralized LQRI with "livq" Control Signals

This architecture is depicted in Figure 33-E and uses a decentralized approach for the LQRI controller, as well as *livq* control signals. The decentralization is done at voltage control area level, building completely separated SVRs for each. This means that each SVR has access only to the information pertaining its area (CN voltage and state feedbacks), which may lead to reduced performance if the latter are not physically (well) decoupled. The advantage of this solution is a simpler controller design, being the matrices size lower than for centralized cases.

## 4.6. Decentralized LQRI with "qref" Control Signals

The SVR architecture F block diagram is shown in Figure 33-F. This architecture uses the decentralized LQRI controller approach described previously (architecture E) but acts on the RPRs by means of *qref* control signals. While preserving the prior architecture's advantages and disadvantages, this one trades off a little higher control

design complexity for the ability to apply much finer control over the sources (due to the determination of a dedicated control signal for each RPR).

# 5. Linearized Model and Tests

In this Chapter, the implementation and test (via Simulink) of all the different SVR architectures presented in the previous Chapter is presented. Simulations are performed using a highly coupled portion of the Italian transmission network as a case study, to compare the dynamic performance of the proposed SVC implementations to the current one when different disturbances are applied. The final goal of such a comparison is the selection of the control architecture most suited for replacing the present Italian SVR for SVC.

## 5.1. Case study

A sector of the Italian transmission network was chosen as a case study to determine a suitable implementation of the above-mentioned MIMO control methodologies for a transmission network's SVR, as well as to assess the resulting dynamic performance. This portion, which covers approximately 26 thousand square kilometres, is made up of 65 HV buses (i.e. real electrical substations) and 11 RPRs (both conventional synchronous generator power plants and wind farms). This specific case study was chosen due to its large electrical coupling among its buses that is also

geographically wide enough to support many SVC CNs. As a consequence, in this case study 5 CNs were chosen based on their short circuit power and sensitivity coupling (i.e., the 5 buses with the highest short circuit power and the lowest reactive power/voltage sensitivity one to the other).

The case study model (SVR excluded) is composed by the following elements: generators/reactive power sources, primary voltage control systems of each RPR, reactive power control system of each RPR, tertiary voltage control references, HV transmission network (lines, transformers, etc.), loads (aggregated loads at HV/MV substations). It is reasonable to apply some simplifying hypotheses to the system's mathematical modelling, given the bandwidth/dynamic of SVC on transmission networks (equivalent time constants of tens of seconds).

## 5.2. Modelling Hypotheses

Firstly, the SVC concerns small variations with respect to the system's nominal voltage. As a result, the system can be represented by means of a linearized model, where load changes can be applied as disturbances with respect to the operating point, and RPRs reactive power injection variations only depend on the SVC control signals. Furthermore, such an approach allows all RPRs that are not used for SVC to be treated as fixed power sources, removing them from the linearized model (under the hypothesis that their reactive power control system is correctly operating, i.e., keeps a fixed reactive power despite voltage variations at source terminals).

Secondly, only the dynamic behaviour relevant to the SVC should be considered, ignoring any faster/slower dynamic, thus using simplified models for the components. In particular, the HV network becomes a passive network composed of algebraic impedances, with electric transients disregarded. The internal dynamics of RPRs can likewise be ignored, modelling them as gains. Because primary voltage control systems are substantially faster than SVC, they can be modelled with gains as well. However, it was decided to keep them in the model for future testing with SVRs with higher control bandwidth (in a possible future scenario where all the conventional power plants are

shut-off). Reactive power control systems must be modelled since their dynamics are similar to those of SVCs and they are the most significant contributors to the whole system's transient behaviour in the given bandwidth. Multiple models can be employed depending on the level of detail required during the SVR design. In the most basic model, a first order transfer function is utilized, whereas in the most complicated model, a complete digital twin of a SART can be used [20]. Tertiary voltage control is a non-dynamic layer, providing a set of constant reference voltages for the SVC.

Finally, because the case study is a high-voltage transmission power system, the Carpentier hypothesis holds true [48][49]. As an outcome, the active power-frequency and reactive power-voltage channels are entirely distinct and independent; the frequency and the active power variables can be removed from the case study model, and the transmission system's passive components can be modelled using the voltage-reactive sensitivity matrix [$S$], whose elements are defined as follows:

$$S_{ij} = \frac{\partial v_i}{\partial q_j} \tag{5.1}$$

where $v_i$ is the voltage of *i-th* bus, and $q_j$ is the reactive power injected/absorbed in the *j-th* bus.

All the variables, matrices, and signals use the *p.u.* relative representation, with a common power base of 100 MVA and voltage bases that depend on the specific section of the system. Moreover, being the system model a linearized one, it uses the variations in the signals in respect to the linearization (operating) point. For the sake of conciseness, the word "variation" has been left out of the rest of the study.

## 5.3. System's Mathematical Model

The mathematical model of the system has been built in Matlab Simulink environment. The Simulink block diagram is shown in Figure 34, where all the involved signals (shown as arrows) are array-type. The "CNs voltage references" block (on the

left) represents the variation in the voltage reference sent by the TVC to the SVR, while $\Delta V_{CN}$ is the variation in the voltage of the CNs (system's output).

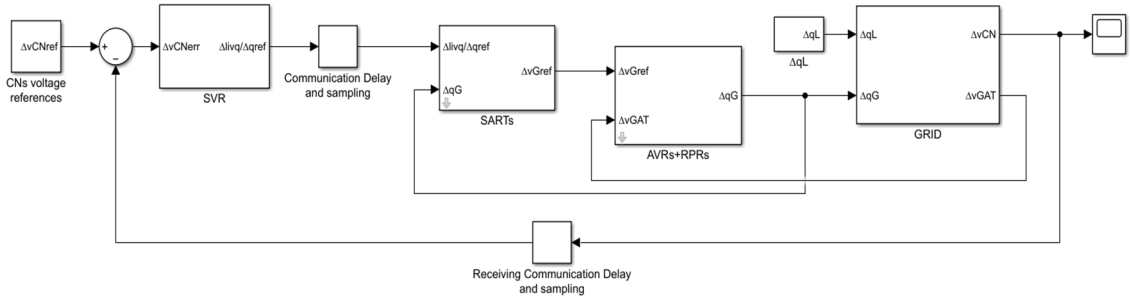


Figure 34 - System's mathematical model in Matlab Simulink environment

The four main subsystems of Figure 34 are:

- "Voltage Regulator" block, implementing the SVC function for the system;
- "SARTs" block, representing the reactive power loops of the RPRs;
- "AVRs+RPRs" block, modelling the primary voltage control loops (which include the model of the RPRs and their AVRs);
- "GRID" block, modelling the transmission network.

### 5.3.1. "Voltage regulator" block

The content of this subsystem varies, following the Table 1 architectures. Regardless of the utilized control approach, this block is responsible for receiving the CNs' voltage error ($\Delta v_{CNerr}$ in Figure 34) and determining the proper control signals to be sent to the SARTs block. The output can either be a $\Delta livq$ or a $\Delta qref$ signal, depending on the specific SVR architecture.

### 5.3.2. "SARTs" block

Inside this block the reactive power loops of the RPRs are modelled. At present, this function is carried out in Italy by the SART apparatuses (as described in the previous Chapter 2). Specifically, the reactive power reference signals coming from the

SVR are compared with the reactive power produced ($\Delta q_G$) by the RPRs. The resulting error is elaborated by a PI controller, which determines the set point ($\Delta v_{Gref}$) for the AVRs. Following the previously described modelling hypotheses, the SARTs models implement the equation:

$$\Delta v_{Gref} = (U \ - \Delta q_G) * \left( K_P + K_I \frac{1}{s} \right) \tag{5.2}$$

where $U = \Delta livq$ or $\Delta qref$, depending on the specific SVR architecture being simulated.

The $K_P$ and $K_I$ parameters in eq. (5.2) are selected by means of simulations, to ensure an equivalent time constant (of the reactive power variation at the source terminals) after a reference signal step that is equal to 8 s for conventional power plants, and equal to 3 s for renewable energy sources.

### 5.3.3. "AVRs+RPRs" block

This block is a representation of the RPRs' PVC loop. The block is composed of the models of the sources as well as their AVRs (which control the generator exciter and ensure that the MV voltage at its terminals follows the reference signal).

The employed models are simplified as a result of the simplifying assumptions mentioned above. The AVR is a PI controller, which receives the voltage reference sent by the SART ($\Delta v_{Gref}$) and compares it with the voltage at the source terminals ($\Delta v_{GAT}$) to provide a suitable control signal for the source ($\Delta v_{ex}$) [5]:

$$\Delta v_{ex} = \left(\Delta v_{Gref} - \Delta v_G\right) * \left( K_{P_{AVR}} + K_{I_{AVR}} \frac{1}{s} \right) = \left(\Delta v_{Gref} - \Delta v_G\right) * \mu \frac{1 + s\,T_v}{s} \tag{5.3}$$

For both conventional and renewable power plants, the control gains $K_{PAVR}$ and $K_{IAVR}$ (or equivalently $\mu$ and $T_v$ parameters) are selected by means of simulations to guarantee an equivalent time constant of about 1 s after a reference signal step.

The source models are different, depending on their type. Synchronous generators use a first order model [14]:

$$\Delta v_G = \frac{h_e}{1 + T_e s} \Delta v_{ex} \tag{5.4}$$

where $h_e = 0.5$ and $T_e = 3.2$.

Conversely, a unitary gain was chosen for modelling the RES (due to the very fast voltage dynamics of their power electronics interfaces).

Finally, the voltage at the power plant's point of common coupling with the transmission system ($\Delta v_{GAT}$) is used in this block to determine the reactive power injected in the network ($\Delta q_G$), by means of the equivalent power plant transformers' reactance ($x_T$):

$$\Delta q_G = \frac{\left(\Delta v_G - \Delta v_{G\_AT}\right)}{x_T} \tag{5.5}$$

### 5.3.4. "GRID" block

The "GRID" block implements equation (5.1). In fact, the input to this block is the full range of reactive powers exchanged in each transmission system's bus, whether they are absorbed by loads ($\Delta q_L$) or injected by RPRs ($\Delta q_G$). Since the system model is linearized, the power variation of the loads in steady state is equal to zero. However, such input has been kept in the mathematical model in order to test the system with reactive power disturbances. The block's output contains the voltage at all system buses, including the CNs' voltage and the sources' voltage at point of common coupling with the transmission system.

### 5.3.5. Additional elements in the model

The system in Figure 34 includes sampling and communication delays models for both sending and receiving channels (the SVR, the CNs, and the RPRs are scattered on

a large area and must comply with the available communication infrastructure capabilities). To do this, both the "Communication delay and sampling" blocks include a transport delay and a zero-holder function. Transport delays for both channels were adjusted at 0.02 s in the case study. The sampling time for the receiving channel (which is supposed to use PMUs for CNs voltage measurement) has been set to 0.2 s, while the sampling time for the sending channel (which is assumed to use the current SCADA - Supervisory Control And Data Acquisition) has been set to 4 s.

## 5.4. Performance Evaluation and Results Comparison

The dynamic regulation performance of the SVR architectures in Table 1 has been assessed by applying them to the case study system. Specifically, the implementation of the SVRs in the mathematical model built in Matlab-Simulink environment (Figure 34) enabled the application of specific disturbances to the system, and the comparison of the resulting transients. It is worth noting that the SVR designs' control parameters provide equivalent voltage regulation performance to the actual SVC in terms of reaction to reference changes. This was accomplished through the use of a model-based design technique. Each regulator has been implemented in the case study model, resulting in several independent models; in each of them, a voltage reference step has been applied to all the CNs at the same time. The SVR parameters were then modified until the dynamic voltage response of each model was comparable (i.e., equivalent time constant) to the current Italian SVR system.

To test and compare the dynamic performance of the regulators, three different perturbations have been chosen. Each perturbation has been conceived for testing a specific aspect of the SVR architectures, as explained in the following.

Perturbation 1): change in the voltage reference of two CNs by +1%, while keeping the other CNs' references constant; this allows testing the ability in decoupling the voltage control actions of the SVR architectures.

Perturbation 2): change in the reactive power load of two buses by -10%, while keeping the other loads constant; this allows testing the capability of rejecting reactive power disturbances of the SVR architectures.

Perturbation 3): +1% step change in the voltage of one CN; this allows testing the ability of the SVR architectures in rejecting voltage disturbances.

Being the tests done on a linearized model, the results are represented in terms of variations with respect to the operating point in which the system was before the application of the perturbations. In this regard, all the perturbations are applied at $t$=100$s$, while the whole simulation lasts for 600$s$. The results are expressed in relative numbers, where the CNs voltages start from 1 *p.u.* and the reactive power starts from 0 *p.u.*

### 5.4.1. Perturbation 1), results and discussion

This specific perturbation was chosen to test the ability of the different SVR architectures in decoupling the voltage control actions among the CNs. The test is particularly demanding for the case study power system, being the case study transmission system characterized by high electrical coupling between its substations. As previously mentioned, the test involves changing the voltage reference of CN1 and CN2 by +1%, while keeping the rest of the CNs' references constant. Figure 35 to Figure 46 depict the results of this test for the six SVR architectures, in terms of CNs' voltages (a) and RPRs' reactive power (b) variations. As can be clearly seen, all the architectures using *livq* control signals fail the test. Specifically, architecture A (the current SVR architecture - Figure 35) and architecture C (Figure 39) do not reach the target CNs' voltages, while architecture E (Figure 43) presents poorly controlled voltage transients. This is caused by cross-actions between the RPRs, whose reactive power injections significantly affect each other (due to the high electrical coupling between the substations). These cross-actions cannot be effectively compensated using the same control signal acting on several sources (i.e., *livq*). Moreover, the common control signal leads to reactive power saturation in several sources. On the other hand, all the

architectures using *qref* control signals, which are specifically calculated for each RPR, can reach the required voltage with properly controlled transients. Architecture B (Figure 37) is capable of totally decoupling the voltage control actions, while architecture D (Figure 41) and architecture F (Figure 45) still present some coupling, which is properly compensated by the regulator after the first part of the transient. Regarding the reactive power distribution among the RPRs, architecture B (Figure 38) presents the best one among all the successful SVR architectures. Indeed, the decoupling control approach can apply the minimum amount of reactive power required to achieve the target voltages, by means of the cancellation between the decoupling and the system matrices (as depicted in paragraph 3.2). Conversely, both architectures D and F present a wider distribution of reactive power among RPRs (Figure 42 and Figure 46). All the successful architectures have a SVR capable of requesting higher (in magnitude) reactive power injections to the RPRs that are electrically closer to the CNs where a voltage reference variation is applied, and lower to the farther ones.

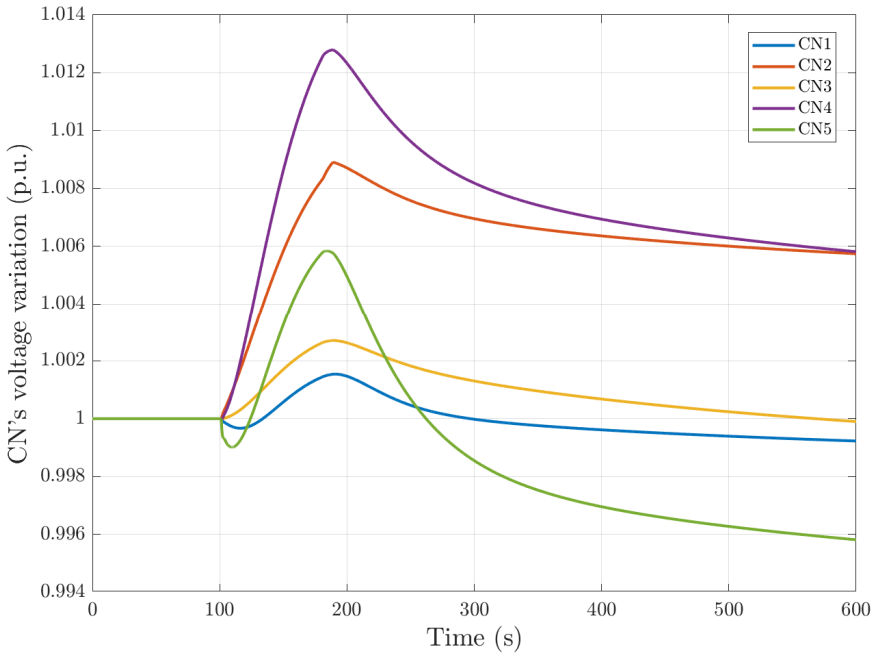


Figure 35 - Perturbation 1), architecture A, CN's' voltage

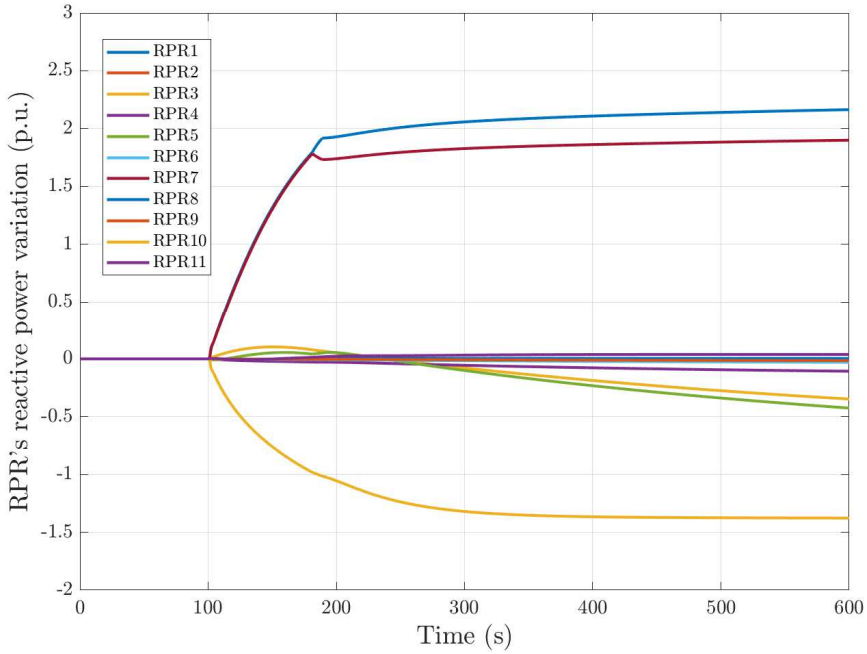


Figure 36 - Perturbation 1), architecture A, RPRs' reactive power

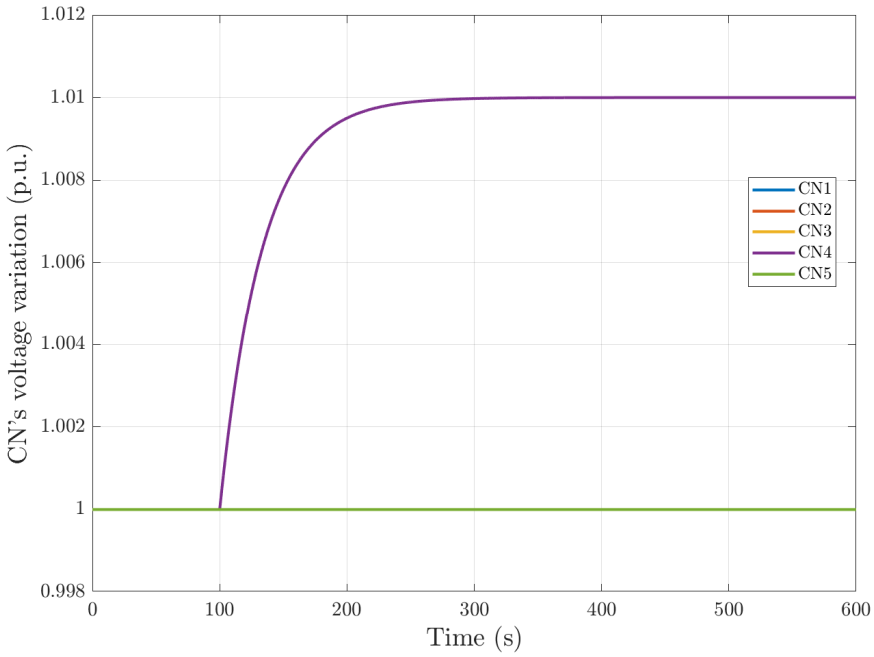


Figure 37 - Perturbation 1), architecture B, CNs' voltage

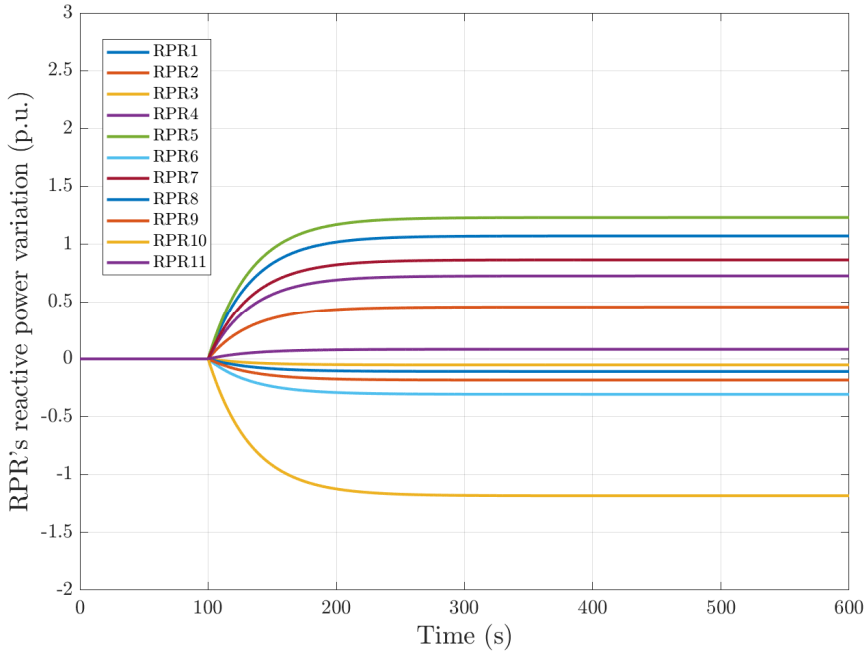


Figure 38 - Perturbation 1), architecture B, RPRs' reactive power

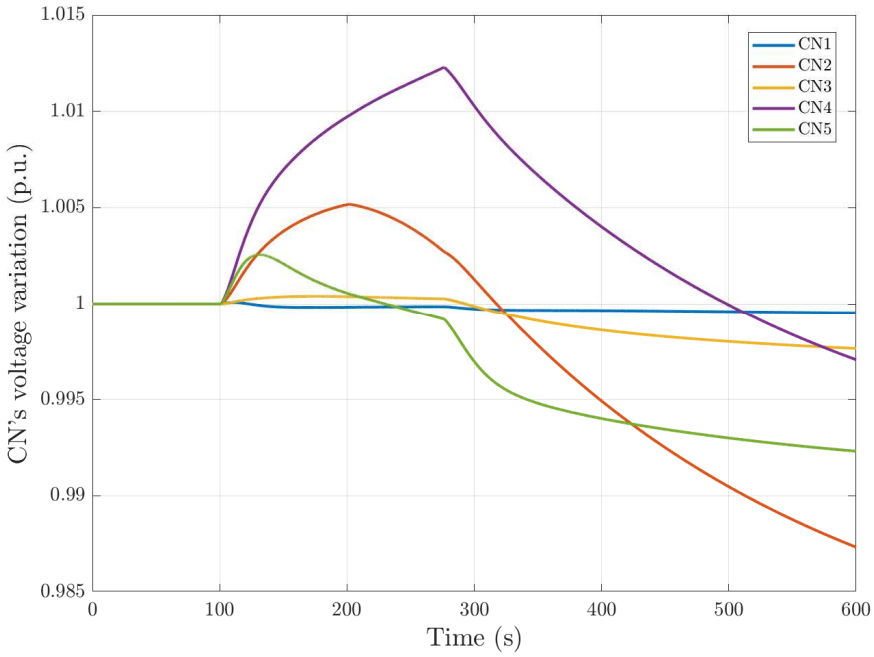


Figure 39 - Perturbation 1), architecture C, CNs' voltage

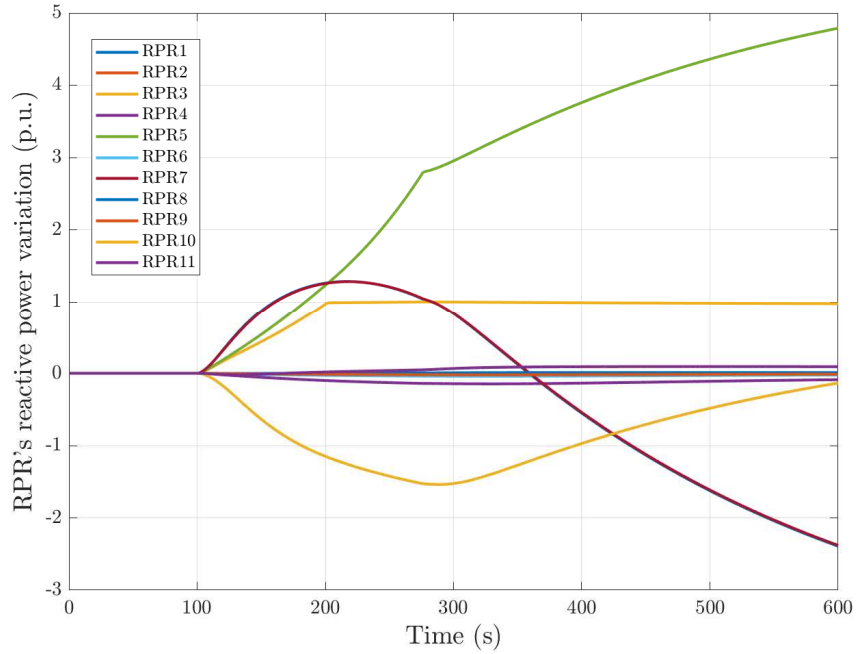


Figure 40 - Perturbation 1), architecture C, RPRs' reactive power

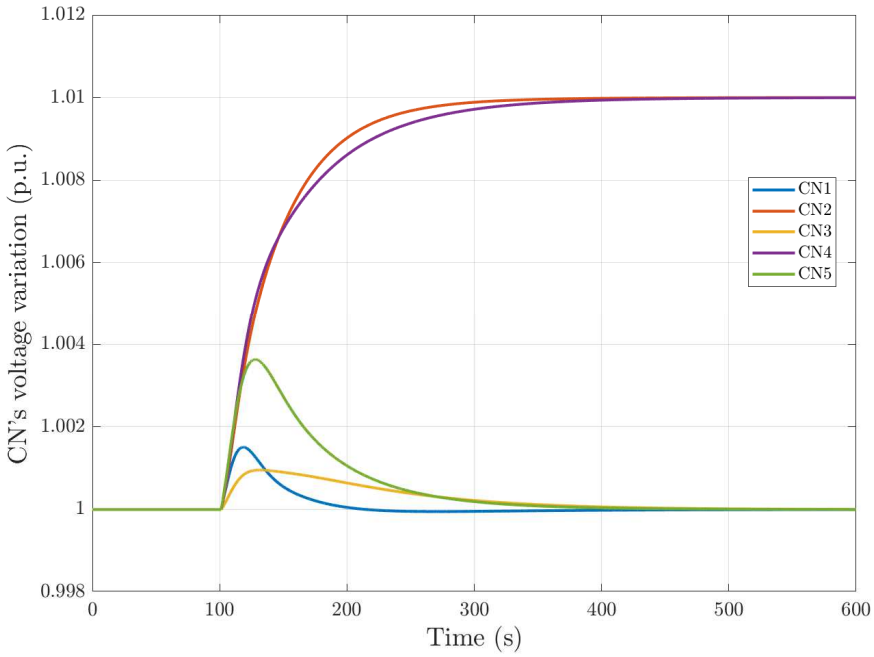


Figure 41 - Perturbation 1), architecture D, CNs' voltage

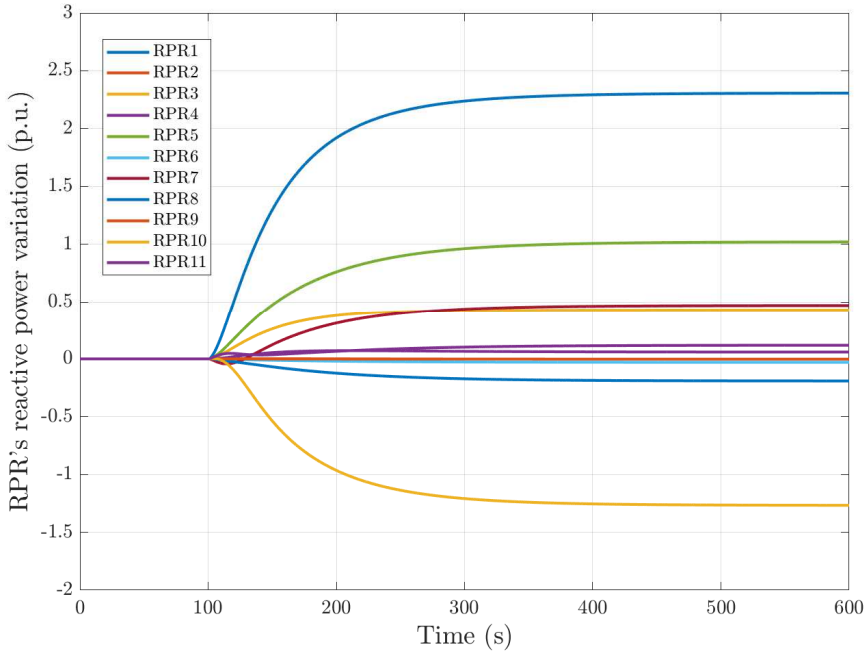


Figure 42 - Perturbation 1), architecture D, RPRs' reactive power

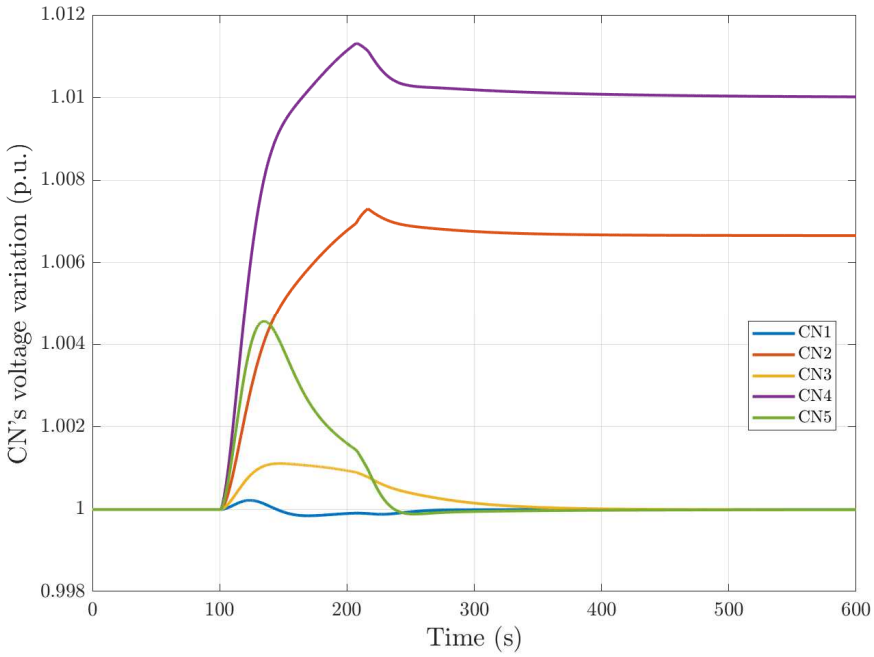


Figure 43 - Perturbation 1), architecture E, CNs' voltage

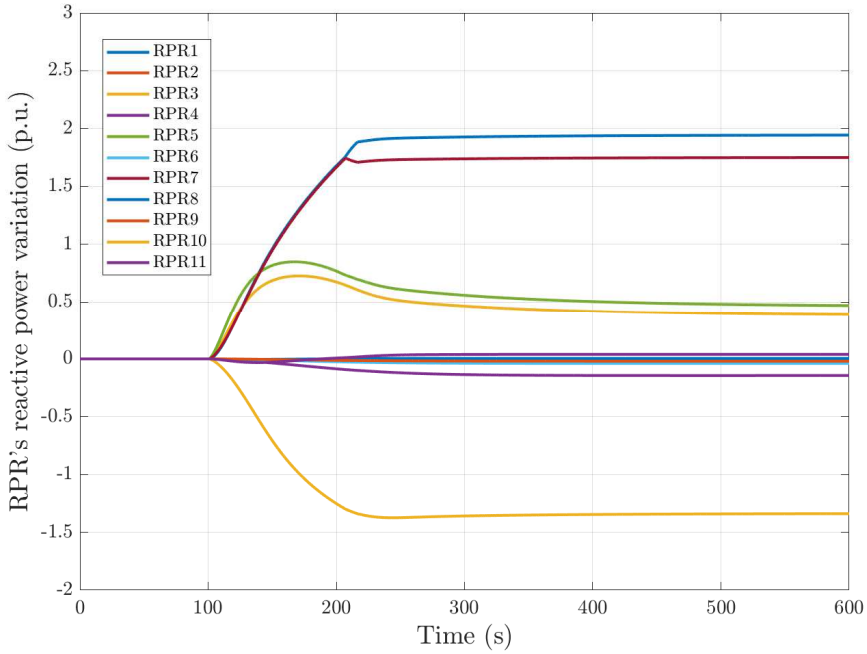


Figure 44 - Perturbation 1), architecture E, RPRs' reactive power

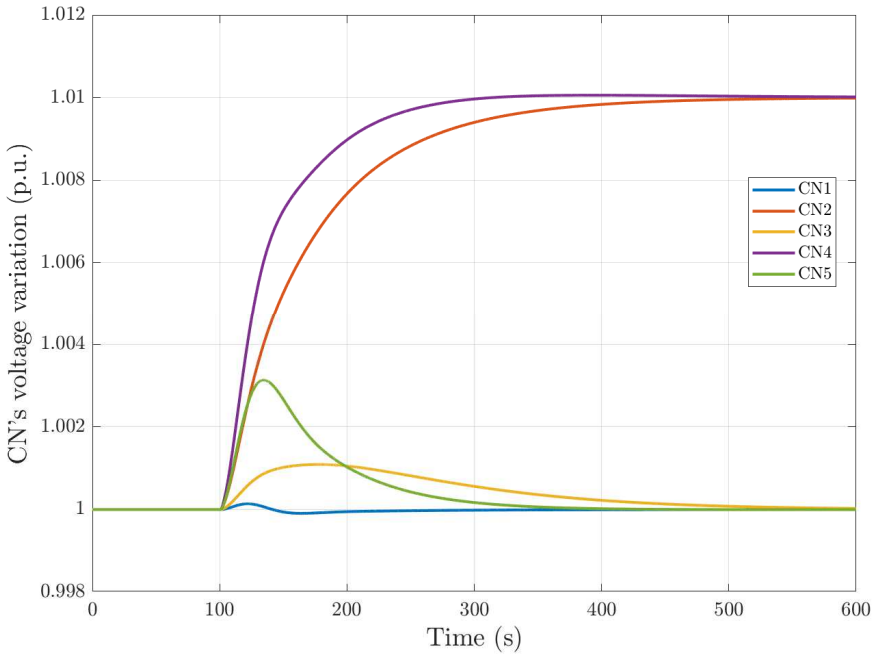


Figure 45 - Perturbation 1), architecture F, CNs' voltage

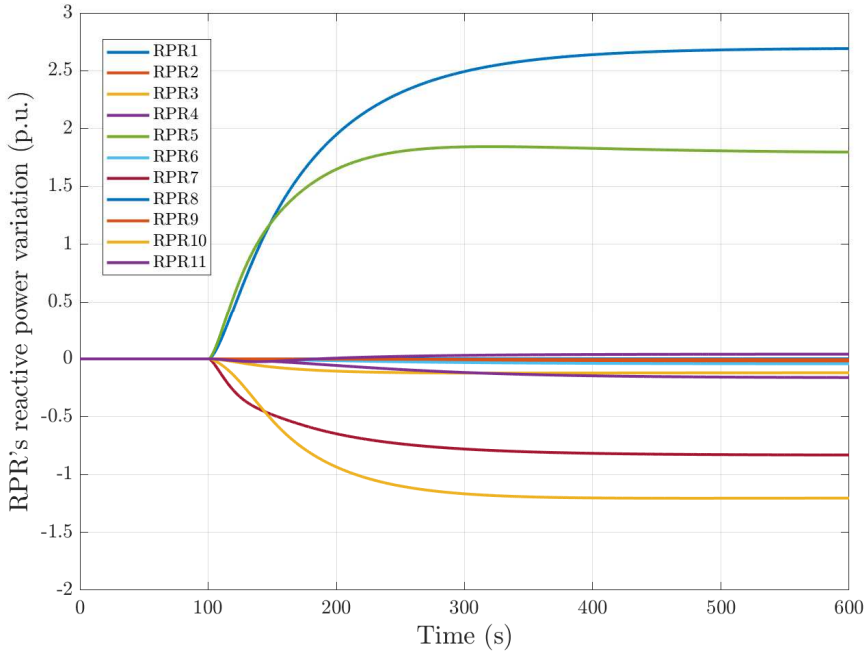


Figure 46 - Perturbation 1), architecture F, RPRs' reactive power

### 5.4.2. Perturbation 2), results and discussion

The purpose of this test is to evaluate the ability of the SVR architectures in rejecting reactive power disturbances in the power system. The perturbation applied to the system is a change in the reactive power load of two buses by -10%, while keeping the rest of the loads at the same previous value. Figure 47 to Figure 58 show the dynamic response of the six SVR architectures to this perturbation, by means of the CNs' voltage and RPRs' reactive power traces. The actual SVR architecture (A - Figure 47) is capable of driving back the CNs voltage at the pre-disturbance value, although requiring a very long time (voltages have not returned to an equilibrium state after more than 500 s past the perturbation). Architecture B (Figure 49), architecture D (Figure 53), and architecture F (Figure 57) are all capable of recovering the pre-perturbed voltages in an acceptable amount of time, with the first (Figure 50) presenting the minimum amount of RPRs' reactive power change, and the second (Figure 54) and third (Figure 58) progressively requiring higher variations. Architectures C (Figure 51 and Figure 52) and E (Figure 55 and Figure 56) still respond satisfactorily in terms of

voltages, but achieving such goal requires higher RPRs' reactive power with respect to the other configurations.

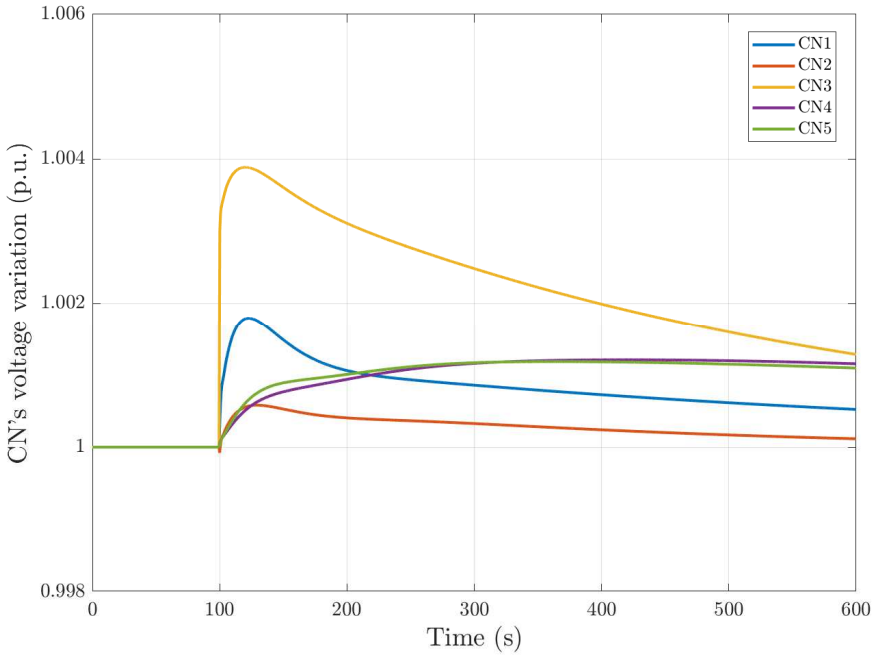


Figure 47 - Perturbation 2), architecture A, CNs' voltage

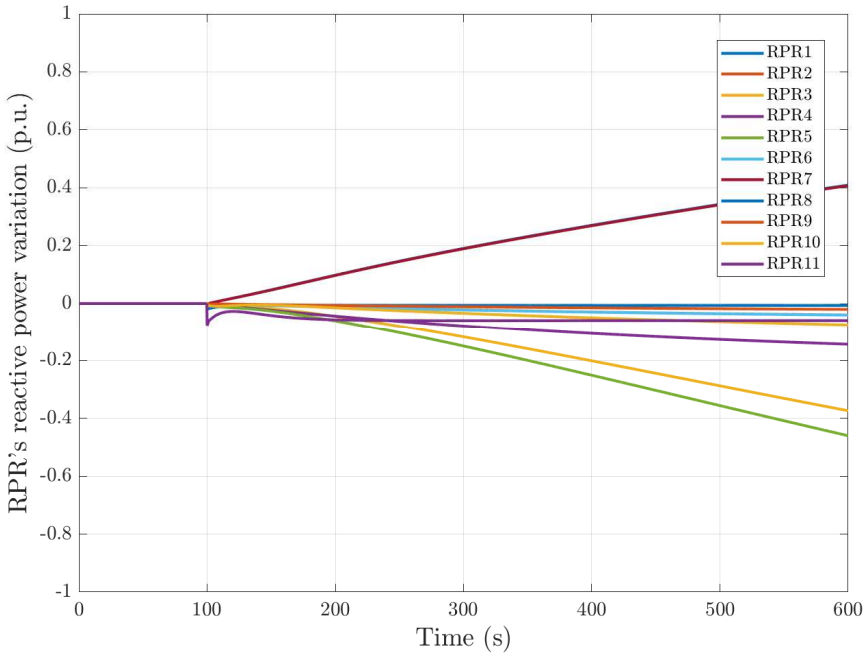


Figure 48 - Perturbation 2), architecture A, RPRs' reactive power

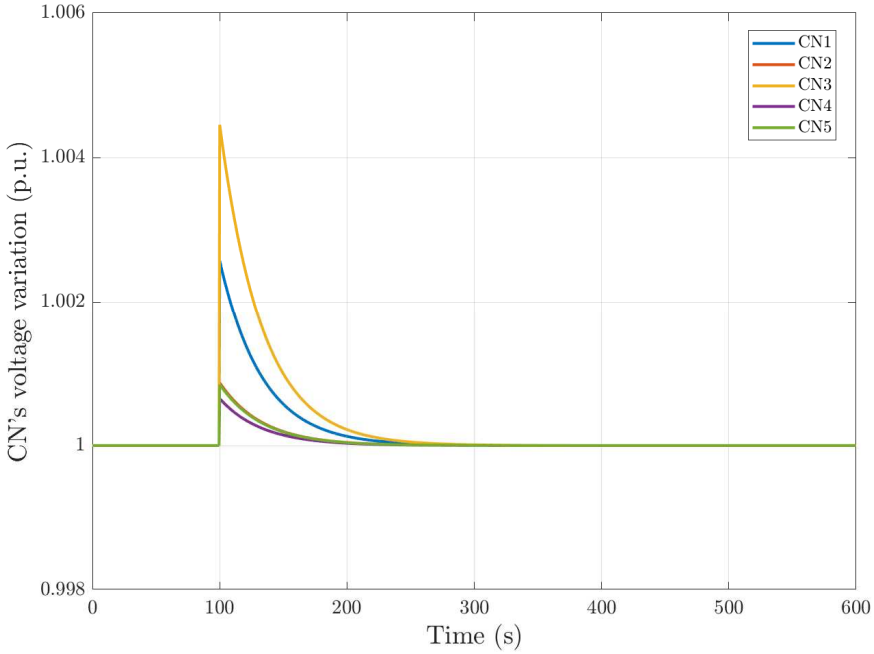


Figure 49 - Perturbation 2), architecture B, CNs' voltage

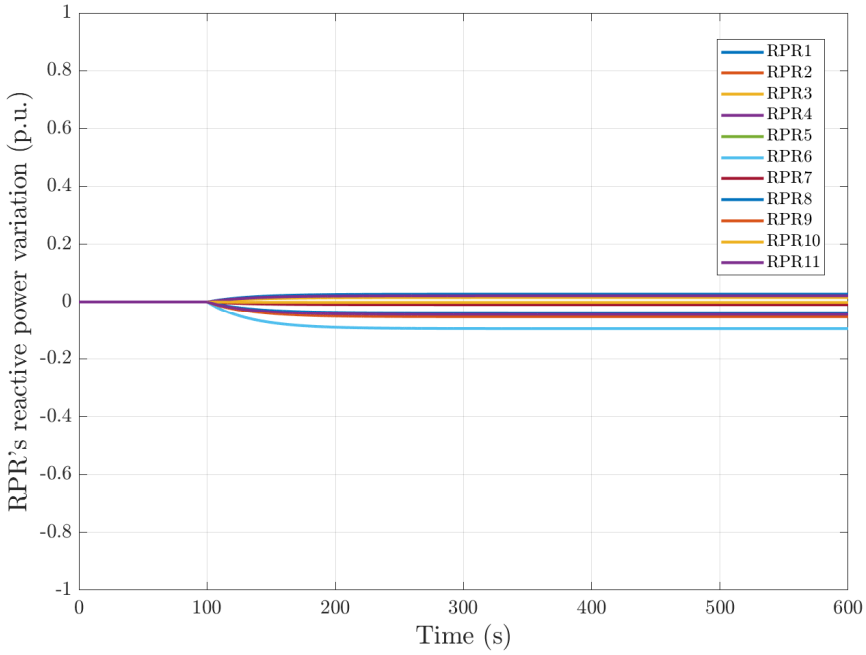


Figure 50 - Perturbation 2), architecture B, RPRs' reactive power

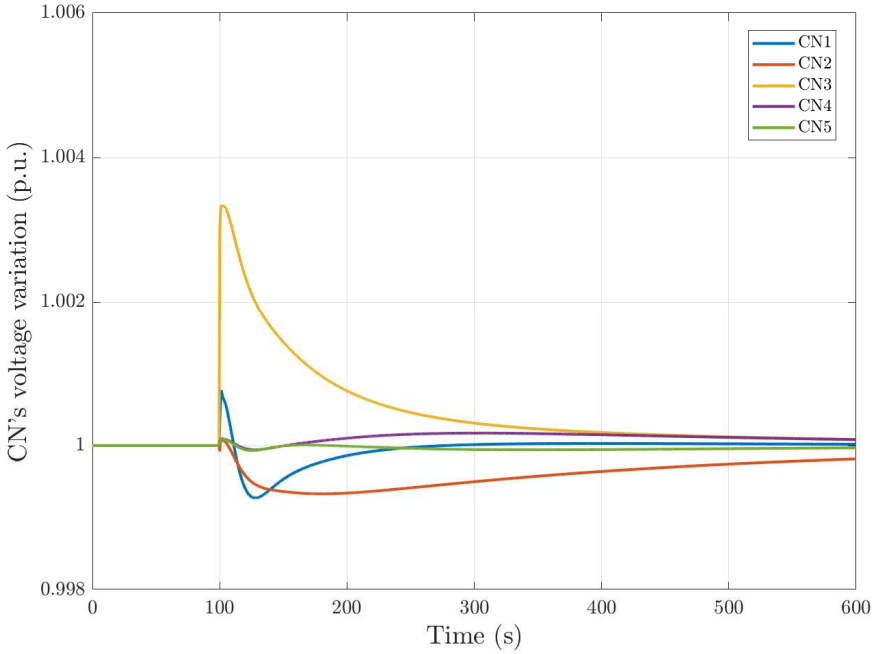


Figure 51 - Perturbation 2), architecture C, CNs' voltage

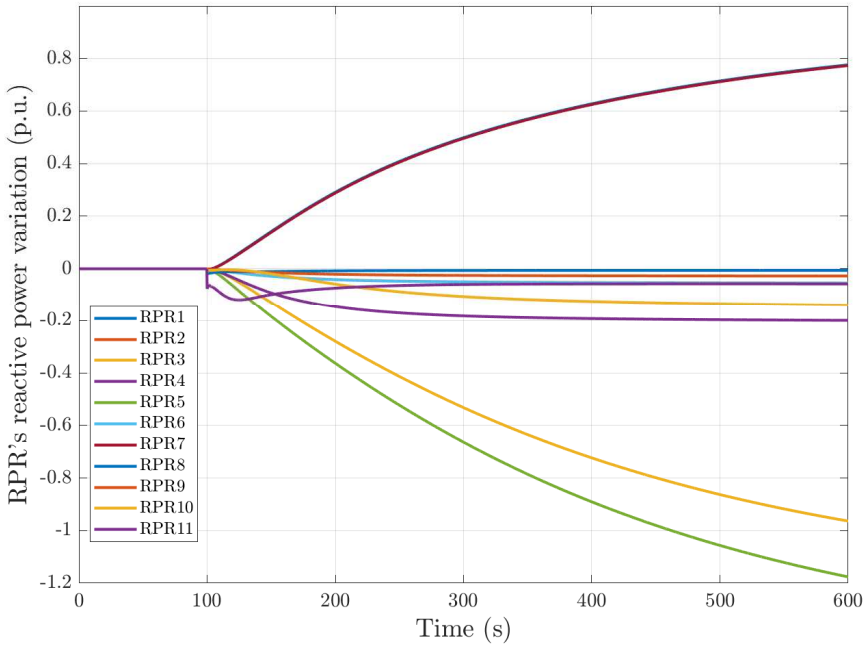


Figure 52 - Perturbation 2), architecture C, RPRs' reactive power

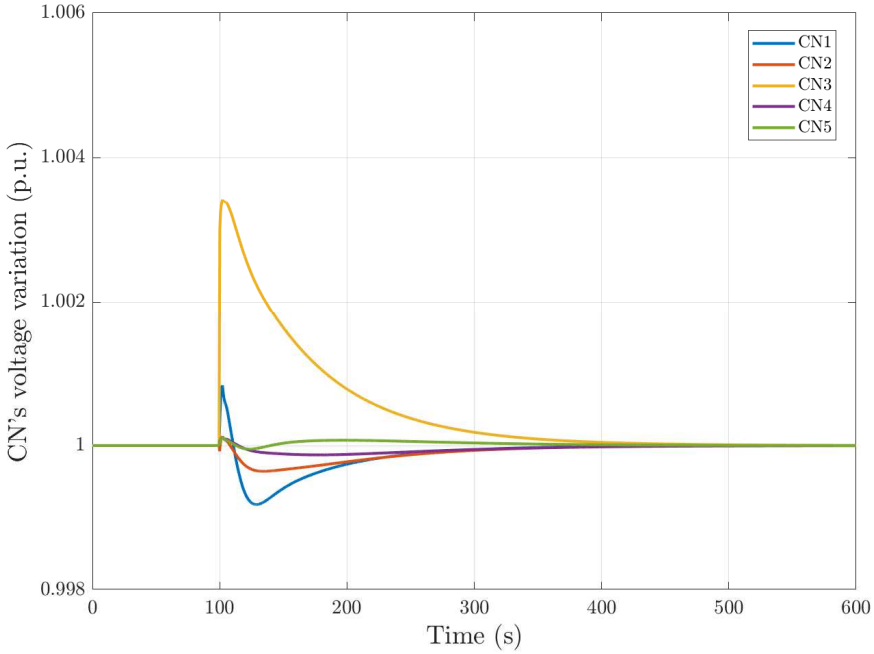


Figure 53 - Perturbation 2), architecture D, CNs' voltage

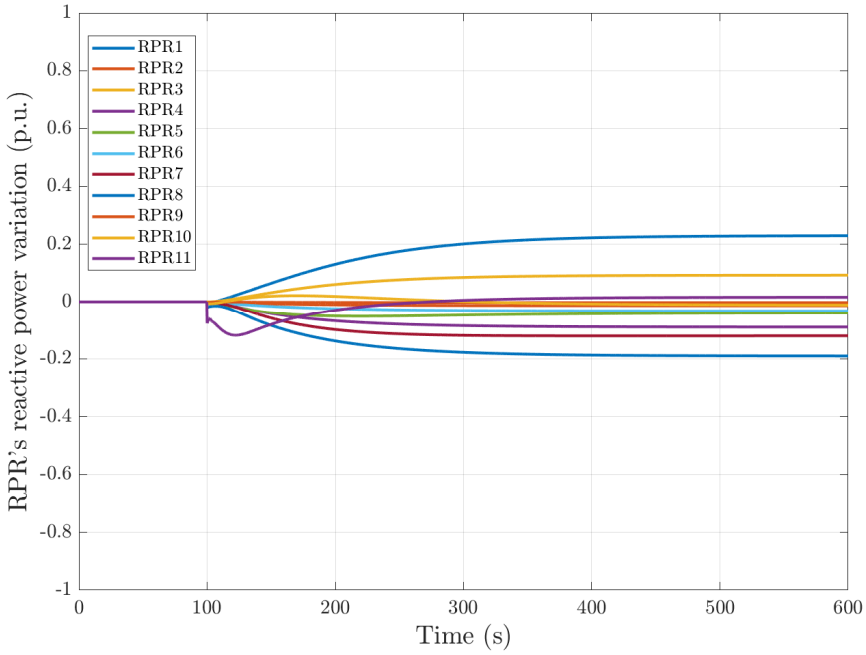


Figure 54 - Perturbation 2), architecture D, RPRs' reactive power

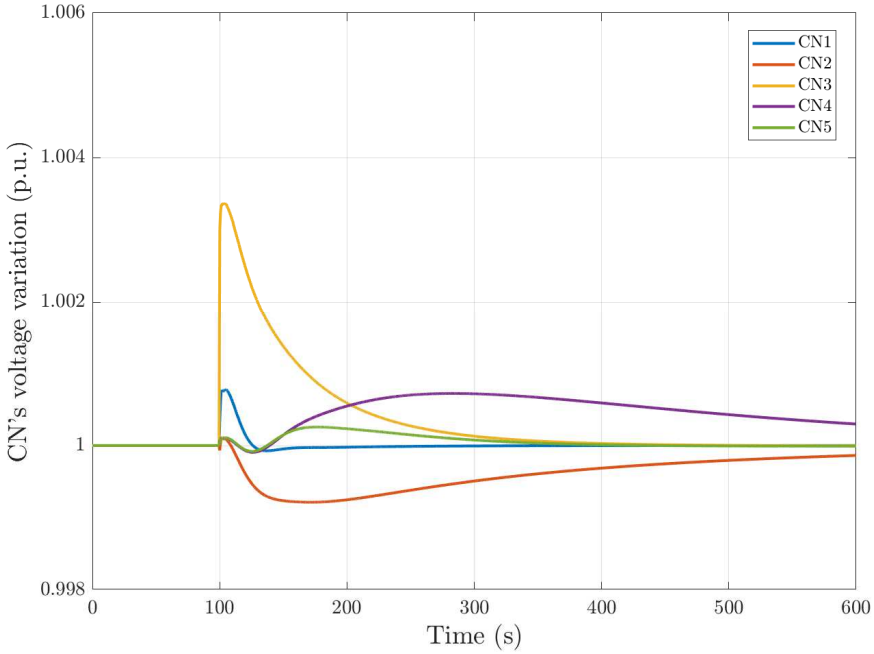


Figure 55 - Perturbation 2), architecture E, CNs' voltage

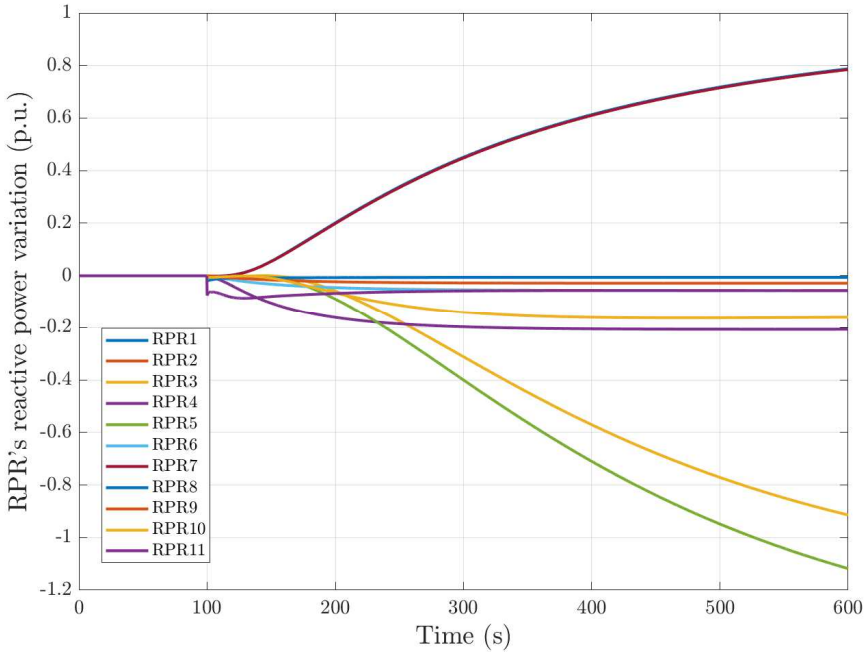


Figure 56 - Perturbation 2), architecture E, RPRs' reactive power

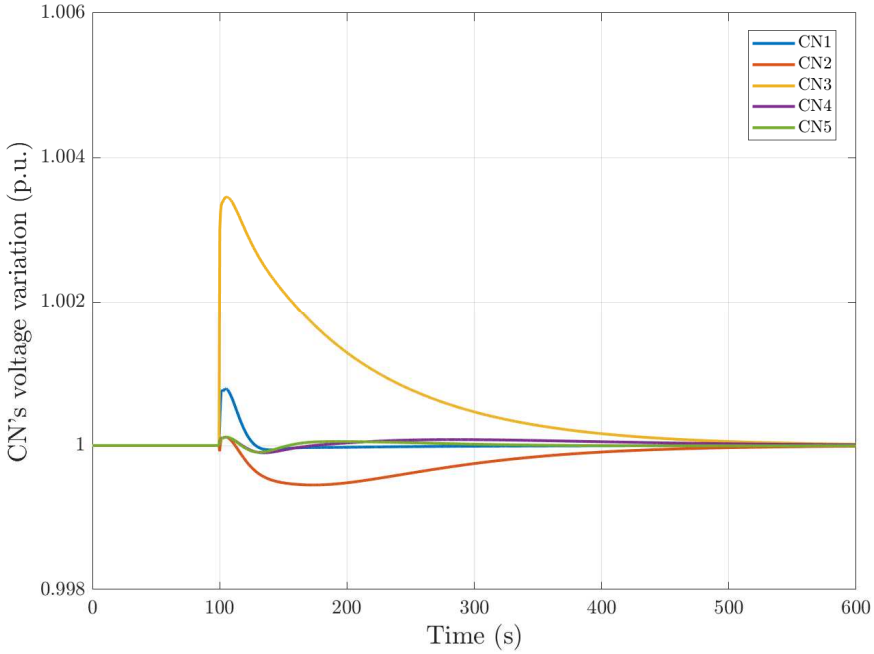


Figure 57 - Perturbation 2), architecture F, CNs' voltage

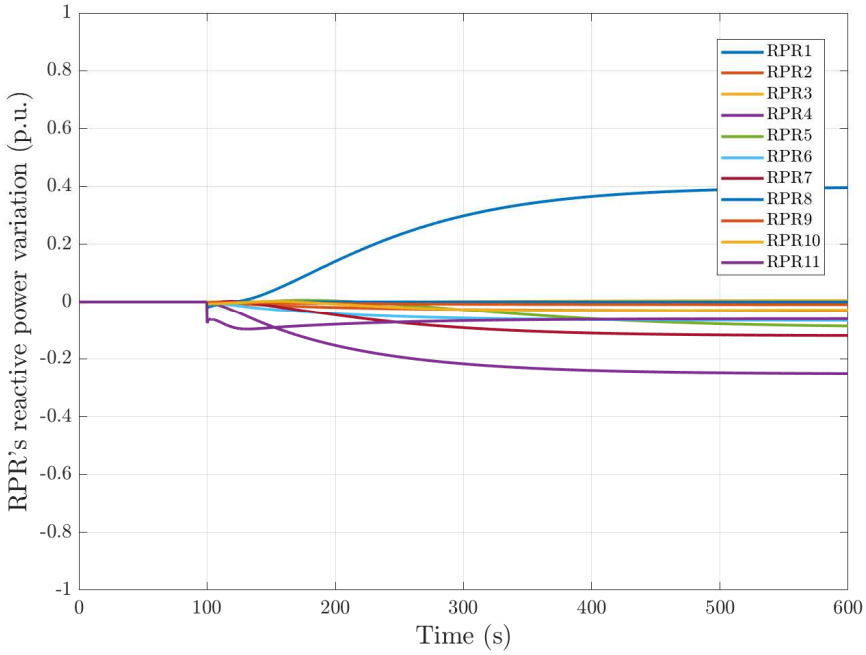


Figure 58 - Perturbation 2), architecture F, RPRs' reactive power

### 5.4.3. Perturbation 3), results and discussion

The perturbation 3 application had the purpose of evaluating the SVR capability of rejecting a sudden change in a CN's voltage, ensuring the recovery of the correct voltages in the network. The applied perturbation is a step increase of 1% in the voltage of $CN_1$. The dynamic performance of the architectures in study, when this perturbation is applied, are shown in Figure 59 to Figure 70. As before, each figure presents the CNs' voltages and the corresponding RPRs' reactive power variations. The actual SVR (Figure 59), while being capable of recovering the correct voltage after the perturbation, presents a very high time constant, which is well above the acceptable one for SVC. Moreover, it causes one source to reach its reactive power saturation limit (Figure 60). Architecture C (Figure 63) completely fails the test, presenting diverging CNs' voltages. Among the three architectures using the with *livq* control signal, only architecture E (Figure 67) recovers the correct voltages after the applied perturbation, although it does it while saturating two RPRs (Figure 68). The architectures using the *qref* control signal are all capable of managing the applied perturbation (Figure 61, Figure 65, and Figure 69). Specifically, architecture B (Figure 62) and D (Figure 66) show a similar behaviour in terms of reactive powers distribution among RPRs, where the second is slightly worse in ensuring the decoupling among the CNs (Figure 65). Architecture F, while presenting a dynamic response in CN voltages like the previous two (Figure 69), forces one RPR (green trace in Figure 70) to supply a significantly larger reactive power in comparison to them.

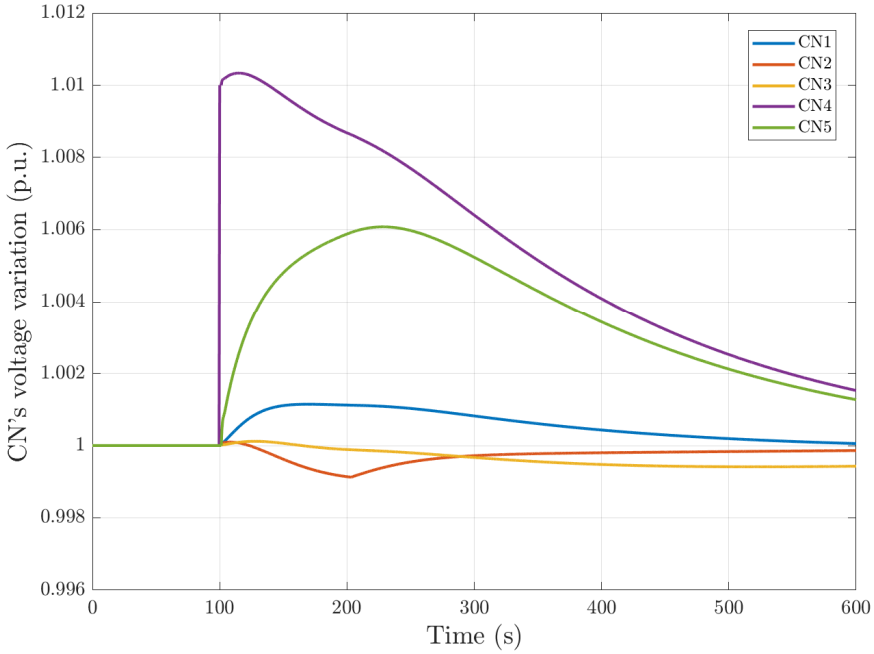


Figure 59 - Perturbation 3), architecture A, CNs' voltage

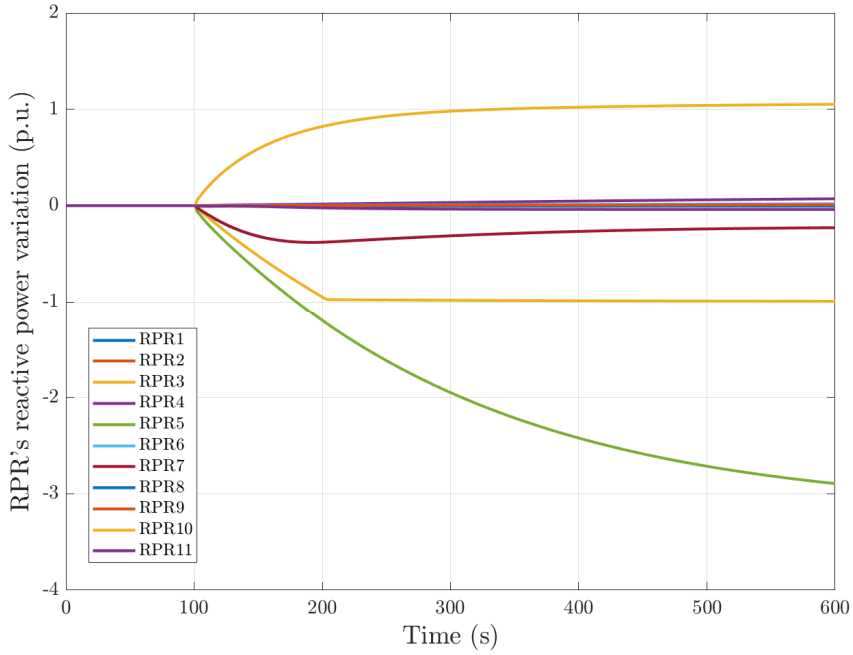


Figure 60 - Perturbation 3), architecture A, RPRs' reactive power

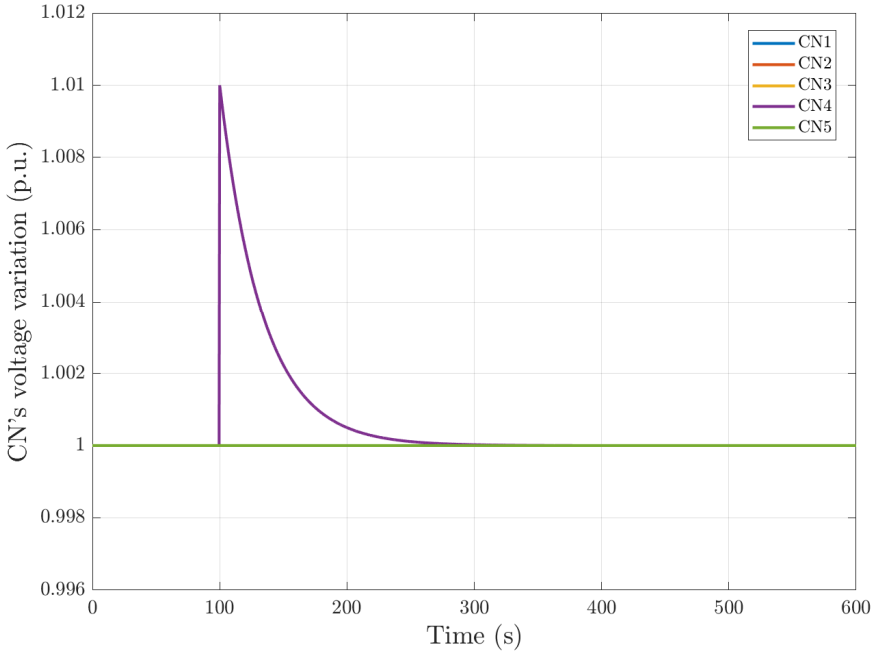


Figure 61 - Perturbation 3), architecture B, CNs' voltage

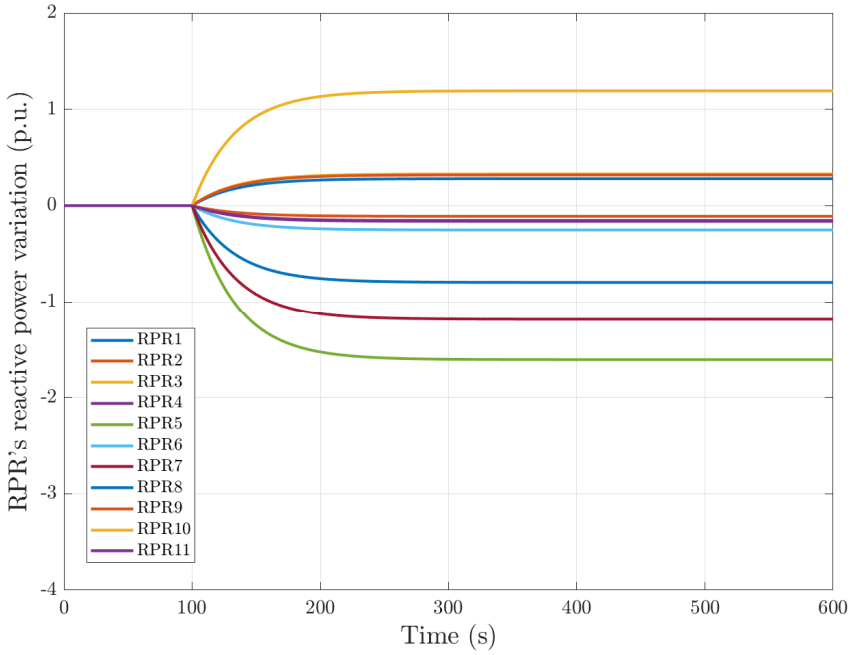


Figure 62 - Perturbation 3), architecture B, RPRs' reactive power

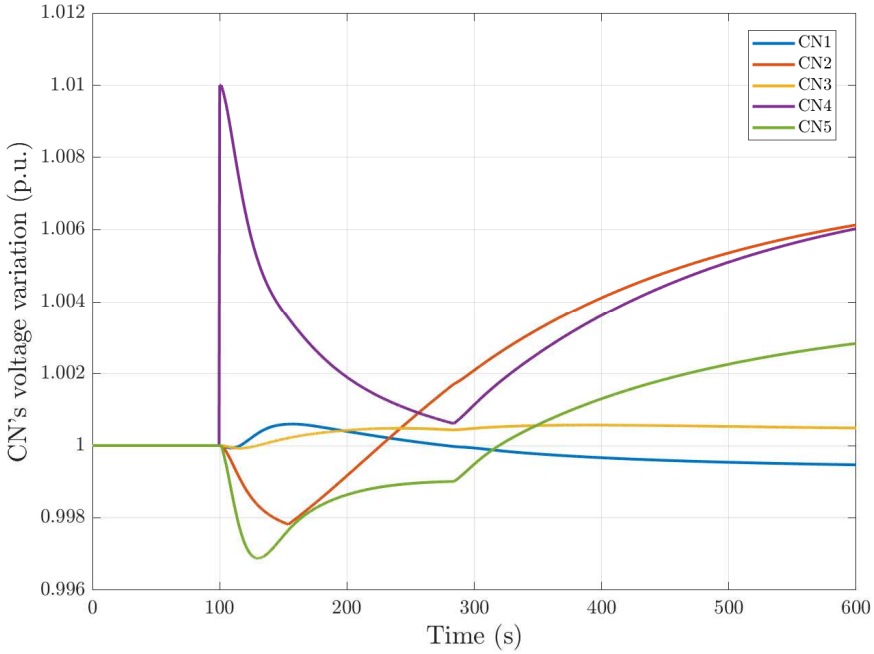


Figure 63 - Perturbation 3), architecture C, CNs' voltage

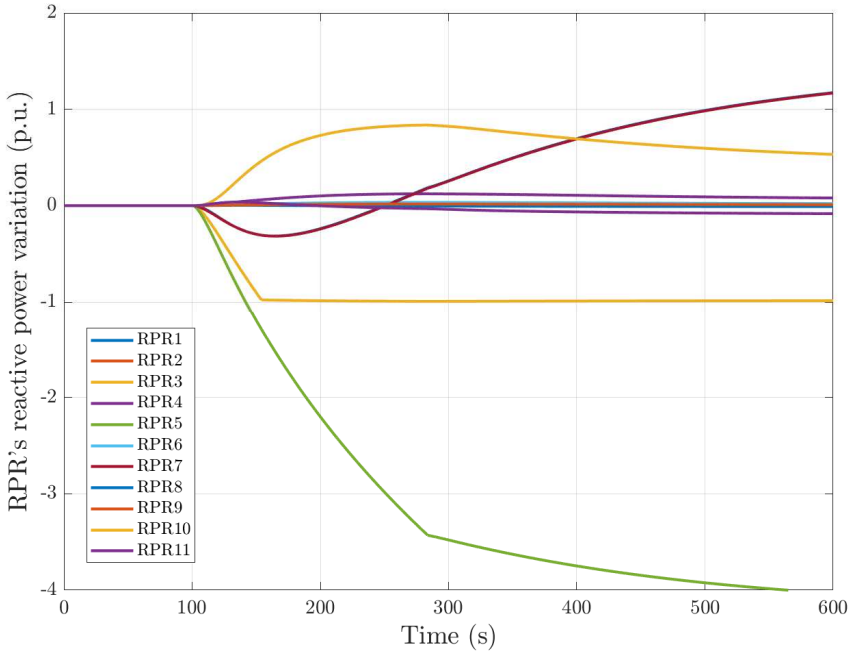


Figure 64 - Perturbation 3), architecture C, RPRs' reactive power

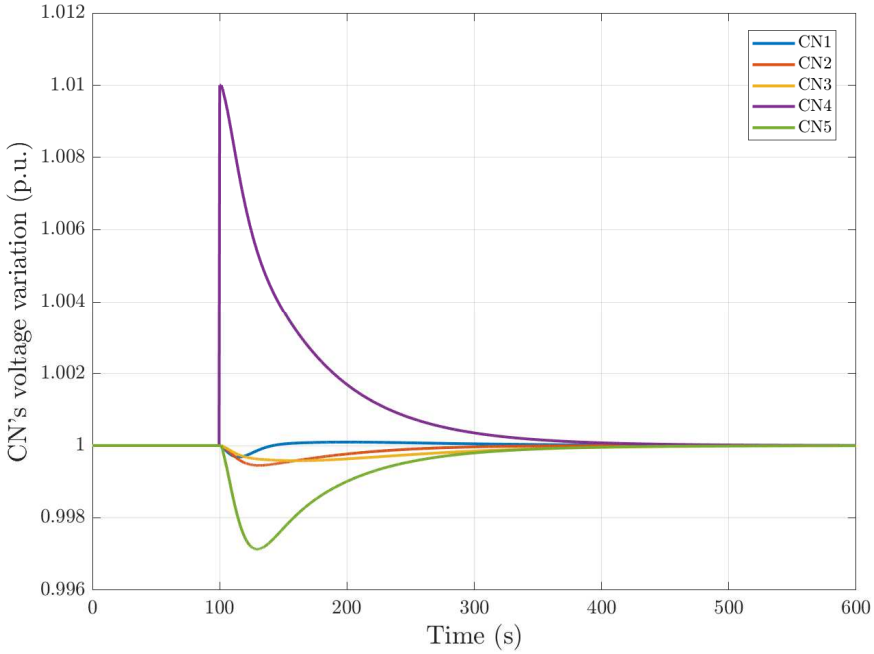


Figure 65 - Perturbation 3), architecture D, CNs' voltage

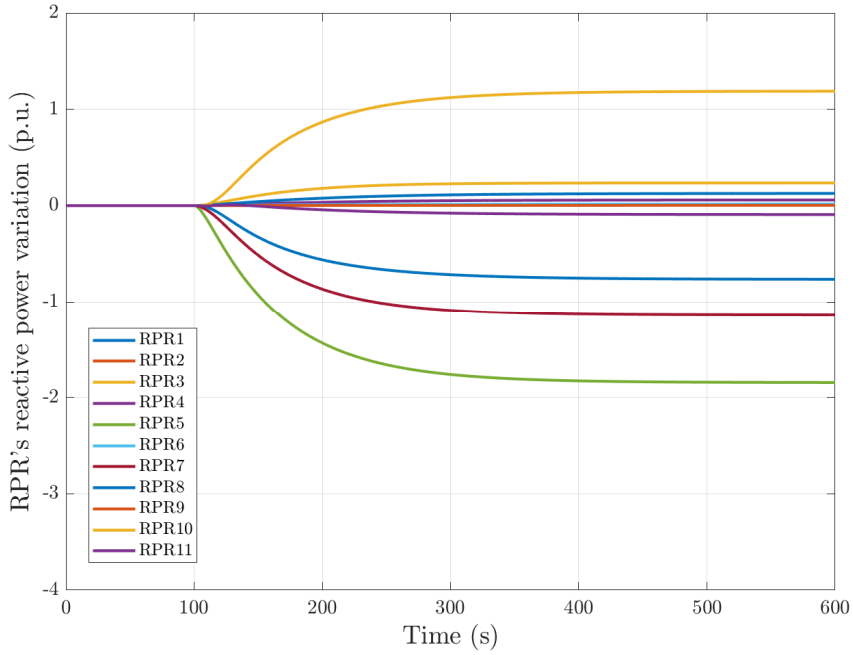


Figure 66 - Perturbation 3), architecture D, RPRs' reactive power

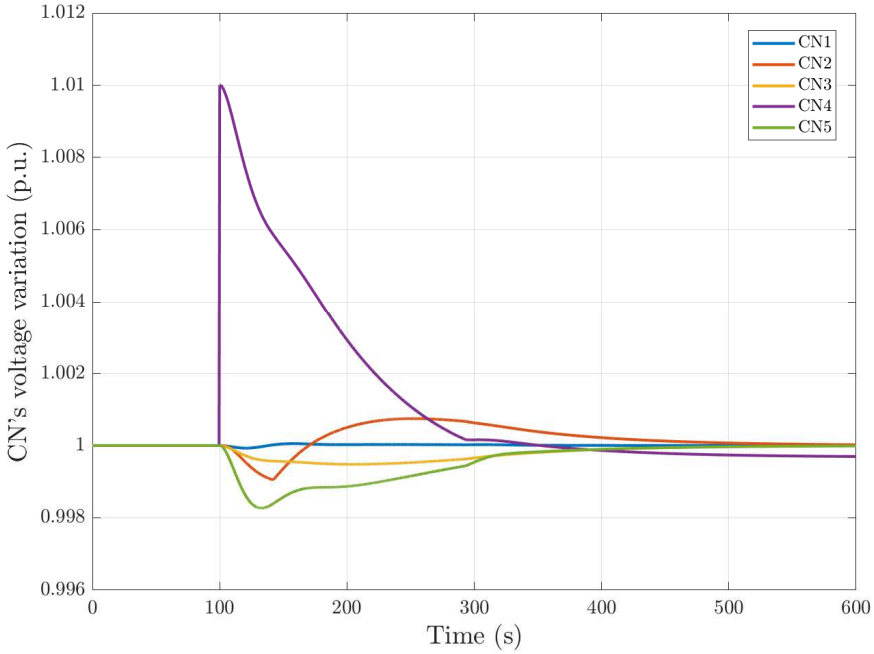


Figure 67 - Perturbation 3), architecture E, CNs' voltage

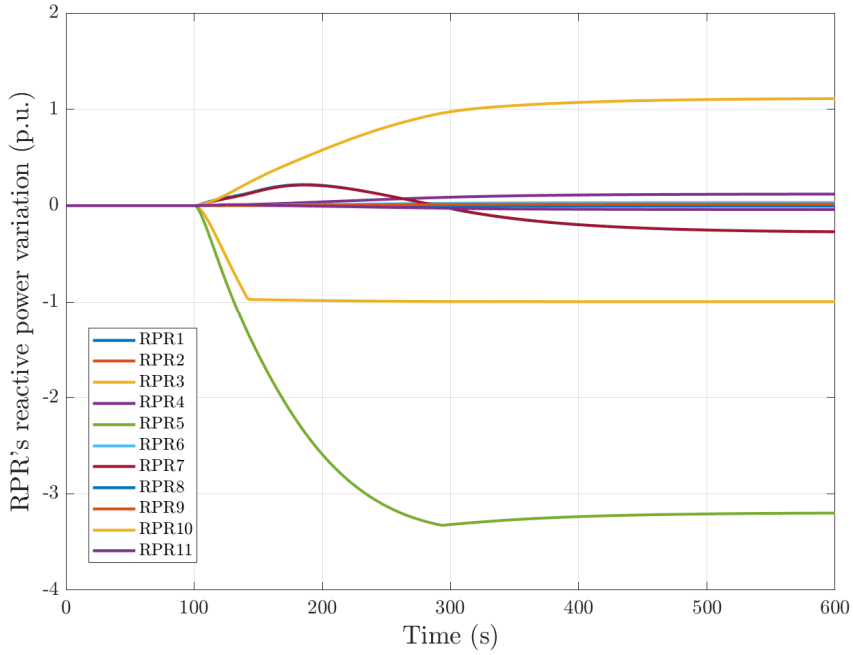


Figure 68 - Perturbation 3), architecture E, RPRs' reactive power

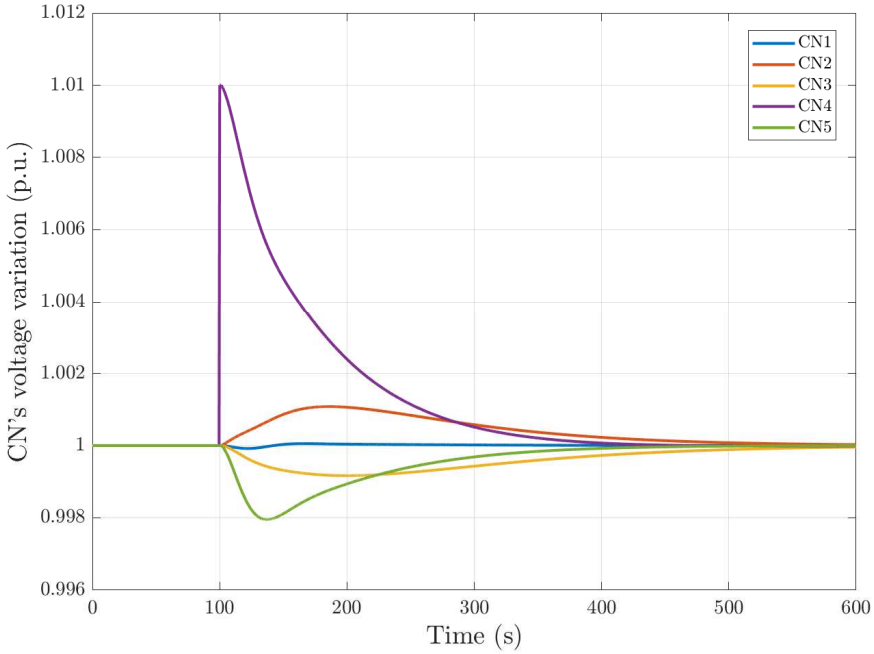


Figure 69 - Perturbation 3), architecture F, CNs' voltage

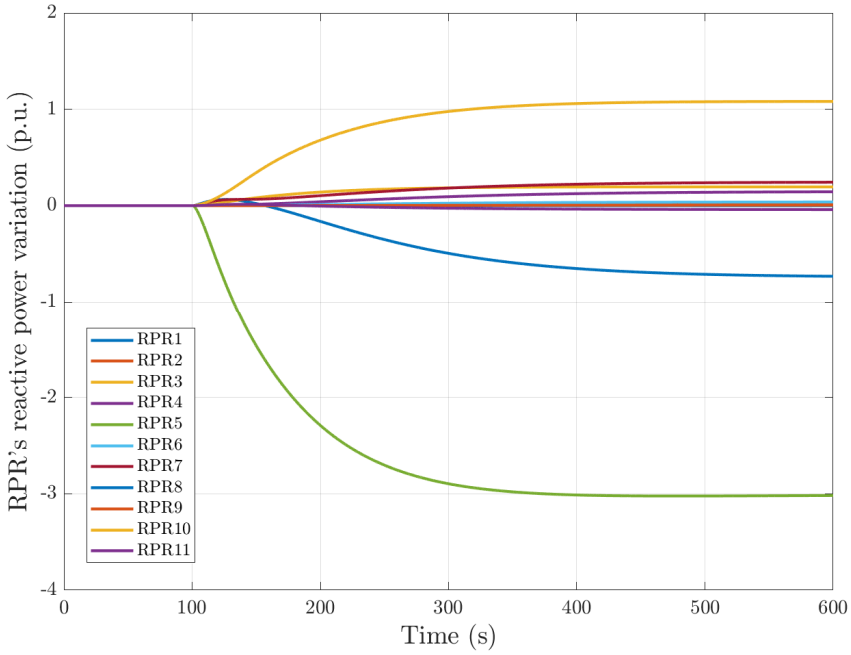


Figure 70 - Perturbation 3), architecture F, RPRs' reactive power

## 5.5. Results Comparison

The outcomes of the simulations above presented are summarized in Table 2, to allow an easier comparison of the achieved results. In the table, the results have been depicted using a qualitative performance rating, ranging from a non-acceptable response (--) to a very good response (++).

Table 2 - Summary of the results, qualitative performance evaluation

| **Architecture** | **Perturbation 1)** | **Perturbation 2)** | **Perturbation 3)** |
|---|---|---|---|
| A | - | -- | - |
| B | ++ | ++ | ++ |
| C | -- | - | -- |
| D | + | + | + |
| E | - | - | - |
| F | + | + | - |

According to Table 2, the only two architectures that exhibit at least an adequate response to all perturbations are B (based on Decoupling Control) and D. (the centralized LQRI controller using *qref* as control signals). As a result, these two architectures can be used for further tests in order to find the best solution for building up a secondary voltage regulator in a transmission network.

The results also suggest that all of the architectures that use the *livq* signal in a highly coupled transmission network for the scope of SVC are unsuitable. This is due to the RPRs' failure to distribute reactive power control operations correctly, as demonstrated by simulations. Furthermore, when comparing design D and F outcomes, it is clear that an SVR with entire network state knowledge has an advantage over a distributed controller approach. Indeed, the former enables improved reactive power sharing and, as a result, improved voltage management.

## 5.6. Control Adaptivity

As can be observed from Table 2, both architectures B and D have proven to be adequate for use as SVC in the case study transmission system, with acceptable

responses to all disturbances. However, both control approaches (decoupling for architecture B and LQRI for architecture D) on which these two SVR architectures are based require the determination of the power system's operative state (transfer function for the decoupling control, state space representation for the LQRI) for calculating the control parameters (decoupling matrix for architecture B, and state feedback gain matrix for D). This implies the need of recalculating the control parameters when the power system's operative state changes (e.g., due to loads' reactive power variation, lines' opening/closing, power plants' connection/disconnection, etc.).

As a result, while developing an SVR for SVC, a reasonable level of adaptivity must be incorporated (also due to the paragraph 2.2 explanation). While the definition of the algorithms for SVR adaptivity is beyond the scope of this study, it is worth noting how the two architectures indicated above respond to power system state fluctuation. As a result, the dynamic voltage regulation performance of designs B and D is shown in this paragraph when the control parameters are estimated in one operative state while the system is operated in another. Specifically, perturbation 2 (reactive power load variation of -10% on two load buses) is applied to the case study system with the SVR control parameters calculated for the simulations paragraph 5.4, but the sensitivity matrix $[S]$ of the power system is changed with one calculated for a low-load scenario (i.e., night operation, which presents several open lines).

Observing Figure 71 and Figure 72, architecture B is unable to control the voltage in such an operating condition. Conversely, architecture D (Figure 73 and Figure 74) is still capable of correctly manage the perturbation, despite the variation in the network matrix. This demonstrates the robustness of LQRI control, which guarantees asymptotic stability also in presence of variations/inaccuracies in the system's parameters [35]. Given these results, it can be affirmed that architecture D is the best one among the ones considered, for the goal of implementing a SVR for SVC on a highly coupled transmission network. It should be noticed that managing adaptivity in an LQRI regulator (which is the control approach used in architecture D) still requires a specific approach and additional blocks with respect to Figure 33-D ones, as discussed in [47].

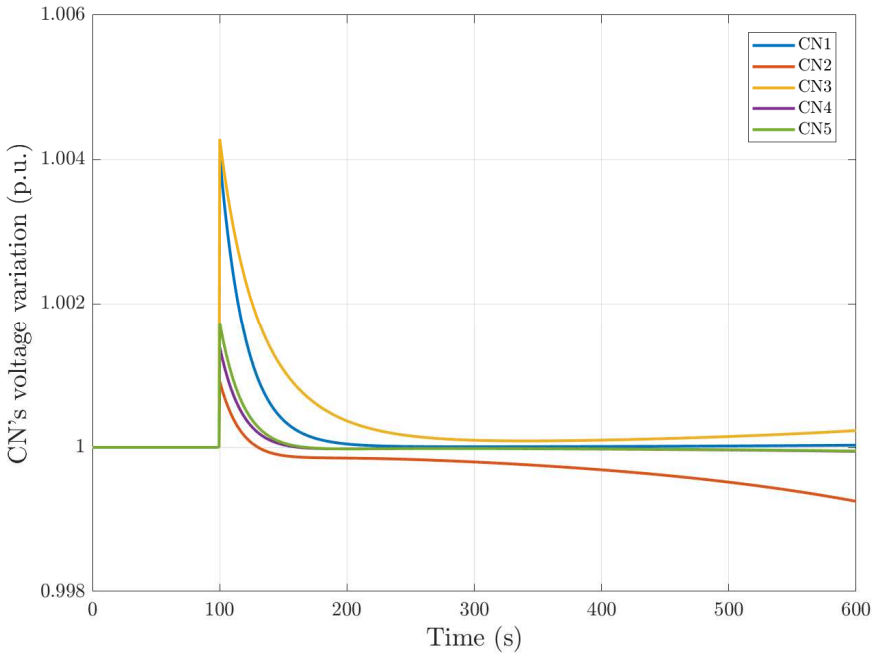


Figure 71 - Perturbation 2) applied to the low-load system, architecture B, control parameters calculated on networks' normal configuration, CNs' voltage

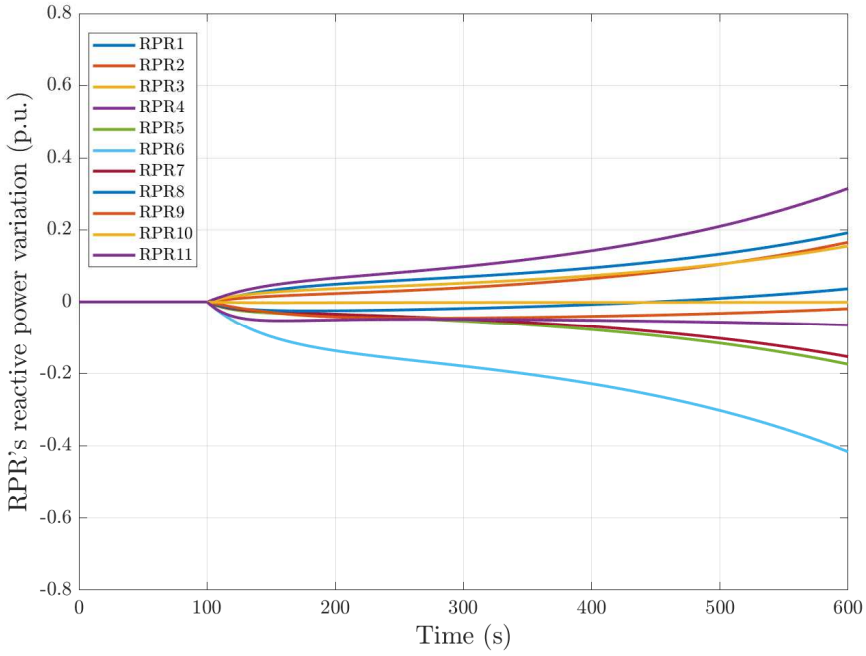


Figure 72 - Perturbation 2) applied to the low-load system, architecture B, control parameters calculated on networks' normal configuration, RPRs' reactive power

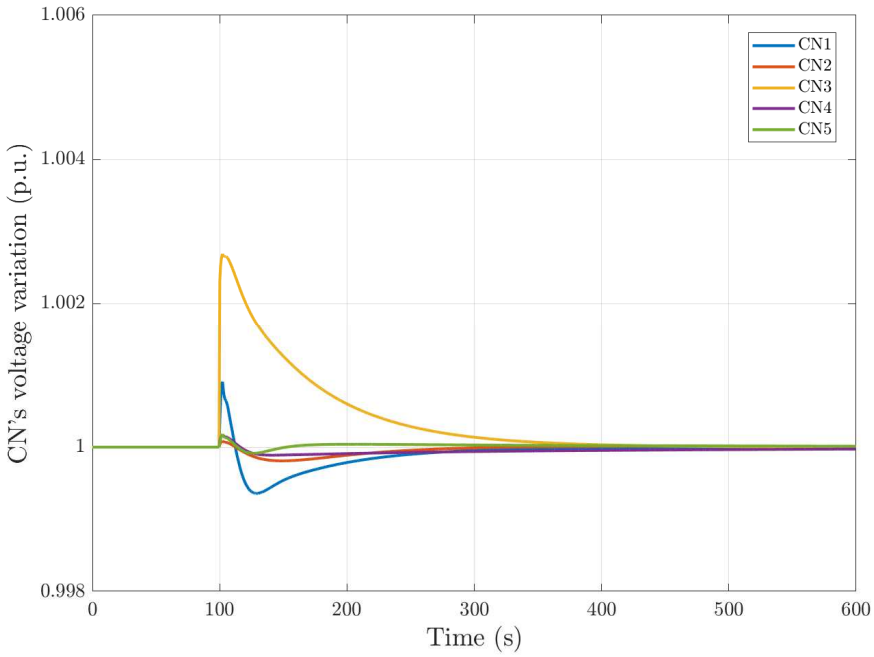


Figure 73 - Perturbation 2) applied to the low-load system, architecture D, control parameters calculated on networks' normal configuration, CNs' voltage

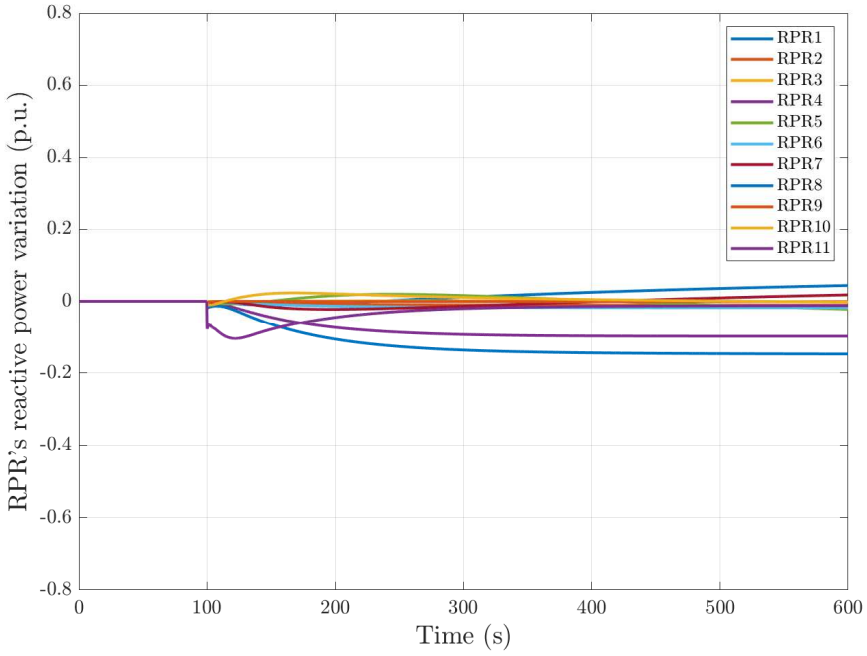


Figure 74 - Perturbation 2) applied to the low-load system, architecture D, control parameters calculated on networks' normal configuration, RPRs' reactive power

## 5.7. Remarks

It should be noted that the best architecture for implementation as an Italian SVR, i.e. the controller based on centralized LQRI with *qref* control signals, no longer relies on the concept of control area, which appears to be an outdated rationale as a result of the various network changes described in the paragraph 2.1 study. In fact, once a portion of the network has been chosen, which could be an entire region (the region is currently a set of control areas that refer to a single Terna Control Center), all of the power plants belonging to it will be managed by a single SVR in an optimum manner for the voltage control of each selected CN (the difficulty of finding a border for this controller remains unsolved, but theoretically, a border for each network to be voltage controlled can always be found, even if it is the entire Italy).

Regarding CNs, the problem of finding them on the basis of the long-term overall decrease in short-circuit power of strong nodes (due to RES massive exploitation and grid improvement, as presented in paragraph 2.3) is greatly reduced, as the geographical portion of the territory (and therefore the number of HV nodes within it) will be much greater compared to the present control areas. Furthermore, by having an SVR capable of reacting to network changes, the SVR will be able to adjust CNs based on regulatory optimizations that can be performed.

Finally, the issue of the controller's internal parameters adaptivity, which caused the network event described in paragraph 2.2, is overcome with this type of new controller due to its intrinsic stability and robustness, as well as the ability to real-time recalculate the characteristic matrix $[K]$ during changes of network operating conditions. In this regard, Paragraph 6.2 describes the full transition from one matrix $[K]$ to another gain control matrix $[K']$, reacting to a crucial network modification.

# 6. LQRI Implementation as SVR for Italian Transmission Network

In the previous Chapter, after intensive testing of various voltage architectures based on two distinct approaches, the centralized LQRI sending *qref* signals was determined to be the most suitable for SVR for the Italian SVC.

However, several issues must be solved to real-world design such SVR, among which there is the determination of the system states to be fed back to the controller for ensuring its correct operation. This requires identifying the variables that are directly measured in a transmission system, determine if they can be useful for the LQRI state feedback, and finally study the different solution effects on the regulation performance. In this regard, the focus is here made towards solutions that can be applied at short/medium-term, thus considering as much as possible the present voltage control architecture and the present measurement and communication infrastructure [54]. Moreover, a specific effort is made towards solutions that do not need the implementation of complex state estimation systems, to avoid increasing the complexity of the control system design and operation.

Additionally, the RPRs can be connected and removed during system operation, as well as their remote reactive power control function can be enabled and disabled. As a result, the system's actuator number changes several times throughout time. This special topic of LQRI optimal control application to SVC in a power system is handled specifically here, using a bumpless control transfer logic scheme.

## 6.1. State Feedback Selection and Measurement for the Application of an LQRI as SVR

The selection of the state variables to be fed back to the controller is critical, because in a complex system there are a huge number of states and using all of them may be impractical (or even impossible). However, ignoring some states (by applying simplifying hypotheses to the typical state-space representation of the system used to create the LQRI) may result in poor control performance. Moreover, even if the LQRI designed on the simplified model provides acceptable results, the chosen states may still be unusable for the feedback, being them not available in the specific application (because they are not measured, or even are not measurable). To address this issue, a new set of sensors for measuring a non-measured state can be added to the controlled system, or a state estimator can be introduced to derive the state based on the available measures. However, this increases the system's cost and complexity. As a result, it is worth investigating if the variables currently recorded in the Italian transmission system (in terms of the scope of secondary voltage regulation) can be employed, either directly or via a simple signal conditioning strategy.

The simplest approach for defining the feedback states for an LQRI regulator is to take the *x(t)* state array from the controlled system's state space representation. Indeed, it is sufficient to construct the mathematical model of the system and then transform it into its state-space form (if it was not explicitly constructed in such form) to acquire the list of feedback signals to be routed to the controller. Such list can be also inferred from other forms of mathematical model. As an example, in block diagram form it is possible to use as state array the output signals of the integrator blocks (although

this requires manipulating the model equations to use only integrations in the model, and never derivations). However, the determination of the $[A]$ and $[B]$ matrices of the state space representation is critical for the controller design, as shown in the previous section, thus building the system model in such form is considered a required step.

### 6.1.1. State feedback availability for LQRI

In this study, the system mathematical model used for simulations and tests is the same explained in paragraph 5.3 following the hypothesis in paragraph 5.2, thus the LQRI as SVC uses the voltage of the CNs for the integral feedback. Such variables are measured either through a SCADA system, or through a more modern PMU-based system [55],[56],[57]. The latter is here considered, and this specific feedback section is kept constant in all the different simulations.

Given the above-described simplifying hypotheses, the system's state array to be transmitted back to the LQRI is made up of the RPRs reactive power loop output signals (i.e., the signal at the output of the integral part of its PI regulator). This option serves as the foundation for comparing the other alternatives presented in this work. While this is the best solution because it is completely consistent with the mathematical description of the LQRI controller, it is not possible to use the reactive power loop output signals as the feedback set of states. Indeed, such signals are not now available to the SVC controller because no previous requirement was established. Thus, it is required an overhaul of the voltage control system in order to use them, which includes changes in the transmission operator systems, in the data communication infrastructure, and in the control and measurement system installed in each RPR. An often-applied solution to this issue is the design of state observers, for inferring the required states from the available measures, through Kalman estimators or other approaches [58], [59]. However, the simplification hypotheses depicted in the paragraph 5.2 make it possible to achieve a simple model, whose complexity mainly lies in the significant dimension of the related matrices for a transmission system (where hundreds of nodes and tens of RPRs are present). Thus, in order to avoid either a complete redesign of the voltage regulation architecture or the development of sophisticated state estimators, it is worth

investigating if measures currently delivered to the current SVC system can be used for feedback to the new LQRI regulator. Indeed, these can be utilized as a direct substitution for the desired state or to estimate the state using basic algebraic equations.

### 6.1.2. Available measures usable for state feedback to the LQRI as SVC

At present, there are several measured variables that are sent from each RPR to the transmission network operator for control and management purposes. These signals are exchanged through a SCADA system, with specific limitations in terms of measurement and transmission performance (e.g., sampling times of about 2-4 s). Such performance may increase in the future (e.g., sampling rate up to 0.02 s), through the introduction of PMU-based measurement and communication systems for the most significant variables, like it is done at present for the voltage of the CNs.

Among the several measured variables, the following have some usefulness for the scope of this study:

- Voltage at HV (network) terminals of the RPR ($v_{AT}$);
- Voltage at MV terminals of each generator/source of the RPRs ($v_{MT1}$, $v_{MT1}$, etc.);
- Reactive power injected by the RPR in the HV transmission network ($q_{AT}$);
- Reactive power of each generator/source of the RPRs ($q_{MT1}$, $q_{MT1}$, etc.).

These variables are depicted in Figure 75-a, where a generic RPR is shown. The RPR is connected to the HV transmission network in the point of common coupling ($P_{CC}$) and is composed by several generators/sources. The latter are endowed with their primary voltage control loops and transformers ($x_{T1}$, $x_{T2}$, etc.), and are coordinated in order to provide the required reactive power to the network.

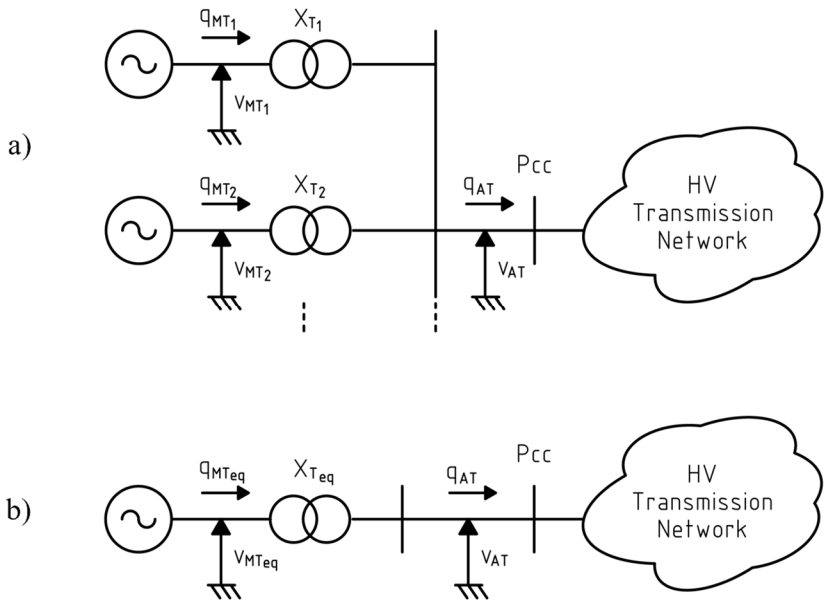


Figure 75 - Notional scheme of an RPR composed by multiple generators/sources: a) multi-generator system, b) equivalent single generator model

The PVC loop is also of relevance because the mathematical model only covers RPRs used for SVC. This means that the sources' voltage at the terminals is directly regulated and the reactive power is the result of that voltage's interaction with the HV network. As an outcome, the first step in this scenario is to check if the measured voltages may be utilized to replace the required status feedback. The voltage at the MV terminals in the above-depicted mathematical system model is proportional to the reactive power loop output signals, i.e., the mathematically determined state. This is due to the fact that PVC systems and generators/sources are in steady-state and hence have constant gains. However, such measure is not constituted by a single signal, but by multiple ones if the given RPR is made up by several generators/sources. Consequently:

- the MV voltage signal array for each RPR must be properly conditioned, for obtaining a single value that is representative of the entire RPR as a whole (i.e., building its single-generator equivalent model, as shown in Figure 75-b;
- the MV voltage signal array can be used as it is, leading to a rise in complexity (system order and matrices size) in the LQRI controller design.

The second method involves to use the voltage at the RPR's HV terminals, which already considers the entire set of generators/sources as an aggregated equivalent.

However, because such a measurement location is separated from the generators/sources by transformers, it generates an offset signal in relation to the MV one. Although the dynamic is largely retained, the existence of voltage drops on the transformers that vary with the reactive power flow may cause some transients to be reinforced or dampened.

Using the reactive power injected by the RPRs in the transmission network can be considered as the third solution, but it presents some criticalities. In fact, in a transmission system the reactive power flows are a consequence of the voltage differences between the network nodes. Thus, both the reactive power of a single generator/source and the reactive power of the entire aggregated RPR are affected by the interaction of the voltage at the generator/terminals source's with the voltage of the network node to which the RPR is attached. As a result, reactive power is proportional to both the state of the single RPR and the state of all the other RPRs in the network. Because of the presence of mixed dynamics that were not addressed during the LQRI design process, it is difficult to directly employ reactive power as a substitute for state feedback for the LQRI SVC regulator. For this reason, it makes no difference whether the reactive power of each individual generator/source or the aggregated reactive power of the entire RPR is used, as the latter is roughly equivalent to the sum of the former (the power measured on the HV side includes the transformers reactive power, which can be considered constant given the system operation at voltages that are close to the rated ones).

A fourth approach can be proposed, which uses a combination of most of these available measures to both make available the required state feedback signal and solve the issue of using additional signal conditioning for providing the voltage of the equivalent generator/source from the several separated signals sent by each RPR. In particular, it is possible to use the measures that already consider the RPR as a single source (i.e., the HV ones), to evaluate the equivalent MV voltage of the aggregated source.

This can be made using the following equation:

$$v_{MT_{eq}} = v_{AT} + x_{T_{eq}} \cdot q_{AT} \tag{6.1}$$

where $v_{MTeq}$ is the voltage at MV terminals of the equivalent generator/source for the RPR, $v_{AT}$ is the measured voltage at HV (network) terminals of the RPR, $x_{Teq}$ is the equivalent reactance of the MV/HV transformers of the RPR, and $q_{AT}$ is the aggregated reactive power of the RPR. In the following paragraph, all these approaches are tested by means of simulations, and the results are presented, discussed, and compared with the mathematical defined state.

### 6.1.3. Dynamic regulation performance tests of different state feedback signals

In this paragraph the system performance using the above-mentioned different state feedback are presented. All the simulations are performed with the same LQRI controller, designed using the simplified mathematical model in state-space representation discussed in Chapter 5 [60].

The following results are obtained in response to a 1% difference in the SVC voltage references for two CNs, while the other three are held constant. Simulations with load variation have shown comparable findings and are consequently not displayed here. Furthermore, in order to eliminate the effect of various factors, the simulations provided here are performed with all measurement signals sampled at the PMU-based performance level. However, simulations with a mixed solution were also performed in relation to the current system condition (CNs voltage measured with PMU and state measured and sent through SCADA). Aside from the presence of minor steps in the resulting traces due to the piecewise input signals, no substantial change is noticed.

The first result concerns the system response while using the state feedback defined through the mathematical modeling approach (i.e., the set of reactive power loops output signals). This result is used as a benchmark for evaluating the other solutions.

The Figure 76 depicts the CNs voltages, which reach the expected reference values with smooth transients and limited coupled dynamics. Being such result obtained with a simulation of a system model that is more complex than the one used for

designing the LQRI, it is demonstrated that the simplifications Chapter 5 do not impair the controller design, while reducing its complexity.

The CNs' voltages for the controller using the RPRs' MV as feedback is shown in Figure 77. Specifically, the model here used for the simulation presents a single generator/source for each RPR, in the hypothesis of having already done the proper conditioning on the measures for achieving a single signal from the multiple MV voltages coming from the field. By comparing the

Figure 76 and Figure 77 results, it is evident that the MV voltage is a suitable substitute for the system state (provided that the correct base changes for the per unit representation are used).

By using the voltage measured on the HV side of the RPRs, the Figure 78 results can be obtained. These are similar to the previous results, despite the presence of the voltage drop on the transformers. It is expected that a more appreciable difference may be found in presence of significant reactive power variations, but such event cannot be evaluated with the linearized model here used. Simulations made using the reactive power as state feedback showed significant issues with the system control, being the reactive power signals dependent on both the single RPR's and the rest of the system's behavior. After introducing a gain (experimentally determined) for adapting the reactive signals range to the voltages one, the results show the unsuitability of such feedback (voltage oscillations and increased cross-coupling between the CNs' transients, shown in Figure 79).

Finally, the results using the feedback obtained by means of the fourth approach of paragraph 6.1.2 (i.e., obtaining the MV equivalent voltage for each RPR using the reactive power and voltage measures on the HV side) are shown in Figure 80. The results show that the proposed algebraic state calculation made on the basis of the available measures is a feasible solution for the LQRI as SVR. Moreover, the comparison of Figure 80 with Figure 76 shows equal transients, in both shape and magnitude. Thus, this solution can be suitable for introducing an LQRI controller for SVC in the transmission

network, while limiting its complexity and removing the need of a complex state observer.

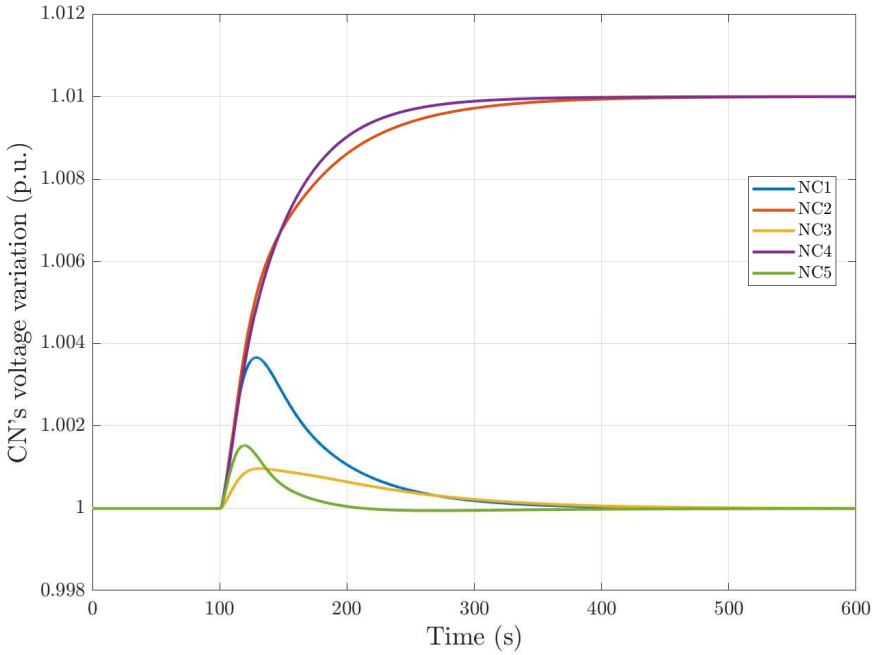


Figure 76 – CNs' voltage, LQRI with the state feedback defined using system's mathematical model

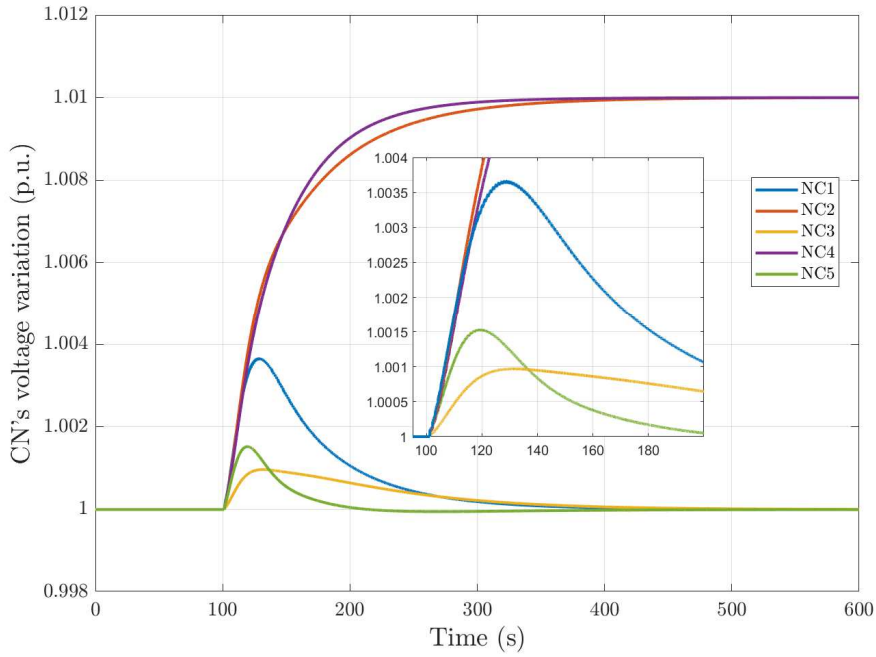


Figure 77 – CNs' voltage, LQRI with the measured RPRs' MV voltage used as state feedback

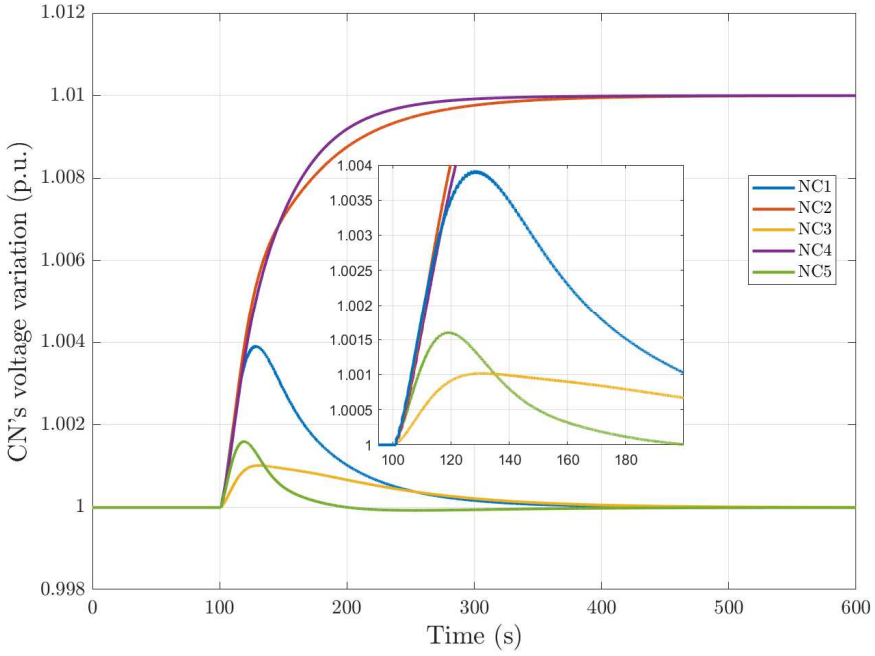


Figure 78 – CNs' voltage, LQRI with the measured RPRs' HV voltage used as state feedback

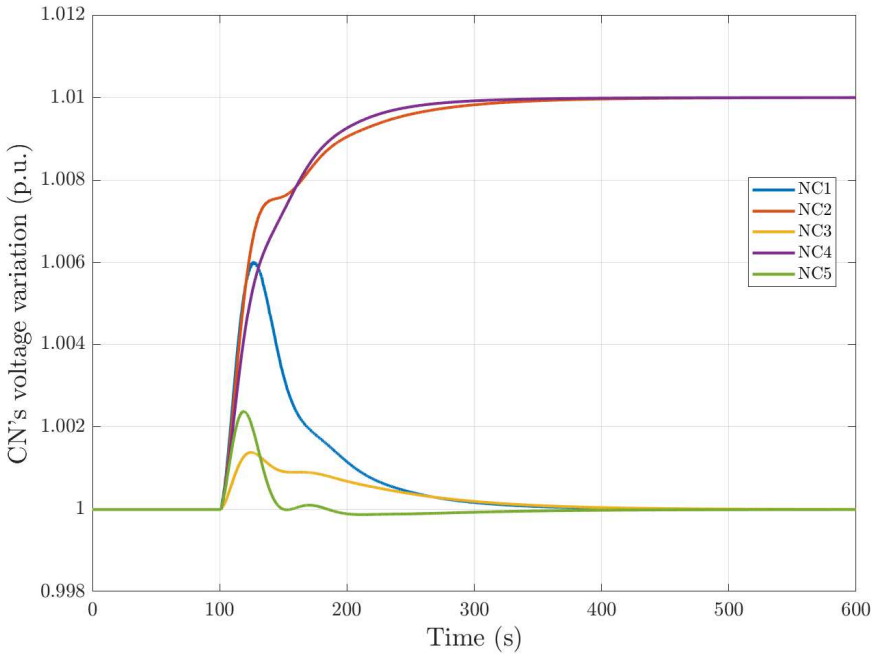


Figure 79 – CNs' voltage, LQRI controller with the RPRs reactive power used as state feedback

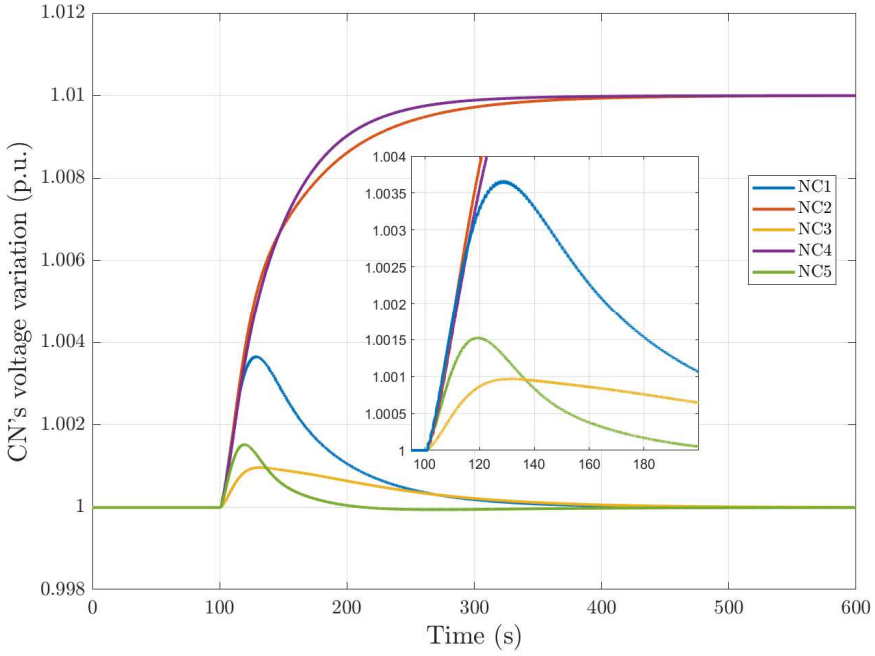


Figure 80 – CNs' voltage, LQRI controller with the calculated MV voltage used as state feedback

## 6.2. Bumpless Transfer Scheme for a LQRI Controller Used as SVR

The determination of the feedback control gain matrix $[K]$ is based on the determination of the system's state-space representation matrices, and thus on the solution of the Riccati equation (as shown in paragraph 3.3). However, it is relevant to notice that the application of an LQRI to the transmission system SVC is effective as long as the system (3.1): does not change in structure, does not change in parameters, works in an operating point that is not so far from the original one (i.e., the one used for the calculation of the Riccati equation solution $[S]$). If these constraints are violated, the equation model (3.1), the matrix $[S]$, and consequently the control gain matrix $[K]$ must be determined again. It should be noted that changes may occur not only in magnitude of the matrices, but also in their dimensions.

One of the operations causing a change in the system structure is the enabling or disabling of the SVC function in the RPRs, which can be mathematically seen by the (3.1) system as a change in the number of system states and input signals, and by the controller as a change in the number of the actuators. This makes it necessary to

recalculate a new feedback control gain matrix [$K$], which has a different size and values in respect to the previous one, and to apply the control signals to the new RPRs' set. (It is important to notice that RPRs can have the secondary voltage control function enabled or disabled, provided that the constraints on system's controllability given in paragraph 3.3 are verified, i.e., the number of RPRs must not be lower than the number of CNs). [$K$] doesn't have a dynamic because it is a matrix of algebraic gains. Thus, any alteration in its value causes an immediate shift in the reactive power reference signals transmitted to the RPRs. The results showed in the following demonstrate that the outcome is an undesirable transient on both the reactive powers and voltages of all nodes. As a result, the LQRI controller must have a bumpless transfer function to reduce the voltage transient that occurs after the control system change caused by the enabling or disabling of the RPR's SVC function. Such function can be designed to face both programmed and unexpected events, providing the best results in the former case, and an acceptable behaviour in the latter case. In this study only the base design is considered, taking into account programmed variations.

### 6.2.1. Bumpless transfer design

As previously explained, a change in feedback control gain matrix [$K$] (and a variation in RPR's number, depending on the specific event considered) is required when the system changes its structure, or change its parameters, or works in an operating point that is far from the original one. Such change can be considered as a complete control system switch, from the controller with the [$K$] matrix to a new one with the newly calculated [$K'$] matrix. This change can be managed using a proper bumpless transfer technique, whose task is to guarantee smooth transients and continuity of the control signals when switching from a controller to another. Several proposals are available in literature for obtaining the bumpless transfer. Some of them are based on $H_\infty$ [61], other are based on Model Predictive Control [62], and there are even techniques capable of providing anti-windup function for controllers with integral elements [63]. In [45] the technique proposed in [63] has been chosen and improved for a decoupling PI regulator applied to the transmission network SVC. Hence, for this work the same

technique has been selected, and properly modified and improved, for solving the switching issue related to an LQRI control.

The base idea of the technique here used is to provide a conditioning signal to the controller that needs to be activated, on the basis of the output of the controller that needs to be deactivated. Such conditioning signal must prepare the new controller for the switch over, ensuring a limited impact of the discontinuity on the system. In Figure 81 is depicted the bumpless transfer scheme here applied, which allows to switch between two properly dimensioned LQRI controller, identified by means of the two feedback control gain matrices $[K]$ (the former one) and $[K]'$ (the entering one). Before the controller switch, the system is controlled by the upper branch (by applying $qref_1$ to the output), while after the switch the control is taken by the lower branch (by applying $qref_1'$ to the output). The output of the new controller must be initialized as closely as possible to the output of the old one in order to prevent a discontinuity in *qref* when shifting the controller, by means of a conditioning signal based on the error between the actual control output towards actuators (*qref*), and the controller output ($qref_1$ or $qref_2$). Using the output error between the controllers allows not only the conditioning signal to force them to be equal, but also ensures that the conditioning signal is automatically disabled when the controller takes action (its output and the signal to actuators becomes equal).

Being the technique here used based on the equality between the two controller outputs, an integral component is required. Differently to what has been done in [45], where the PI controllers where capable of nullify the input error, here additional integrators (marked as *Int* in Figure 81) must be added, being the LQRI integral action applied only on the CNs voltage feedback. Although such new integrators allow the bumpless switch between the two controllers, they introduce a new issue. I.e., they cause an offset in the system feedback for the new controller, leading to a variation in the controller response in respect to the design one. Thus, additional feedback must be added to the integral function, to ensure the integrator unloading after the controller switching. The gain of the integrator unloading feedback can be selected freely, on the basis of the desired system response. In general, selecting a high gain ensures fast recovery of the

state feedback offset, but causes an appreciable transient on the system output (which can reach the same magnitude of a switch between the controllers without the bumpless function). Conversely, selecting a very low gain ensures negligible transients in the system at controllers' switch and in the following period, but keeps the states offset for long time and thus makes the controller work outside its design point. In this study, a feedback gain equal to 0.1 has been selected using simulations. As stated in [63] and [45], the primary feedback of this bumpless transfer technique double as anti-windup compensators, if saturations are present in the control signals (Figure 81).

Besides the integral action on the controllers' output error, the conditioning section must also ensure the proper size of the feedback signals array, as well as their physical and mathematical coherence with the states used by the LQRI controller. In fact, there are several issues that make it impossible direct feedback of the integrator output to the state. First, the size of the system state array *z(t)* and the size of the

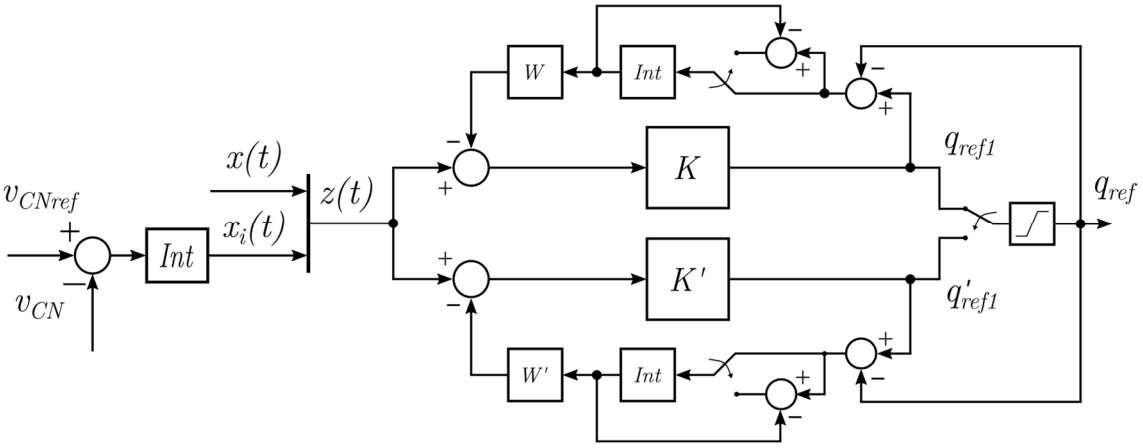


Figure 81 - Bumpless transfer scheme for LQRI as SVR

controller output to actuators array *qref* are different. Second, if the switch between controllers is initiated by a change in RPRs number, the two controllers also have diverse output array dimension to each other ($qref_1$ vs. $qref_2$). Third, the output to actuators is proportional to reactive power, while the input state is proportional to different physical variables depending on the chosen states to be fed-back to the controller. For the latter, in this work the feedback from RPRs is the output of their reactive power loops, thus being proportional to a voltage, while the integral part feedback is the output of the CNs

voltage error integrators, thus being proportional to a reactive power. Thus, the conditioning section must apply three steps to ensure the correct feedback. Step one: the *qref* linked to the RPRs that are not used for the SVC are constrained to zero. Step two: the controllers' output error linked to the same RPRs is removed from the feedback. Step three: the collection of reactive power reference errors that results is multiplied by a suitable matrix, represented by $[W]$ and $[W']$ in Figure 81, to ensure mathematical and physical coherency.

The latter are calculated as follows:

$$[W] = [K]^{-1} \tag{6.2}$$

$$[W'] = [K']^{-1} \tag{6.3}$$

where the matrix inversion operation is substituted with the Moore-Penrose pseudoinverse when required (i.e., for all the cases in which $[K]$ or $[K']$ are not square matrices). In Figure 81, the operations on the signals arrays to match the dimensions are not shown, to retain readability.

### 6.2.2. LQRI with bumpless scheme tests

In order to test the effectiveness of the above described bumpless transfer technique, the Chapter 5 model has been used. As described in Chapter 5, the system is modelled using the network's sensitivity matrix $[S]$ and the RPRs' first order dynamic. The $S$ matrix is determined fixing a standard network's working point and solving the load flow problem. The scheduled deactivation of the SVC function in one RPR perturbs the system. This is accomplished by cutting off the RPR's *qref* input signal while maintaining a constant level of the reactive power it was injecting into the grid. The simulation results for a SVR with (Figure 82, Figure 83, and Figure 84) and without (Figure 85, Figure 86, and Figure 87) the bumpless transfer function are described in the following. Since the model is linearized, all CNs' initial voltages are set to 1 *p.u.* although having a reactive power equal to 0 *p.u* (the simulations evaluate the variations in respect to the operating point). It is relevant to notice that the reference values sent to the

RPRs (Figs. 5 and 8) are different from the reactive power injected into the network (Figure 83 and Figure 86), because the latter depend also on the voltages on the network, and thus on the reactive power of the loads and all the other RPRs.

At time equal to 20 *s,* two CNs' voltage reference is changed (from 1 to 1.01 *p.u.*), with the aim of demonstrating the LQRI control's effectiveness in managing system voltage and reactive power. As clearly visible in Figure 82 and Figure 85, the LQRI control is able to leading the two CNs to their new setpoints, while keeping the others at a constant level. This is obtained by adjusting the reference point for reactive power (Figure 83 and Figure 86), and subsequently the reactive power injected into the network (Figure 84 and Figure 87), of all the RPRs.

At time equal to 300 *s,* the SVC function in one RPR is disabled leading to the need of changing the feedback control gain matrix $[K]$ to $[K]'$. As a consequence, the reactive power reference of chosen RPR has been set to zero and it stops following the reactive power command from the LQRI regulator (Figure 83 and Figure 86, blue trace), and its reactive power injected into the grid only follows voltage variations in the adjacent nodes (Figure 84 and Figure 87, blue trace). The modification of matrix $[K]$ occurs concurrently. As a result of the latter, the system without a bumpless transfer function experiences undesirable CNs voltages dynamics (Figure 82) since all reactive power references changed abruptly (Figure 83). On the other hand, the system with the bumpless transfer function shows extremely little voltage variation (Figure 84) because it requires the controller output to match the entering controller output before the switching instant. The effect of the integrator unloading in the conditioning signal section of the bumpless transfer scheme is also visible from Figure 85 to Figure 87, with the reactive powers that slowly change towards their correct steady-state values (the ones presented also by the system without the bumpless transfer function), and limited voltage variations.

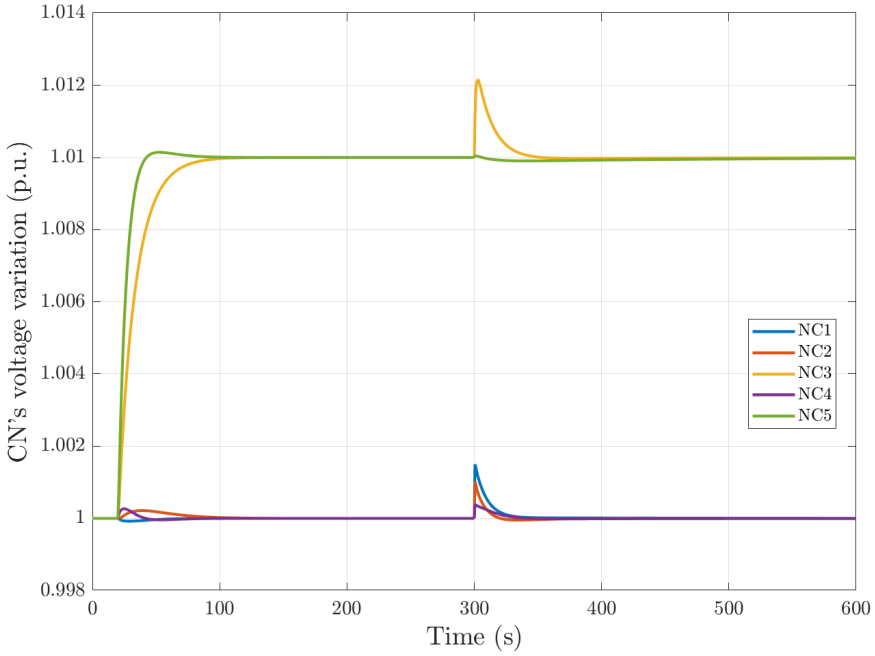


Figure 82 - CNs' voltage with LQRI control without bumpless transfer

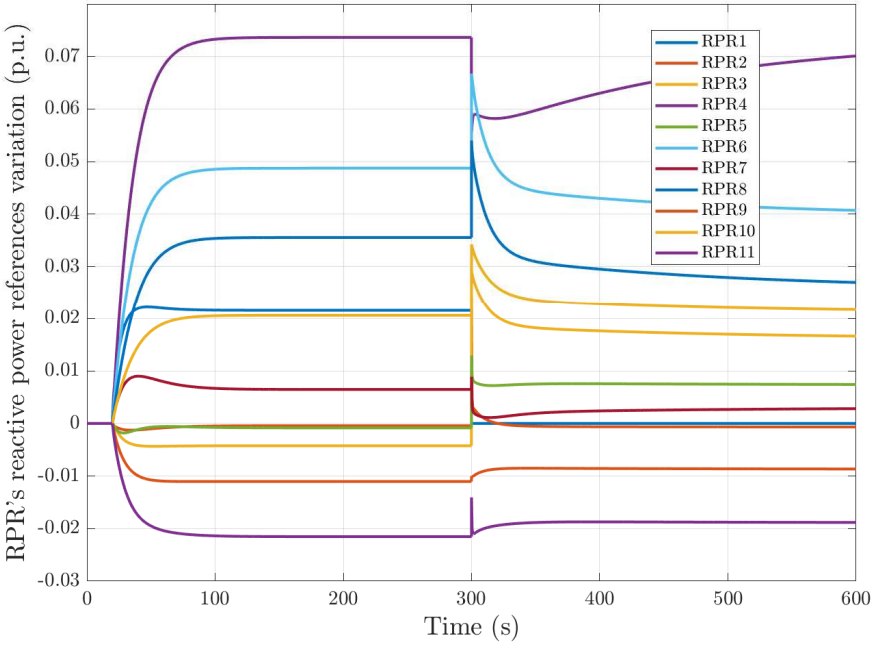


Figure 83 - Reactive power references variation of RPRs with LQRI control without bumpless transfer

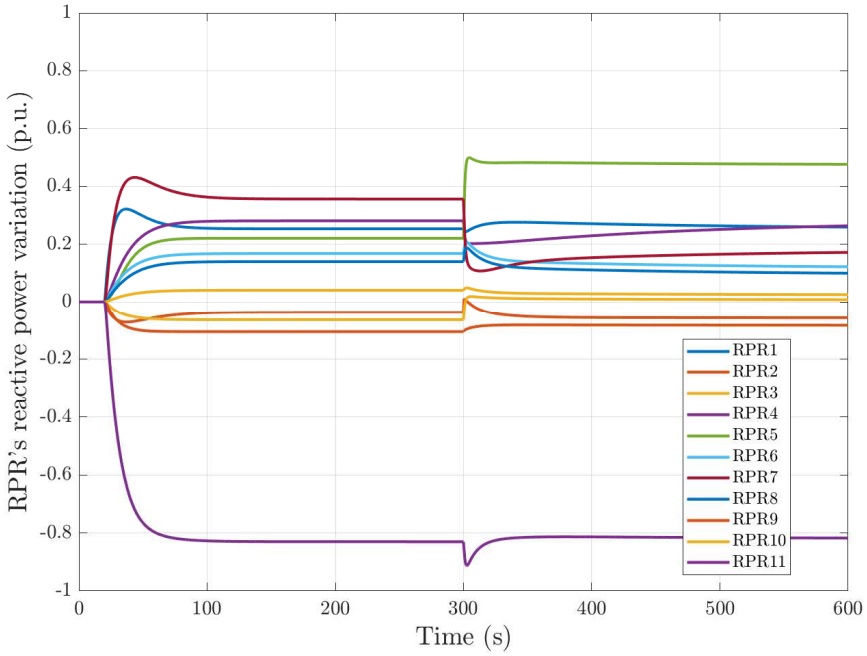


Figure 84 - Reactive power variation of RPRs with LQRI control without bumpless transfer

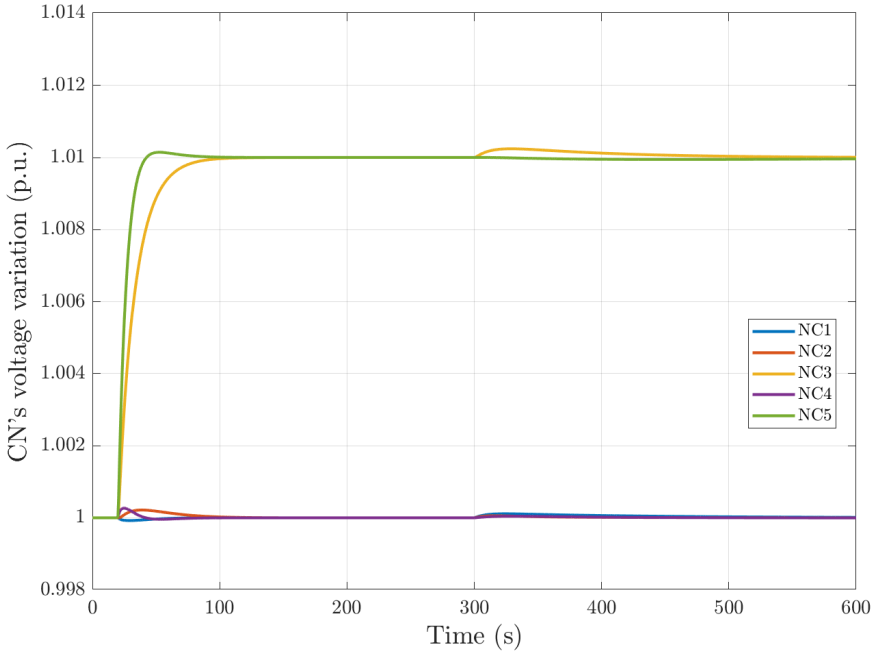


Figure 85 - CNs' voltage with LQRI control with bumpless transfer

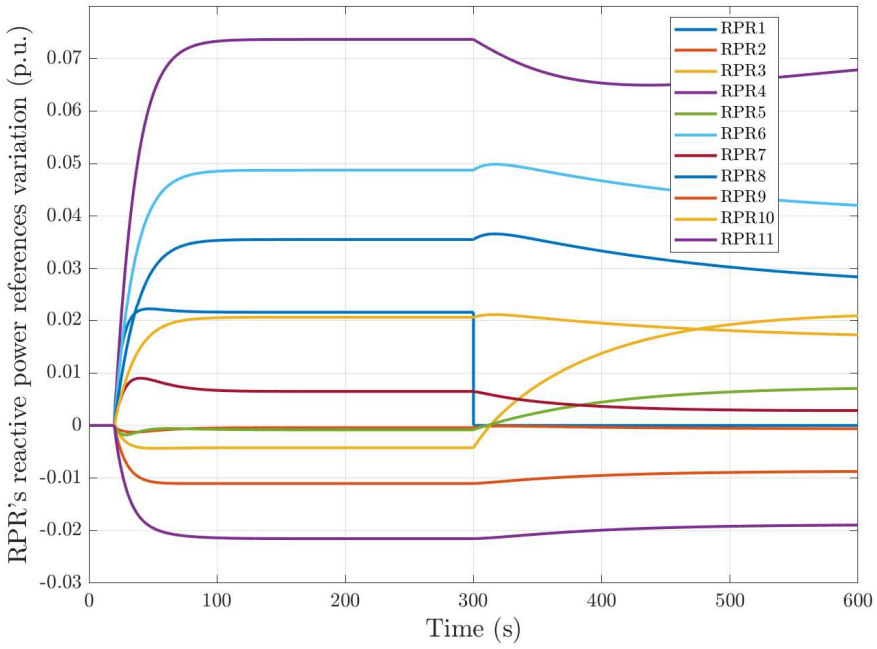


Figure 86 - Reactive power references variation of RPRs with LQRI control with bumpless transfer

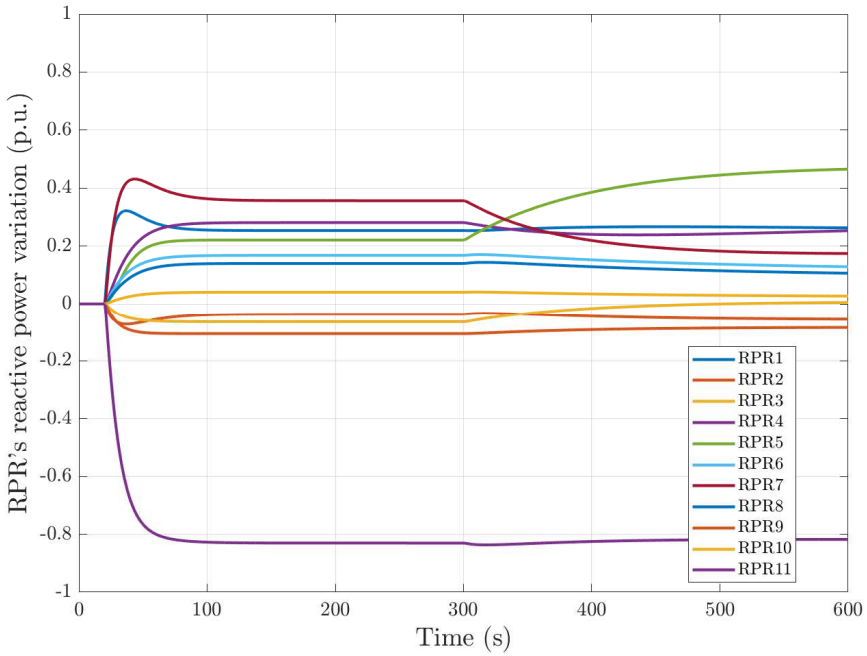


Figure 87 - Reactive power variation of RPRs with LQRI control with bumpless transfer

# 7. Non-Linear Model and Tests

In order to support the findings presented in the preceding Chapter (i.e. paragraphs 6.1 and 6.2), an improved and more complex model (shown in Figure 88 as a blocks scheme) (with respect to the one of paragraph 5) of the Italian transmission network was designed and implemented. Furthermore, this kind of more detailed model is useful for testing the real SVR LQRI model (which will be used by Terna, the Italian TSO) in off-line mode on a HIL (Hardware In the Loop) or SIL (Software In the Loop) concept scheme. The LQRI model developed for Terna, which is able to be compiled in C language and to run in a 0.5s real-time, has been built up by the laboratory D-ETEF (Digital Energy Transformation & Electrification Facility) team of the Engineering Department of University of Trieste, to whom the thesis author belongs. Thus, for the sake of completeness, some peculiar design features are here presented, without going deep on the whole SVR LQRI model.

## 7.1. Modelling Hypothesis and Case Study

This model included all buses with nominal voltages of 220 and 150 kV, in addition to the previously (paragraph 5.1) examined 380 kV buses. As a result, the total

number of buses increased from 65 to 416. The integration of 5 power plants capable of supporting secondary voltage regulation was considered within this detailed model. However, one of these power plants stayed idle within the specific operating scenario chosen for this research (a snapshot obtained from the real transmission system in operation). In this scenario, a single CN was used to boost the efficacy of the bumpless LQRI control. The model used in this section is based on a recursive power flow of the whole network. A short explanation about power flow calculation is outlined in Appendix B.

Therefore, the voltage of all the case study buses (which includes the CNs voltages $v_{CN}$) is calculated by means of a power flow algorithm, operating on the transmission system model, which is iterated until convergence at every sampling step of the overall simulation. In particular, the specific power flow algorithm utilized is Newton Rapson, with a sampling step for the power system simulation equal to 0.1 s. Conversely, the LQRI controller runs at 0.5 s sampling step, which is representative of a possible real case implementation in the SVC architecture. The generators' voltages ($v_G$) are an input to the power flow algorithm and are determined by the voltage regulation architecture's different layers. Specifically, the generators' voltages are the output of a reactive power control loop, which uses as a reference the *qref* signal coming from the LQRI controller. The latter is compared with the actual reactive power injected by the power plants $q_{AT}$, which is a power flow output, to calculate the error for the reactive power control loop. The *qref* are obtained using the SVR LQRI (most performing architecture of paragraph 5.6), based on the bumpless scheme for LQRI tested in paragraph 6.2, which receives as input from the TVC the CN's voltage reference $v_{CNref}$. The latter also embeds the system's state evaluation described in [60] and paragraph 6.1, using the power plants' HV side voltage $v_{GAT}$ and the power plants' reactive power $q_{AT}$ signal. The state steady state form calculation is performed as outlined in paragraph 7.2.

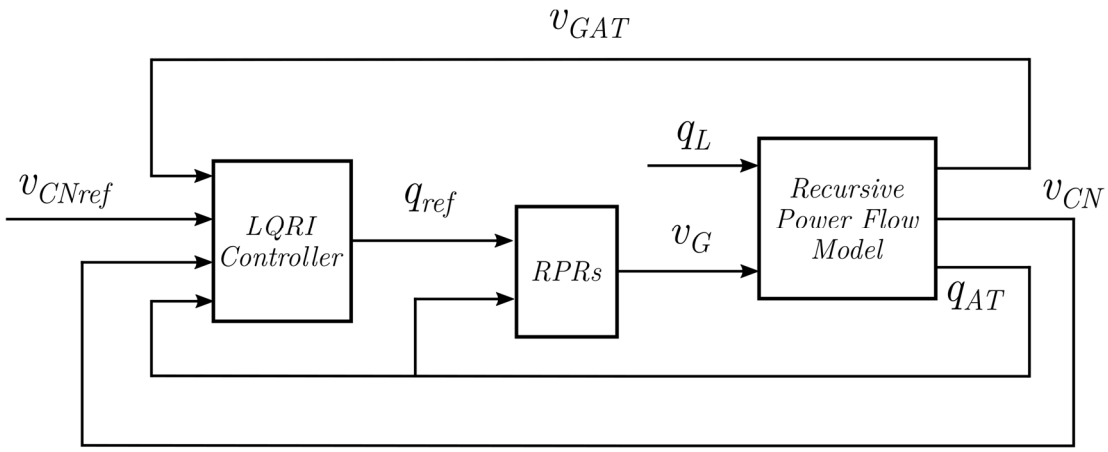


Figure 88 - Blocks scheme of recursive power flow model for SVR LQRI tests

## 7.2. Steady State Form Determination for LQRI

On the basis of the study [60] reported in paragraph 6.1, here is presented how to determine the steady state form starting from the Terna's available measures. Starting from the admittance matrix $[Y]$ of the under-study network subdivided in MV generation nodes (identified with subscript G) and load nodes HV (identified with subscript L), it is possible to obtain its real part $[G]$ (matrix of the conductances) and its imaginary part $[B]$ (matrix of the susceptances):

$$\begin{bmatrix} Y_{LL} & Y_{LG} \\ Y_{GL} & Y_{GG} \end{bmatrix} = \begin{bmatrix} G_{LL} & G_{LG} \\ G_{GL} & G_{GG} \end{bmatrix} + j \begin{bmatrix} B_{LL} & B_{LG} \\ B_{GL} & B_{GG} \end{bmatrix} \tag{7.1}$$

1. As a result, it is possible to compute the matrix $[H]$ as follows [5]:

$$[H] = -[B_{LL}^{-1}] * [B_{BLG}] \tag{7.2}$$

where $[H]$ relates loads voltages to generators voltages by the following ratio:

$$\Delta v_L = [H]\Delta v_{G_{MT}} \qquad \text{with} \qquad \Delta q_L = 0 \tag{7.3}$$

2. At this point it is possible to calculate the state form of the system:

$$\begin{cases} \dot{x} = [A]x + [B]y \\ y = [C]x \end{cases} \quad \rightarrow \quad \begin{cases} \Delta \dot{v_{G_{MT}}} = [A]\Delta v_{G_{MT}} + [B]\Delta v_{NC} \\ \Delta v_{NC} = [C]\Delta v_{G_{MT}} \end{cases} \tag{7.4}$$

where $\Delta v_{G_{MT}}$ is the system state, namely the MV of the power plant's equivalents, $\Delta v_{NC}$ are CNs' voltages and the matrices $[A]$, $[B]$ and $[C]$ are calculated as follows:

$$A_{ij} = \begin{cases} A_{ii} = \frac{(H_{ii} - x_{Ti} - 1)}{T_{r_i} * x_{T_i}} \\ A_{ij} = \frac{H_{ii}}{T_{r_i} * x_{T_i}} \end{cases} \qquad B_{ij} = \begin{cases} B_{ii} = \frac{1}{T_{r_i}} \\ B_{ij} = 0 \end{cases} \qquad C_{ij} = H_{NCNC_{ij}} \tag{7.5}$$

where $T_{r_i}$ is the time constant of the *i-th* power plant's reactive cycle, $x_{T_i}$ is the equivalent reactance of the *i-th* equivalent power plant, and $H_{CNCN_{ij}}$ is the $[H]$ submatrix matrix CNs only.

3. Once the state form has been determined, it is possible to implement the relationships for the determination of the $[K]$ matrix of the LQRI controller:

$$K = R^{-1}(B^T P) \tag{7.6}$$

where $[P]$ is the only positive symmetrical and semi-definite solution of the associated Riccati algebraic equation:

$$PA + A^T P + Q - PBR^{-1}B^T P = 0 \tag{7.7}$$

As a result, the case study model following the equation (3.1) and using eq. (7.5) is described through the following *A, B* and *C* matrices:

$$A = \begin{bmatrix} -2.180 & 0 & 0 & 0 \\ 0 & -3.503 & 0 & 0 \\ 0 & 0 & -41.791 & 0 \\ 0 & 0 & 0 & -8.348 \end{bmatrix}$$
$$B = \begin{bmatrix} 0.1250 & 0 & 0 & 0 \\ 0 & 0.1250 & 0 & 0 \\ 0 & 0 & 0.1250 & 0 \\ 0 & 0 & 0 & 0.1250 \end{bmatrix} \tag{7.8}$$
$$C = [1.3722 \;\; 2.0720 \;\; 25.5554 \;\; 5.6810]$$

## 7.3. SVR LQRI Adaptivity

As explained in paragraph 6.2, the scheme in Figure 81 represent the conceptual scheme for a bumpless switch from 2 different LQRI regulators. This enables the update of the regulator's $[K]$ matrix using the LQRI approach without producing any step variation of the SVR outgoing vectors of reference reactive power variation. The switch

management between the outgoing controller and the incoming controller implements a logic of the following type:

*IF (there was a variation in the [K] matrix)*

*DO (compare the outputs of the two LQRI controllers)*

*IF (the error between the output of the incoming regulator and that of the outgoing regulator is less than a certain tolerance)*

*DO (switch)*

*IF (the time elapsed by the change in the [K] matrix is less than a certain time limit)*

*DO (wait)*

*ELSEIF*

*DO (switch)*

In practice, the switch's management is susceptible to a variation of the [*K*] matrix, which is recalculated in response to variations of:

- Matrix [*H*] (hence the network set-up, being the matrix [*H*] derived from the admission matrix *Y)*;
- Control Nodes;
- Remote control signal of regulating power plants (output or input of a regulating power plant);
- Service presence of regulating power plants (switching off or on);

Following a change in the [*K*] matrix, the process in charge of managing the bumpless switch is queried. Its inputs are two crucial switch parameters: an error tolerance between the *qref* vectors output to the two instances LQRI1 and LQRI2, and a switch time limit. The maximum switch time was added to avoid a lack of convergence within the tolerance on *qref* vectors preventing the switch from being executed and, as a result, keeping a non-updated LQRI in the presence of significant network variations. Both parameters are settable based on requirements.

## 7.4. Network Data Acquisition

The Recursive Power Flow Model (RPFM) (as well as the SVR LQRI developed for Terna, for the calculation of matrix $[Y]$) needs all the network data in order to being able to reconstruct the entire network set-up.

```
%% IEEE 30-BUS TEST SYSTEM DATA
%           IEEE 30-BUS TEST SYSTEM (American Electric Power)
%     Bus  Bus  Voltage  Angle  ---Load---- ----Generator---  Static Mvar
%     No  Type   Mag.   Degree  MW    Mvar  MW  Mvar Qmin Qmax +Qc/-Ql
bus = [1   3     1.06     0     0.0   0.0   0    0    0    0      0
       2   2     1.043    0    21.70  12.7  40    0  -40   50      0
       3   1     1.0      0     2.4   1.2   0    0    0    0      0
       4   1     1.06     0     7.6   1.6   0    0    0    0      0
       5   2     1.01     0    94.2  19.0   0    0  -40   40      0
       6   1     1.0      0     0.0   0.0   0    0    0    0      0
       7   1     1.0      0    22.8  10.9   0    0    0    0      0
       8   2     1.01     0    30.0  30.0   0    0  -10   40      0
       9   1     1.0      0     0.0   0.0   0    0    0    0      0
       10  1     1.0      0     5.8   2.0   0    0    0    0     19
       11  2     1.082    0     0.0   0.0   0    0   -6   24      0
       12  1     1.0      0    11.2   7.5   0    0    0    0      0
       13  2     1.071    0     0     0.0   0    0   -6   24      0
       14  1     1        0     6.2   1.6   0    0    0    0      0
       15  1     1        0     8.2   2.5   0    0    0    0      0
       16  1     1        0     3.5   1.8   0    0    0    0      0
       17  1     1        0     9.0   5.8   0    0    0    0      0
       18  1     1        0     3.2   0.9   0    0    0    0      0
       19  1     1        0     9.5   3.4   0    0    0    0      0
       20  1     1        0     2.2   0.7   0    0    0    0      0
       21  1     1        0    17.5  11.2   0    0    0    0      0
       22  1     1        0     0     0.0   0    0    0    0      0
       23  1     1        0     3.2   1.6   0    0    0    0      0
       24  1     1        0     8.7   6.7   0    0    0    0    4.3
       25  1     1        0     0     0.0   0    0    0    0      0
       26  1     1        0     3.5   2.3   0    0    0    0      0
       27  1     1        0     0     0.0   0    0    0    0      0
       28  1     1        0     0     0.0   0    0    0    0      0
       29  1     1        0     2.4   0.9   0    0    0    0      0
       30  1     1        0    10.6   1.9   0    0    0    0     0];
```

```
%                          Line code
%      Bus Bus     R         X        1/2 B    Tr.Tap Setting
%      nl  nr    p.u.      p.u.       p.u.        p.u.
line = [1   2   0.0192    0.0575    0.02640        1
        1   3   0.0452    0.1852    0.02040        1
        2   4   0.0570    0.1737    0.01840        1
        3   4   0.0132    0.0379    0.00420        1
        2   5   0.0472    0.1983    0.02090        1
        2   6   0.0581    0.1763    0.01870        1
        4   6   0.0119    0.0414    0.00450        1
        5   7   0.0460    0.1160    0.01020        1
        6   7   0.0267    0.0820    0.00850        1
        6   8   0.0120    0.0420    0.00450        1
        6   9   0         0.2080    0            0.978
        6  10   0         0.5560    0            0.969
        9  11   0         0.2080    0              1
        9  10   0         0.1100    0              1
        4  12   0         0.2560    0            0.932
       12  13   0         0.1400    0              1
       12  14   0.1231    0.2559    0              1
       12  15   0.0662    0.1304    0              1
       12  16   0.0945    0.1987    0              1
       14  15   0.2210    0.1997    0              1
       16  17   0.0824    0.1923    0              1
       15  18   0.1073    0.2185    0              1
       18  19   0.0639    0.1292    0              1
       19  20   0.0340    0.0680    0              1
       10  20   0.0936    0.2090    0              1
       10  17   0.0324    0.0845    0              1
       10  21   0.0348    0.0749    0              1
       10  22   0.0727    0.1499    0              1
       21  22   0.0116    0.0236    0              1
       15  23   0.1000    0.2020    0              1
       22  24   0.1150    0.1790    0              1
       23  24   0.1320    0.2700    0              1
       24  25   0.1885    0.3292    0              1
       25  26   0.2544    0.3800    0              1
       25  27   0.1093    0.2087    0              1
       28  27   0         0.3960    0            0.968
       27  29   0.2198    0.4153    0              1
       27  30   0.3202    0.6027    0              1
       29  30   0.2399    0.4533    0              1
        8  28   0.0636    0.2000    0.0214         1
        6  28   0.0169    0.0599    0.065          1];
```

Figure 89 - Example (for IEEE 39 buses) of network data input for recursive power flow model

The input data to the RPFM must be provided with a specific format, just like for other network simulation software based on the acquisition of table data (e.g. Panda Power, Dome, etc.). The code requires two different matrices: one for bus data (named *Bus*) and one for connection data between buses (lines, transformers, named *Line*). In Figure 89 are reported as example respectively the matrix *Bus* and the *Line* matrices belonging to the IEEE 39 Bus test network [64]. It should be mentioned that the IEEE test network is used here for ease of reading because the case study of this subject includes a larger number of busses and lines (422 lines for the bus matrix and 497 lines for the line matrix, only as regards the active components in the network snapshot

provided by Terna for testing) and it would make understanding the structure of the pieces mentioned below needlessly difficult.

These input matrices, for the case study, are built from data that are in the Terna's DAVA and DADIR databases, but the process of its construction is out of this thesis topic. In order to give some further information about Terna's database, the DAVA database contains all of the network's "dynamic" information, such as identification of the busbar systems of the power stations, voltages detected by voltmeters associated with the busbar systems inside the power stations, power statistics of aggregate loads or generators, state of opening/closure elements, and so on. On the opposite, the DADIR database contains "static" network information such as line and transformer parameters, line's power station origin and destination, generator capability curves, and so on. Comparing Figure 89 with the data on the DAVA and DADIR databases we can say that:

- Column 2 of the *Bus* matrix identifies with 1 the PQ buses (hence the load and/or transit buses) with 2 the PV buses (voltage-controlled buses, typically generation buses) and with 3 the *slack bus*;
- Columns 3, 5, 6, 7, and 8 of the *Bus* matrix can be obtained by filtering data from the DAVA database;
- Columns 9 and 10 of the *Bus* matrix, which contain information on the maximum and minimum reactive power of the generator attested to the given bus, can be deduced from the DAVA database;
- Columns 3, 4, and 5 of the *Line* matrix, containing the parameters of lines and transformers, can be determined from the DADIR database data;
- Column 6 of the *Line* matrix, containing the position of the transformer tap changer, can be deduced from the DAVA database;
- Columns 1 of the *Bus* matrix, 1 and 2 of the *Line* matrix, contain the numerical indication of the buses, as a translation from the Terna ID to a numeric index associated with them, which will remain fixed.

The information of the individual bar to which each element of the database is attested is not directly deductible from the data contained in the DAVA or DADIR cards, but it is necessary to intersect several cards of both databases. This information is however necessary for the management of multiple bars, especially in the case of the derivation of several lines on bars of the same station operated separately.

Finally, it should be noted that loads and generators are represented by columns 5, 6, 7, and 8 of the *Bus* matrix, with just the active and reactive power absorbed/produced indicated. In terms of generation, RPRs are represented by their Thevenin equivalents and described by their equivalent bus (which is inserted into the bus matrix), equivalent reactance (inserted as a line between the bus equivalent and the bus AT of central in the matrix line), and the entity of the active and reactive power produced.

## 7.5. Perturbations and Tests

Using the RPFM, 3 different simulation cases have been tested for validating the bumpless LQRI secondary voltage regulator:

1) The first one replicates the perturbation outlined in paragraph 6.2, thus, a full power plant disconnection is modelled.
2) The second one tests the anti-windup ability of the controller; thus, a power plant reactive power capability reduction is carried out, leading one of the actuators to a control action saturation.
3) The third and last type of perturbation consist of an abrupt change of the control node, switching to another node with a different reference point.

All the following simulations are $400s$ long, but the initial $100s$ are dedicated to the power system and controller initialization processes. Thus, they are not shown in the following figures to allow a better readability. Moreover, all the three perturbations have been triggered at the time of $200s$. Finally, all the results shown in this section start with

the same control matrix $[K]$, calculated at the start of the simulation, which is the following:

$$K_{0s} = \begin{bmatrix} 0{,}0757 & 0{,}0690 & 0{,}0719 & 0{,}0798 \\ 0{,}0690 & 0{,}0672 & 0{,}0683 & 0{,}0758 \\ 0{,}0719 & 0{,}0683 & 0{,}0719 & 0{,}0794 \\ 0{,}0798 & 0{,}0758 & 0{,}0794 & 0{,}0888 \end{bmatrix} \tag{7.9}$$

### 7.5.1. Disconnection of an RPR

In this paragraph the response of the system at the disconnection of a power plant that is being used for SVC, using the detailed model, is described. As can be seen in Figure 90, the abrupt disconnection causes an almost 4% transient overvoltage. The reactive power of the disconnected power plant (the blue one in Figure 91) instantly drops to zero (simulating an abrupt breaker opening), while the other RPRs react following the smooth changes in reactive power references provided by the bumpless LQRI regulator. The result is the full compensation of the power plant disconnection, restoring the CN's voltage to its setpoint by distributing the lost reactive power contribution on the remaining power plants. Such a result is obtained by means of the LQRI control matrix $[K]$ recalculation, and the subsequent smooth switch from the former controller to the new thanks to the bumpless transfer scheme. In fact, the disconnection of an RPR equals to a change in the number of actuators for the system, which in turn requires a new control matrix with a new matrix $[K]$ as follow:

$$K_{200s} = \begin{bmatrix} 0{,}0710 & 0{,}0722 & 0{,}0801 \\ 0{,}0722 & 0{,}0759 & 0{,}0839 \\ 0{,}0801 & 0{,}0839 & 0{,}0938 \end{bmatrix} \tag{7.10}$$

These results make it possible to state that the RPFM has been properly developed and, at the same time, the LQRI with bumpless transfer scheme provides the expected results. Indeed, although starting from a different operating point and using a different set of simulation conditions, the result is coherent with the one depicted in paragraph 6.2.

### 7.5.2. Reduction in an RPR's reactive power capability

The second perturbation consists in the abrupt reduction of a power plant's reactive power capability while its SVC function is enabled. This phenomenon may happen in the real world when a sudden increase in active power production is demanded. The latter in turn leads to a reduction in the reactive power capability according to the power plant's P-Q curve. The proposed bumpless LQRI controller can compensate such events, by redistributing the missing reactive power to the other RPRs, therefore acting as an anti-windup system in presence of a saturation. In fact, the reduction of a power plant reactive capability can be considered as an actuator saturation, which is automatically taken care by the bumpless transfer scheme thanks to the reactive power limits feedback (provided by the power plants). Such a feature does not require the recalculation of the control matrix $[K]$, which remains equal to the one applied at the start of the simulation: equation (7.9) It can be seen in the Figure 92 and Figure 93 that the reduction of the reactive power of one power plant (the blue line in Figure 93) results in a smooth variation in the other power plants' reactive power references, determined by the voltage regulator in order to properly restore the CN's voltage reference level. In respect to the previous perturbation, the voltage transient is less severe, due to the less severe reduction in the reactive power variation.

### 7.5.3. Change of the control node

The last simulation case concerns the change of the node used as CN, coupled with a related change in reference voltage.

In Figure 94 are represented the CNs' voltages during the perturbation. The first CN (blue trace) has a voltage reference of 1.05 *p.u.*, while the second CN (orange trace) has a voltage reference of 1.02 *p.u.*. At $200s$ the bumpless LQRI switches the control from the first to the second, emulating an operator action, or a fault that leads to the inability of using that CN. The regulator reacts by changing its control matrix $[K]$, while using the bumpless function to ensure a smoot passage to the new operating condition.

The new control feedback gain matrix $[K]$ which enter at $200s$ after the CN change is the following:

$$K_{200s,CN\ change} = \begin{bmatrix} 0{,}0640 & 0{,}0727 & 0{,}0756 & 0{,}0498 \\ 0{,}0727 & 0{,}0882 & 0{,}0902 & 0{,}0593 \\ 0{,}0756 & 0{,}0902 & 0{,}0949 & 0{,}0621 \\ 0{,}0498 & 0{,}0593 & 0{,}0621 & 0{,}0415 \end{bmatrix} \tag{7.11}$$

This also demonstrates how the bumpless LQRI controller is capable of recalculating its control matrix and provide a smooth application of the new control gain, to guarantee the transmission system's power quality. In Figure 95 are depicted the reactive power references of the 5 regulating power plant, where the small changes required to ensure reaching the voltage reference on the new CN are evident. The smooth reactive power dynamic is also appreciable.

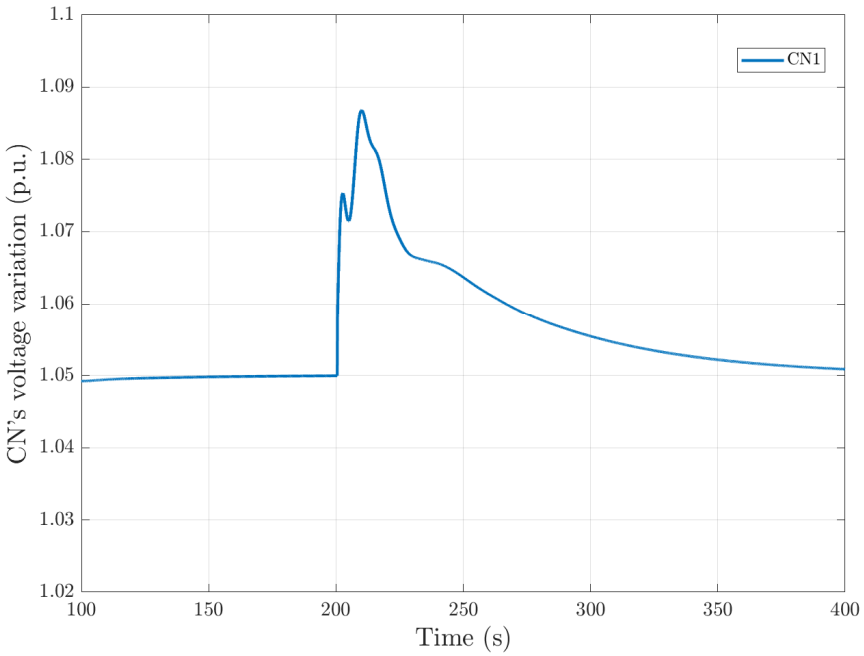


Figure 90 - CN's voltage with bumpless LQRI – recursive power flow model

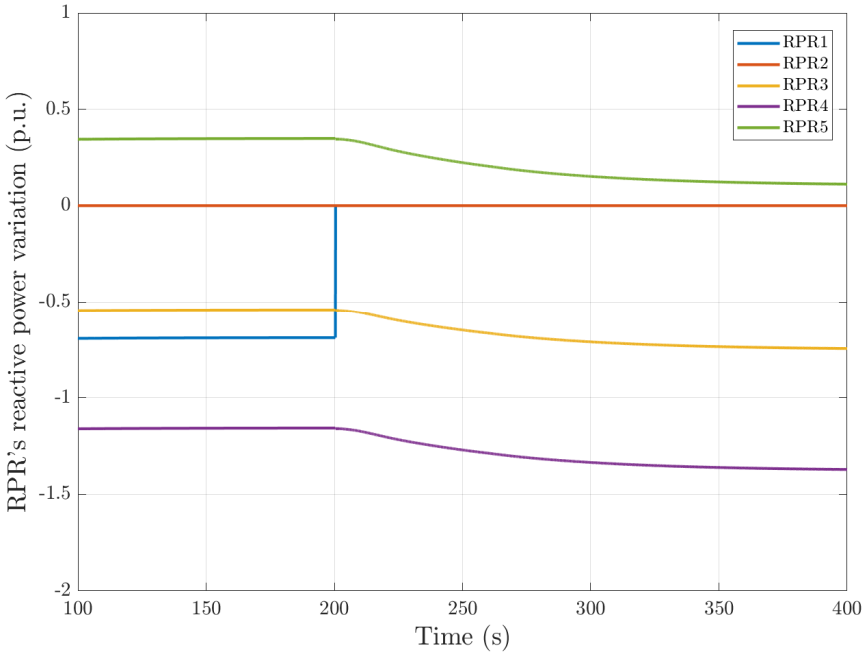


Figure 91 - Reactive power references variation of RPRs with bumpless LQRI – recursive power flow model

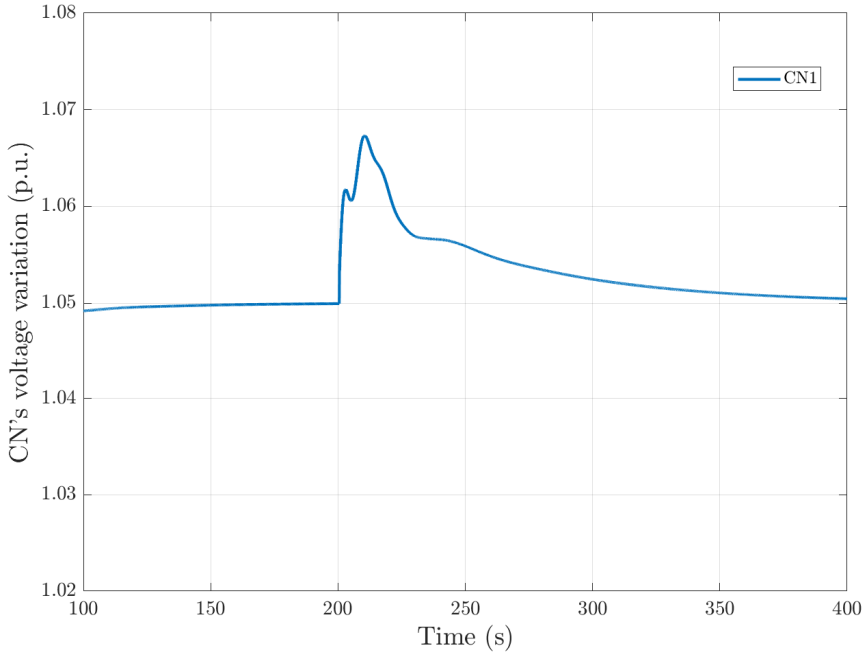


Figure 92 - CN's voltage with bumpless LQRI – recursive power flow model

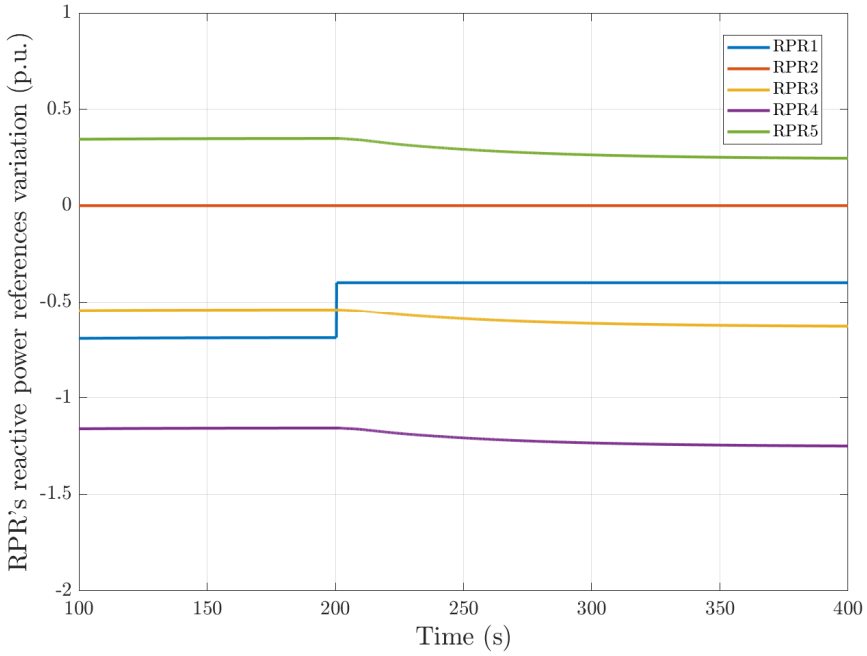


Figure 93 - Reactive power references variation of RPRs with bumpless LQRI – recursive power flow model

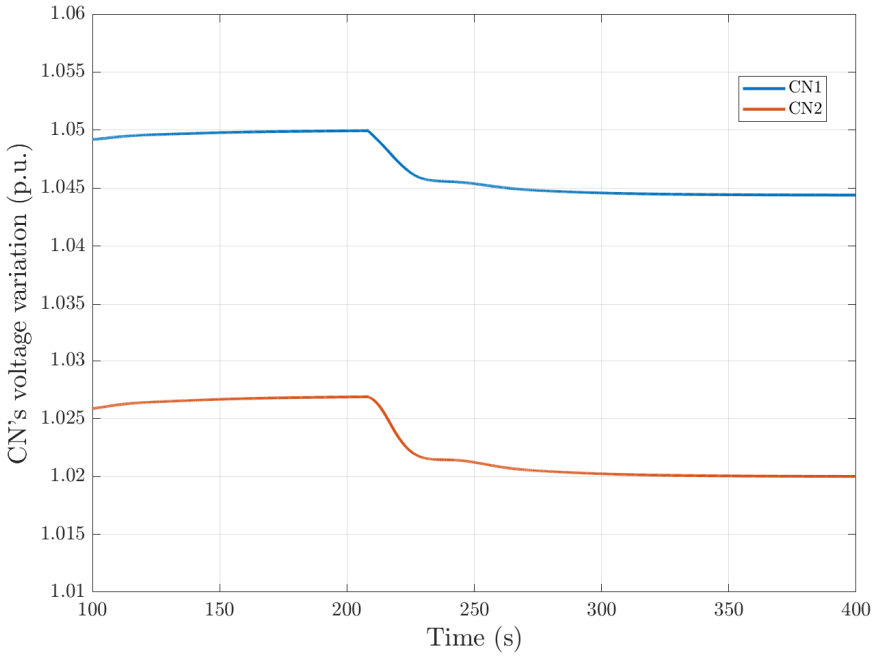


Figure 94 - CN's voltage with bumpless LQRI – recursive power flow model

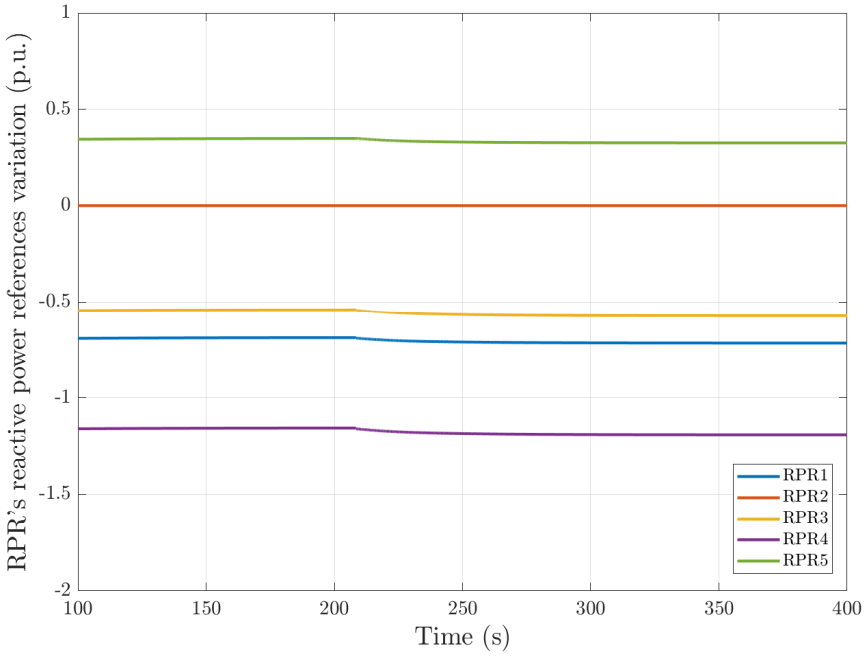


Figure 95 - Reactive power references variation of RPRs with bumpless LQRI – recursive power flow model

# Conclusions

The gradual transition from fossil fuels to renewable energy resources in electric power generation is causing significant changes in power system management and real-time control. Transmission systems are facing a gradual reduction in the number of high-power conventional power plants connected to the grid in favour of small, distributed renewable sources-based power plants (with significantly different dynamic performance), as well as the integration of new power system elements such as VSC HVDC links, STATCOMs, and so on. Furthermore, current wide area voltage control architectures, primarily designed in the 1990s, have some limitations due to technological obsolescence, being based on the fundamental hypothesis of network structure and power flows time invariance. The logical conclusion is that a modern control strategy must be devised.

To this aim, the purpose of this thesis was to show the research studies that were performed in order to design a new secondary voltage regulator for the Italian transmission network, capable of managing the power system evolution (caused by the regulatory aims towards the global warming limitation).

To begin, two in-depth studies on current Italian SVC criticalities was presented. The first one is about the strategy for grouping nodes into control areas and assigning

them PNs. It shows that if both frequency and severity of network structure changes increase, the allocation of PNs and their control areas must be able to keep up. As a result, in order to track the movements of control areas, controlling power plants, and associated PNs, a new SVR must be able to adapt to network changes in real-time. The second study was about power system voltage stability as a consequence of a network event (i.e. a sudden regulating power plant disconnection that happened in a specific part of the Italian grid). The results of such study show that reducing delays in the remote-control chain has a highly stabilizing effect. Moreover, when PMUs are paired with a faster sampling period on the remote-control side, the dampening effect offered by shorter delay times is amplified. Additional emphasis is given to short circuit power following network changes, and its implications for SVC. Short-circuit power changes on transmission network buses may potentially result in tough identification of PNs, envisioning a future wherein RES can participate to control voltage, while at the same time cause issues due to their continuous connection and disconnection due to weather variations. As a result, a new SVR capable of regulating numerous PNs' voltage, as well as managing their frequent switching may be required, in order to optimize the PN selection in response to transmission network changes.

Since some of the assumptions that led the voltage control chain to be approximated as a SISO system (group of power plants controlling a single PN within a single area) in the past may no longer be valid, the research in this thesis focuses on voltage control of a transmission network viewed as a MIMO system. Two different MIMO control approaches are here presented, the Decoupling and the Linear Quadratic Regulator with Integral actions. These two different approaches have been implemented in Matlab-Simulink with a linearized network model in order to test them. Simulation results shows that the architecture with LQRI as SVR, sending dedicated control signals to each power plant, is the solution with the best dynamic performance.

Once the most suitable solution has been selected, the results of specific studies concerning its implementation in a real-world scenario have been explained. Specifically, consideration has been given to the availability of measures from the field and the needs

of the Italian transmission network. Such studies enable the transition from the ideal mathematical model, which is only used for the definition of control algorithms, to a SVR model that is closer to the actual realization. Thus, the system mathematical state reconstruction for the LQRI used as SVR, considering the available measures, has been taken into account. The result is the possibility of using the existing measures/signals that are sent by the power plants for calculating the system state using an algebraic equation, hence avoiding the usage of a complicated state estimator. Another challenge in the implementation of an LQRI as SVR is that its characteristic feedback control gain matrix is dependent on the system mathematical state, the system structure, and the system operating point. The enabling or disabling of the SVC function in the RPRs is one of the actions that causes a change in the system structure, which can be mathematically interpreted as a change in the number of system states and input signals, and by the controller as a change in the number of actuators. In order to avoid abrupt step changes on the control signals, a bumpless transfer scheme has been introduced on the LQRI controller. This scheme enables a smooth transition between distinct gain control matrices, specifically two separate LQRI controllers. When the control gain matrix is modified, simulation of LQRI using the bumpless scheme and the linearized network model yields promising results in terms of smooth dynamics.

Finally, in order to validate the results obtained with the linearized model, as well as demonstrating the correct operation of the resulting SVR, a transmission network nonlinear model based on recursive power flow computations was developed. It can obtain data from the Italian TSO databases (and thus it can be integrated in the Matlab-Simulink model of the LQRI regulator developed for Terna) and executes the power flow algorithm for each simulation time step. Results shows that the nonlinear model, despite the higher level of complexity, provides the validation of the linear model results. Moreover, it demonstrated that LQRI sending dedicated control signals has a good dynamic performance in terms of voltage control and reactive power distribution. Thus, it presents the necessary qualities to deal with the previously described energy transition, such as adaptivity to network changes and the capacity to regulate multiple CNs.

# Appendix A

In general and also under steady-state conditions, power generation and transmission networks have small phase displacements between the voltages at the terminals of their links (see Chapter 4.4.4 of), as well as small resistances and conductances vs reactances and susceptances in their lines and transformers. As a result, real power flows (2.4.88) on the links, as well as real power injections into nodes, are mostly determined by voltage phases. Reactive power flows on connections, as well as reactive power injections into nodes, are primarily affected by voltage amplitudes. In other words, the voltages of various nodes under steady-state conditions are primarily determined by: i) reactive powers injected into the network by generators; ii) reactive powers absorbed by loads; and reactive power flows via the various system components (lines and transformers). For sufficiently long lines with negligible shunt capacitive susceptibility: i) at no load, the voltage at the receiving terminal is greater than the voltage at the sending terminal (Ferranti effect), and the line generates reactive power; ii) at low loads (transmitted real power less than natural load), a line generates reactive power and the voltage at the receiving terminal rises; iii) at high loads (transmitted power greater than natural load), a line absorbs reactive power and the voltage at the

receiving terminal falls; iv) the voltage at the sending terminal is given by the following equation, based on Figure 96:

$$\bar{V_1} = V_2 \cos(\beta a) + j\frac{XP}{V_2} + \frac{XQ_2}{V_2} \tag{A.1}$$

which corresponds to the phasor diagram of FIGURE. Thus, for small phase displacement $\theta_{12}$, we obtain:

$$V_1 - V_2 \cos(\beta a) \cong \frac{XQ_2}{V_2} \tag{A.2}$$

thus, the voltage drop can be calculated as:

$$\Delta V = V_1 - V_2 \cong \frac{XQ_2}{V_2} - V_2\,[1 - \cos(\beta a)\,] \tag{A.3}$$

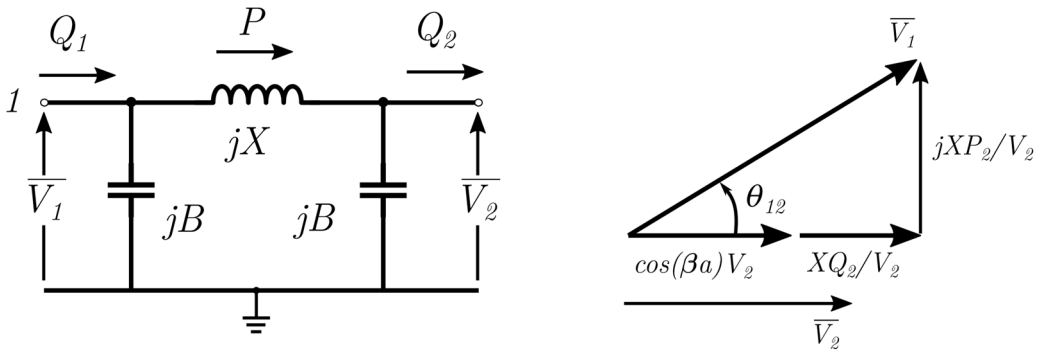


Figure 96 – Long lines equivalent circuit and phasor diagram of voltages

For short lines, where the shunt capacitive susceptance is negligible, and for transformers: i) the generation of reactive power is negligible; ii) the voltage at the sending terminal is given by the eq. (A.1), putting *cos(βa)=1:*

$$\overline{V_1} = V_2 - j\frac{XP}{V_2} + \frac{XQ_2}{V_2} \tag{A.4}$$

which corresponds to the phasor diagram of Figure 97. For small phase displacements $\theta_{12}$, we deduce:

$$\Delta V = V_1 - V_2 \cong \frac{XQ_2}{V_2} \tag{A.5}$$

Finally, eq. (A.3) and (A.5) evidence that voltage drops are mainly due to the reactive load. Thus, the voltage at the receiving terminal remaining equal, an increase in the reactive load $Q_2$ requires an increase in the voltage at the sending terminal and thus an increase of the voltage drop on the line or transformer.

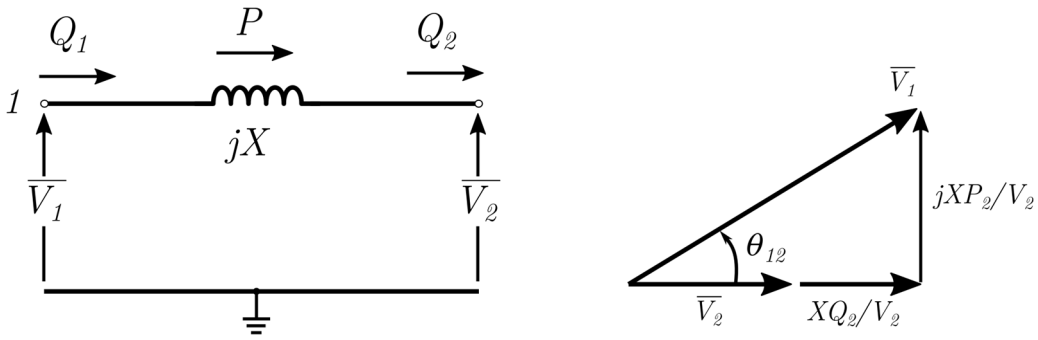


Figure 97 – Short lines and transformers equivalent circuit and phasor diagram of voltages

# Appendix B

A *power flow* analysis in an electric transmission network is a crucial process used to determine the electrical variables (such as voltage, current, and power) in each component of the network (which is a tough task since the transmission network has usually a high grade of interconnection). This type of analysis is essential to ensure the stable and efficient operation of the network, considering the laws of physics and operational constraints. In more technical terms, power flow analysis solves a system of nonlinear equations that describe the flow of power through various components of the electrical network. The system of equations is based on Kirchhoff's laws for currents and voltages at each node of the network. The objective is to find the values of voltages and currents in a way that satisfies the power balance laws for each node.

The power flow equations can be represented in mathematical form as follows, considering a node $i$ with a voltage $V_i$ and complex power $S_i$, the Active Power ($P$) and Reactive Power balances are:

$$P_i = \sum_{j=1}^{N} V_i V_j (G_{ij} \cos(\theta_{ij}) + B_{ij} \sin(\theta_{ij})) \tag{B.1}$$

$$Q_i = \sum_{j=1}^{N} V_i V_j (G_{ij} \sin(\theta_{ij}) + B_{ij} \cos(\theta_{ij})) \quad \text{(B.2)}$$

where:

- $P_i$ and $Q_i$ represent the active and reactive power at node *i;*
- $V_i$ is the voltage at node *i;*
- $G_{ij}$ and $B_{ij}$ are the real and imaginary parts of conductance and susceptance between nodes $i$ and *j;*
- $\theta_{ij}$ is the phase difference between the voltage at nodes $i$ and $j$
- $N$ is the total number of nodes in the network.

The power flow's goal is hence to simultaneously solve these equations for all the unknown variables, thereby obtaining the voltage and power values at each node in the network, ensuring efficient and reliable operation.

In a power flow analysis for an electrical transmission network, inputs and outputs are critical to understanding and evaluating the behaviour of the electrical system.

## Power flow analysis inputs

- Network Data: Configuration of the transmission network, including information on transmission lines, transformers, generators, and loads. These data include power admissions, capabilities, reactors, and other component characteristics;
- Initial Conditions: The initial conditions of the system, such as the initial values of voltages and phases in the network nodes. These conditions may be based on a known operating state or be estimated;
- Operational Requirements: The operational specifications or system requirements, such as the request to maintain specific network nodes at certain voltages or with specific power flows.

## Power flow analysis Outputs

- Voltage and Phase Distribution: voltages and phases at each node or bus in the network, providing a comprehensive view of the electrical variables present in the system;
- Power Flows: active and reactive power flows through each transmission line, transformer, generator, and load in the network. These details are crucial to understanding how energy is distributed and utilized in the system;
- Load on Lines: Currents and loads on different transmission lines, providing insights into line capacity and current loading;
- System Performance: system performance parameters, such as power losses, power factor, voltage violations, and network congestions. These results help to evaluate the efficiency and stability of the system;
- Information on Potential Violations: any situation where operational limits are exceeded, such as line overloads, voltage violations, or other stability issues that may require corrective actions.

# List of Figures

# References


[1] European Commission: Brussels, 'European Commission. Communication, COM/2018/773 Final, a Clean Planet for All. A European Strategic Long-Term Vision for a Prosperous, Modern, Competitive and Climate Neutral Economy'. 2018.

[2] 'Italian Integrated National Energy and Climate Plan'. [Online]. Available: https://ec.europa.eu/energy/sites/ener/files/documents/it_final_necp_main_en.pdf

[3] M. Fermeglia, P. Bevilacqua, C. Cafaro, P. Ceci, and A. Fardelli, 'Legal Pathways to Coal Phase-Out in Italy in 2025', *Energies*, vol. 13, no. 21, Art. no. 21, Jan. 2020, doi: 10.3390/en13215605.

[4] Terna S.p.A., 'Piano di Sviluppo 2023: Evoluzione Rinnovabile e interventi di Connessione'.[Online].Available: [https://download.terna.it/terna/Terna_Piano_Sviluppo_2023_Evoluzione_Rinnovabile_interventi_Connessione_8db254c6c0da24c.pdf](https://download.terna.it/terna/Terna_Piano_Sviluppo_2023_Evoluzione_Rinnovabile_interventi_Connessione_8db254c6c0da24c.pdf)

[5] R. Marconato, *Electric Power Systems: Steady State Behaviour, Controls, Short Circuits and Protection Systems. Second Ed., vol 2.* Milan, Italy: CEI Italian Electrothecnical Comitee, 2002.

[6] S. Corsi, M. Pozzi, C. Sabelli, and A. Serrani, 'The coordinated automatic voltage control of the Italian transmission Grid-part I: reasons of the choice and overview of the consolidated hierarchical system', *IEEE Transactions on Power Systems*, vol. 19, no. 4, pp. 1723–1732, Nov. 2004, doi: 10.1109/TPWRS.2004.836185.

[7] S. Corsi, 'The secondary voltage regulation in Italy', in *2000 Power Engineering Society Summer Meeting (Cat. No.00CH37134)*, Jul. 2000, pp. 296–304 vol. 1. doi: 10.1109/PESS.2000.867599.

[8] V. Arcidiacono, 'Automatic voltage reactive power control in transm. System', presented at the Proc. CIGRE-IFAC Survey Paper E, Florence, Italy, Sep. 1983.

[9] J. P. Paul, J. Y. Leost, and J. M. Tesseron, 'Survey of the Secondary Voltage Control in France : Present Realization and Investigations', *IEEE Transactions on Power Systems*, vol. 2, no. 2, pp. 505–511, May 1987, doi: 10.1109/TPWRS.1987.4335155.

[10] H. Lefebvre, D. Fragnier, J. Y. Boussion, P. Mallet, and M. Bulot, 'Secondary coordinated voltage control system: feedback of EDF', in *2000 Power Engineering Society Summer Meeting (Cat. No.00CH37134)*, Jul. 2000, pp. 290–295 vol. 1. doi: 10.1109/PESS.2000.867598.

[11] J. P. Piret, J. P. Antoine, and M. Subbe et Alii, 'The study of a centralized voltage control method applicable to the Belgian system', Paris, France, 1992, p. paper 39-201.

[12] J. Van Hecke, N. Janssens, J. Deude, and F. Promel, 'Coordinated voltage control experience in Belgium', presented at the Proc. CIGRE, Paris, France, 2000, p. paper 38-111.

[13] J. L. Sancha, J. L. Fernandez, A. Cortes, and J. T. Abarca, 'Secondary voltage control: analysis, solutions and simulation results for the Spanish transmission system', *IEEE Transactions on Power Systems*, vol. 11, no. 2, pp. 630–638, May 1996, doi: 10.1109/59.496132.

[14] M. Polo and C. Scarpa, 'The Liberalization of Energy Markets in Europe and Italy'. Rochester, NY, Jan. 01, 2003. doi: 10.2139/ssrn.381041.

[15] M. Ilic, X. Liu, G. Leung, M. Athans, C. Vialas, and P. Pruvot, 'Improved secondary-new tertiary voltage control', *Power Systems, IEEE Transactions on*, vol. 10, pp. 1851–1862, Dec. 1995, doi: 10.1109/59.476050.

[16] C. W. Taylor, V. Venkatasubramanian, and Y. Chen, 'Wide area stability and voltage control', presented at the Proc. VII SEPOPE, Curitiba, Brazil, May 2000.

[17] G. N. Taranto, N. Martins, D. M. Falcao, A. C. B. Martins, and M. G. dos Santos, 'Benefits of applying secondary voltage control schemes to the Brazilian system', in *2000 Power Engineering Society Summer Meeting (Cat. No.00CH37134)*, Jul. 2000, pp. 937–942 vol. 2. doi: 10.1109/PESS.2000.867497.

[18] F. A. B. Lemos, I. Member, W. Jr, L. Werberich, M. Rosa, and R.-R. Grande, 'Assessment of a Sub-Transmission and Distribution System Under Coordinated Secondary Voltage Control', presented at the 14th PSCC, Sevilla, Spain, Jun. 2002, p. Session 21, Paper 1, Page1-7.

[19] S. Corsi, V. Arcidiacono, M. Cambi, and L. Salvaderi, 'Impact of the restructuring process at ENEL on the network voltage control service', presented at the Proc. IREP, Santorini, Greece, Aug. 1998.

[20] G. Sulligoi, M. Chiandone, and V. Arcidiacono, 'NewSART automatic voltage and reactive power regulator for secondary voltage regulation: Design and application', in *2011 IEEE Power and Energy Society General Meeting*, Jul. 2011, pp. 1–7. doi: 10.1109/PES.2011.6039618.

[21] N. A. Daher, I. Mougharbel, M. Saad, and H. Y. Kanaan, 'Comparative study of partitioning methods used for secondary voltage control in distributed power networks', in *2013 IEEE International Conference on Smart Energy Grid Engineering (SEGE)*, Aug. 2013, pp. 1–7. doi: 10.1109/SEGE.2013.6707897.

[22] J. Zhong, E. Nobile, A. Bose, and K. Bhattacharya, 'Localized reactive power markets using the concept of voltage control areas', *IEEE Transactions on Power Systems*, vol. 19, no. 3, pp. 1555–1561, Aug. 2004, doi: 10.1109/TPWRS.2004.831656.

[23] P. Lagonotte, J. C. Sabonnadiere, J.-Y. Leost, and J.-P. Paul, 'Structural analysis of the electrical system: application to secondary voltage control in France', *IEEE Transactions on Power Systems*, vol. 4, no. 2, pp. 479–486, May 1989, doi: 10.1109/59.193819.

[24] M. Shaaban, 'Improved regional coordination of generation voltage control', in *2008 IEEE 2nd International Power and Energy Conference*, Dec. 2008, pp. 175–179. doi: 10.1109/PECON.2008.4762457.

[25] F. Milano, 'An open source power system analysis toolbox', in *2006 IEEE Power Engineering Society General Meeting*, Jun. 2006, p. 1 pp.-. doi: 10.1109/PES.2006.1708946.

[26] F. Marzolla *et al.*, 'Study on zoning procedures for Secondary Voltage Regulation', in *2020 IEEE International Conference on Environment and Electrical Engineering and 2020 IEEE Industrial and Commercial Power Systems Europe (EEEIC / I&CPS Europe)*, Jun. 2020, pp. 1–8. doi: 10.1109/EEEIC/ICPSEurope49358.2020.9160700.

[27] S. R. Alvarez, E. H. L. Mazo, and J. E. Oviedo, 'Evaluation of power system partitioning methods for secondary voltage regulation application', in *2017 IEEE 3rd Colombian Conference on Automatic Control (CCAC)*, Oct. 2017, pp. 1–6. doi: 10.1109/CCAC.2017.8276463.

[28] P. K. Chan, M. D. F. Schlag, and J. Y. Zien, 'Spectral K-way ratio-cut partitioning and clustering', *IEEE Transactions on Computer-Aided Design of Integrated Circuits and Systems*, vol. 13, no. 9, pp. 1088–1096, Sep. 1994, doi: 10.1109/43.310898.

[29] N. Muhammad, 'Kohonen Neural Network Clustering For Voltage Control In Power Systems', *TELKOMNIKA*, vol. 8, Aug. 2010, doi: 10.12928/telkomnika.v8i2.612.

[30] J. Mezquita, H. Mehrjerdi, S. Lefebvre, M. Saad, P. J. Lagacé, and D. Asber, 'A secondary voltage regulation approach for Hydro-Québec in transmission level', *Electric Power Systems Research*, vol. 121, pp. 183–191, Apr. 2015, doi: 10.1016/j.epsr.2014.11.016.

[31] J. Mezquita, D. Asber, S. Lefebvre, M. Saad, and P. Lagacé, 'Power Network Partitioning with a Fuzzy C-Means', *Proceedings of the IASTED International Conference on Power and Energy Systems and Applications, PESA 2011*, Dec. 2011, doi: 10.2316/P.2011.756-024.

[32] O. Abdalla, H. Habib, and A. Abdel-Ghany, 'Secondary and Tertiary Voltage Control of a Multi-Region Power System', vol. 1, pp. 37–59, Sep. 2020, doi: 10.3390/electricity1010003.

[33] H. Mehrjerdi, S. Lefebvre, M. Saad, and D. Asber, 'A Decentralized Control of Partitioned Power Networks for Voltage Regulation and Prevention Against Disturbance Propagation', *IEEE Transactions on Power Systems*, vol. 28, no. 2, pp. 1461–1469, May 2013, doi: 10.1109/TPWRS.2012.2225154.

[34] N. A. Daher, I. Mougharbel, M. Saad, H. Y. Kanaan, and D. Asber, 'Pilot buses selection based on reduced Jacobian matrix', in *2015 IEEE International Conference on Smart Energy Grid Engineering (SEGE)*, Aug. 2015, pp. 1–7. doi: 10.1109/SEGE.2015.7324611.

[35] H. Sun, Q. Guo, B. Zhang, W. Wu, and B. Wang, 'An Adaptive Zone-Division-Based Automatic Voltage Control System With Applications in China', *IEEE Transactions on Power Systems*, vol. 28, no. 2, pp. 1816–1828, May 2013, doi: 10.1109/TPWRS.2012.2228013.

[36] B. Hernandez, C. A. Canizares, J. M. Ramirez, B. Hu, and M. Liu, 'Secondary and Tertiary Voltage Regulation Controls Based on Regional Optimal Power Flows', in *2018 Power Systems Computation Conference (PSCC)*, Jun. 2018, pp. 1–7. doi: 10.23919/PSCC.2018.8442443.

[37] H. Su, F. Kang, and C. Liu, 'Transmission Grid Secondary Voltage Control Method Using PMU Data', *IEEE Transactions on Smart Grid*, vol. 9, no. 4, pp. 2908–2917, Jul. 2018, doi: 10.1109/TSG.2016.2623302.

[38] H.-Y. Su and C.-W. Liu, 'An Adaptive PMU-Based Secondary Voltage Control Scheme', *IEEE Transactions on Smart Grid*, vol. 4, no. 3, pp. 1514–1522, Sep. 2013, doi: 10.1109/TSG.2013.2272583.

[39] H.-Y. Su, Y.-C. Chen, and Y.-L. Hsu, 'A Synchrophasor Based Optimal Voltage Control Scheme with Successive Voltage Stability Margin Improvement', *Applied Sciences*, vol. 6, no. 1, Art. no. 1, Jan. 2016, doi: 10.3390/app6010014.

[40] H.-Y. Su and T.-Y. Liu, 'WAMS-based coordinated automatic voltage regulation incorporating voltage stability constraints using sequential linear programming approximation algorithm', *Electric Power Systems Research*, vol. 163, pp. 482–490, Oct. 2018, doi: 10.1016/j.epsr.2018.07.024.

[41] O. H. Abdalla, H. H. Fayek, and A. M. Abdel Ghany, 'Secondary Voltage Control Application in a Smart Grid with 100% Renewables', *Inventions*, vol. 5, no. 3, Art. no. 3, Sep. 2020, doi: 10.3390/inventions5030037.

[42] W. Qi, Z. Lingzhi, and Z. Shuangxi, 'A novel fuzzy logic secondary voltage controller', in *Proceedings. International Conference on Power System Technology*, Oct. 2002, pp. 2589–2593 vol.4. doi: 10.1109/ICPST.2002.1047254.

[43] A. Karl Johan and R. M. Murray, *Feedback Systems: An Introduction for Scientists and Engineers, Second Edition*. [Online]. Available: http://fbsbook.org/

[44] 'Skript Control Systems II - Gioele Zardini - V1.pdf'. Accessed: Oct. 06, 2023. [Online]. Available: https://n.ethz.ch/~gzardini/cs2pvk/Theory/Skript%20Control%20Systems%20II%20-%20Gioele%20Zardini%20-%20V1.pdf

[45] G. Sulligoi *et al.*, 'Reactive Power Resources Management in a Voltage Regulation Architecture Based on Decoupling Control', in *2021 AEIT International Annual Conference (AEIT)*, Oct. 2021, pp. 1–6. doi: 10.23919/AEIT53387.2021.9626889.

[46] W. S. Levine, *Control System Advanced Methods, The Control Handbook*, 2nd Edition., vol. Chapter 27: Decoupling Control. CRC Press, 2011.

[47] A. Vicenzutti, F. Marzolla, G. Sulligoi, G. M. Giannuzzi, and C. Pisani, 'Reactive Power Resources Management in a Voltage Regulation Architecture Based on LQRI Control', in *2022 IEEE International Conference on Environment and Electrical Engineering and 2022 IEEE Industrial and Commercial Power Systems Europe (EEEIC / I&CPS Europe)*, Jun. 2022, pp. 1–6. doi: 10.1109/EEEIC/ICPSEurope54979.2022.9854638.

[48] W. S. Levine, *Control System Advanced Methods, The Control Handbook*, 2nd Edition., vol. Chapter 17: LQRI Control. CRC Press, 2011.

[49] B. Kedjar and K. Al-Haddad, 'DSP-Based Implementation of an LQR With Integral Action for a Three-Phase Three-Wire Shunt Active Power Filter', *IEEE Transactions on Industrial Electronics*, vol. 56, no. 8, pp. 2821–2828, Aug. 2009, doi: 10.1109/TIE.2008.2006027.

[50] H. G. Malkapure and M. Chidambaram, 'Comparison of Two Methods of Incorporating an Integral Action in Linear Quadratic Regulator', *IFAC Proceedings Volumes*, vol. 47, no. 1, pp. 55–61, Jan. 2014, doi: 10.3182/20140313-3-IN-3024.00105.

[51] S. Corsi, M. Pozzi, M. Sforna, and G. Dell'Olio, 'The coordinated automatic voltage control of the Italian transmission Grid-part II: control apparatuses and field performance of the consolidated hierarchical system', *IEEE Transactions on Power Systems*, vol. 19, no. 4, pp. 1733–1741, Nov. 2004, doi: 10.1109/TPWRS.2004.836262.

[52] J. Carpentier, 'Optimal power flows', *International Journal of Electrical Power & Energy Systems*, vol. 1, no. 1, pp. 3–15, Apr. 1979, doi: 10.1016/0142-0615(79)90026-7.

[53] J. L. Carpentier, 'Optimal Power Flows: Uses, Methods and Developments', *IFAC Proceedings Volumes*, vol. 18, no. 7, pp. 11–21, 1985, doi: https://doi.org/10.1016/S1474-6670(17)60410-5.

[54] G. Sheng, Y. Liu, D. Duan, Y. Zeng, and X. Jiang, 'Secondary voltage regulation based on wide area network', in *2009 IEEE Power & Energy Society General Meeting*, Jul. 2009, pp. 1–7. doi: 10.1109/PES.2009.5275928.

[55] 'IEEE Guide for Phasor Data Concentrator Requirements for Power System Protection, Control, andMonitoring', *IEEE Std C37.244-2013*, pp. 1–65, May 2013, doi: 10.1109/IEEESTD.2013.6514039.

[56] 'IEEE Standard for Synchrophasor Measurements for Power Systems', *IEEE Std C37.118.1-2011 (Revision of IEEE Std C37.118-2005)*, pp. 1–61, Dec. 2011, doi: 10.1109/IEEESTD.2011.6111219.

[57] 'IEEE Standard for Synchrophasor Data Transfer for Power Systems', *IEEE Std C37.118.2-2011 (Revision of IEEE Std C37.118-2005)*, pp. 1–53, Dec. 2011, doi: 10.1109/IEEESTD.2011.6111222.

[58] R. E. Kalman, 'Contributions to the Theory of Optimal Control'. 1960.

[59] H. Tebianian and B. Jeyasurya, 'Dynamic state estimation in power systems using Kalman filters', in *2013 IEEE Electrical Power Energy Conference*, Aug. 2013, pp. 1–5. doi: 10.1109/EPEC.2013.6802979.

[60] A. Vicenzutti, F. Marzolla, G. Sulligoi, G. M. Giannuzzi, and C. Pisani, 'Study on the State Feedback Selection and Measurement for the Application of an LQRI Secondary Voltage Regulator to a Transmission System', in *2022 20th International Conference on Harmonics & Quality of Power (ICHQP)*, May 2022, pp. 1–6. doi: 10.1109/ICHQP53011.2022.9808441.

[61] Y. Zhao and J. Zhao, '$H_ınfty$ Reliable Bumpless Transfer Control for Switched Systems With State and Rate Constraints', *IEEE Transactions on Systems, Man, and Cybernetics: Systems*, vol. 50, no. 10, pp. 3925–3935, Oct. 2020, doi: 10.1109/TSMC.2018.2871335.

[62] T. C. S. Wibowo and N. Saad, 'Steady-state bumpless transfer MPC using external feedback of Manipulated Variables', in *2010 International Conference on Intelligent and Advanced Systems*, Jun. 2010, pp. 1–6. doi: 10.1109/ICIAS.2010.5716165.

[63] Y. Peng, D. Vrancic, and R. Hanus, 'Anti-windup, bumpless, and conditioned transfer techniques for PID controllers', *IEEE Control Systems Magazine*, vol. 16, no. 4, pp. 48–57, Aug. 1996, doi: 10.1109/37.526915.

[64] 'IEEE 39-Bus System - Illinois Center for a Smarter Electric Grid (ICSEG)'. Accessed: Oct. 18, 2023. [Online]. Available: https://icseg.iti.illinois.edu/ieee-39-bus-system/.